FIBER OPTICS SENSOR TECHNOLOGIES FOR INNOVATIVE CONDITION MONITORING APPLICATIONS

LAI CHUN CHEUNG

PhD

The Hong Kong Polytechnic University

2019

The Hong Kong Polytechnic University

Department of Electrical Engineering

FIBER OPTICS SENSOR TECHNOLOGIES FOR INNOVATIVE CONDITION MONITORING APPLICATIONS

LAI CHUN CHEUNG

A thesis submitted in partial fulfillment of the requirements for the degree of Doctor of Philosophy

November 2015

CERTIFICATE OF ORIGINALITY

I hereby declare that this thesis is my own work and that, to the best of my knowledge and belief, it reproduces no material previously published or written, nor material that has been accepted for the award of any other degree or diploma, except where due acknowledgement has been made in the text.

_________________________________ (Signed)

LAI, Chun Cheung (Name of student)

Dedication

To my beloved parents, Lai Bing Wah and Li Chai Yin

Abstract

This study aimed to explore a new area of development in optical fiber sensing - using the Fiber Bragg Grating (FBG) as a sensing element with real-life applications. The proposed new development is in the field of information technology, and fully utilize the advantages of FBG-based sensors as the foundation of the new area, benefiting many modern industries in this information age.

To demonstrate the concept, a case study focused on railway application is presented. The case study included setting up a Smart Railway Health-Condition Monitoring (SRHM) system, including an FBG-based sensors network and information technology algorithms, for monitoring the health condition of all trains in the fleet.

The FBG has become very popular in recent years because of its advantages of high capacity, small size and long-distance of application. Thus, it has been used in different fields and excellent performances have been recorded. Railway systems involve numerous high-voltage systems that may be sensitive to, or emit, electromagnetic (EM) waves. Compared to electronic type sensors, the FBG is the most suitable candidate for railway application because of its EM interference (EMI) immunity and zero-emission of EM waves.

The SRHM system proposed, connects four FBG-based sensors as follows: (1) Track Settlement Level Sensor, (2) Axle Counting Sensor, (3) Weight Balance Sensor, and (4) Vibration Index (VI) Sensor. The VI was selected for investigation to demonstrate the proposed new research direction and extended usage. Furthermore, to distinguish

the identity of each train and its corresponding data, radio frequency identification (RFID) tags were installed in all cars of the trains. After a year of experimentation, the data and results illustrated that SRHM performance was satisfactory. The research showed that, the VI values of a train is correlated to the Out-of-Roundness (OOR) of the wheels. The SRHM system recorded that VI dropped to very low values after re-profiling of the wheels. Thereafter, the VI grows gradually and then increases more rapidly over longer timescales. This finding fits the Weibull distribution for lifetime failure analysis. The data from a year of testing was used as a reference for comparison with OOR levels, which is one of the factors measured in determining the maintenance quality of the fleet.

The findings show that VI data did help in improving maintenance efficiency. In the experiment, historical VI values for the whole fleet were fed back to the maintenance planning personnel. Any train with a higher VI was given a higher priority within the maintenance process, which includes wheel re-profiling. After three months, the overall VI values dropped gradually and continued to drop in the next three months. In fact, the maximum VI values dropped from 18.4 to 12.9 during the first three-month period and then to 9.9 by the end of the second three-month trial period. Additionally, a 3A-Warning system was proposed which related to the degree of vibration.

The results from the SRHM system also showed that 55.2% of the wheel re-profiling normally carried out was not necessary, when VI values showed that the related OOR values were within the acceptable range. In other words, to skip re-profiling these wheels can save a lot of cost and manpower, as well as extending the lifetime of the wheels.

Utilizing the historical data and statistical algorithms, useful information has been extracted and maintenance efficiency increased. The rates of vibration growth predicted by the trend of historical VI values, is used to facilitate a decision-making support system (DSS) for maintenance scheduling. A balanced regime is proposed for wheel re-profiling making use of the Weibull distribution curve, specifically the point at which the curve turns from the low growth region to the high growth region, as the trigger for re-profiling. Hence, the maximum lifetime with minimum resources balance is reached. A Fleet Health Condition Level (FHCL) chart was also derived. Monitoring the health and maintenance quality of the fleet in real-time and in-service was thereby achieved.

Although the SRHM system would improve the quality of railway maintenance, there are some limitations and challenges. Since a train is a very complex machine, vibration derives from different sources and this can vary through time. In addition, OOR is only one of the factors used to estimate the health condition of a train. For accurate estimation, further investigation and more sensors may be added.

Finally, more benefits have been gained by applying FBG sensors in railway maintenance. Safety, cost, labor time, and the lifetime of the wheel are improved significantly. Thus, this research project has demonstrated that, the power of the FBG is expanded if it is applied in collaboration with different sensors and information technologies.

Acknowledgements

I would like to express my sincere gratitude to all those people and organizations who supported this research, specially thank my chief supervisor –Professor S.L. Ho and my co-supervisor –Professor H.Y. Tam. They have displayed much patience in guiding me in the research area, language, in thinking and in other aspects. They have fostered my independence.

Thanks are also due to the *Department of Electrical Engineering* for laboratory facilities and materials support, ensuring that the project finished smoothly.

I am grateful too for the support given by the research engineers in the *Smart Railway Laboratory* and the *Photonics Research Center* in the *Department of Electrical Engineering* in The *Hong Kong Polytechnic University* for the provision of sufficient research samples, equipment and materials to generate enough data.

Special thanks are due to the proofreading reviewers Dr. Raymond W. L. Cheung and Mrs. Elaine Mary Anson, towards improving my English skills in the writing of this thesis.

Table of Contents

List of Figures

List of Tables

List of Abbreviations

3A	Alarm, Alert and Accept
3V	Volume, Velocity and Variety
5V	Volume, Velocity, Variety, Veracity and Value
AI	Artificial Intelligence
ADC	Analog-to-Digital Conversion
ASTM	American Society for Testing and Materials
BOTDA	Brillouin Optical Time Domain Analysis
BOTDR	Brillouin Optical Time Domain Reflectometry
CBM	Condition-Based Maintenance
CM	Corrective/Reactive Maintenance
CRISP-DM	Cross-Industry Standard Process for Data Mining
DIKW	Data, Information, Knowledge and Wisdom
DS	Decision-making Support
DSS	Decision-making Support System
EAC	Electronic Axle Counter
EDF	Erbium Doped Fiber
EDFA	Erbium Doped Fiber Amplifier
EM	Electromagnetic
EMI	Electromagnetic Interference
EMU	Electric-Multiple-Unit
FBG	Fiber Bragg Grating
FFT	Fast Fourier Transform
FHCL	Fleet Health Condition Level

GDSS	Group Decision Support System
GPS	Global Positioning System
ID	Identity
LPF	Low Pass Filtered
LVDT	Linear Variable Differential Transformer
MCDM	Multi-Criteria Decision-making Method
MCM	Machine Condition Monitoring
METRo	Model of the Environment and Temperature of the Roads
MMF	Multimode Fiber
MOI	Micron Optics Incorporation
MR	Modern Railways
NAS	Network-Attached Storage
NDT	Non-Destructive Testing
NN	Neural Network
ODSS	Organizational Decision Support System
OOR	Out-Of-Roundness
OTDR	Optical Time-Domain Reflectometer
PC	Polarization Controller
PDF	Probability Density Function
P-F	Potential Failure
PM	Predictive/Preventive Maintenance
RCM	Reliability-Centered Maintenance
RFI	Radio Frequency Interference
RFID	Radio Frequency Identification
RM	Reactive/Corrective Maintenance

RUL	Residual Usable Lifetime
SMF	Single-mode Fiber
SRHM	Smart Railway Health-Condition Monitoring
T&C	Testing and Commissioning
TBM	Time-Based Maintenance
UV	Ultra-Violet
VI	Vibration Index
WB	Weight Balance

Chapter 1 **Introduction**

1.1 Background

The Fiber Bragg Grating (FBG) [1] Optical fiber sensor has attracted much attention in recent years. It is a sensing element with a grating inscribed in an ordinary optical communication fiber. It does not consume electric power, but rather, is a laser and is non-metallic. It is thereby free of Electromagnetic Interference (EMI) [2] and does not emit electromagnetic (EM) waves. Although there are different categories of optical fiber sensors available nowadays, the FBG has the largest market share due to its advantages in sampling speed and spatial resolution. Owing to its novel advantages [3], [4] over traditional electronic sensors, FBG has been used on a wide range of applications such as health condition monitoring in buildings including the Canton Tower [5], Tsing Ma bridge [6], [7] and machines such as [8] aircraft and railway trains [9]. However, most of the research has developed independently, and the potential for FBG synergy with different sensors as well as information technologies, has never been exploited. This study has demonstrated this synergy, through a real-life application in railway condition monitoring [10], [11] by maximizing the lifetimes of the trains and the safety of passengers.

A railway is an essential transportation system in modern cities, and especially for inter-city, high-speed trains, an increasing number of monitoring system have been developed in many countries. Coverage and market share is increasingly important too, as a result of the reliability and safety of railways. Any accident or delay can cause economic [12], productivity [13] and even life losses. Thus, high efficiency maintenance works for a railway are necessary to maintain a high quality service.

However, the development of condition monitoring in railways has reached a bottleneck, with useful information difficult to collect because of the harsh environment such as extreme weather, track settlement and vibration in the trains. For example, EMI in the railway environment is serious because apparatus and equipment such as the overhead pantograph sustains high voltages up to 25kV, the traction system sustains a high current [14], and the equipment switching mode power sources [15] operate at high frequency. These are electronic noise pollution sources and can interfere with traditional electronic type sensors.

Currently, condition monitoring on a railway is commonly implemented with electronic type sensors such as accelerometers, to measure gearbox vibration [16], [17] for example, and the measurement is usually conducted off-line. The data collected is presented independently and statistical comparisons are lacking among the entire set of asset tests which are carried out.

In this study, vibration due to the wheel/rail interaction [18], [19] was related to the Out-Of-Roundness (OOR) [20]–[22] of train wheels as one component of the health condition of a train. The reason for selecting vibration, is because it represents an early warning symptom of failure as shown in the potential failure-functional (P-F) curve [23]–[25] in Figure 1. The operation of any machine always generates vibration with varying amplitude and frequency depending on different health conditions such as loosening between mechanical components [26]. Owing to the vibration, more symptoms, such as noise, heat and even fire are generated. Thereby, for a proper maintenance strategy, actions should be taken, in the order Zone-1 to Zone-4. Although ultrasound gives an even earlier sign [27] of failure than vibration, it was not selected because its frequency is too high for demodulation in a FBG system [28].

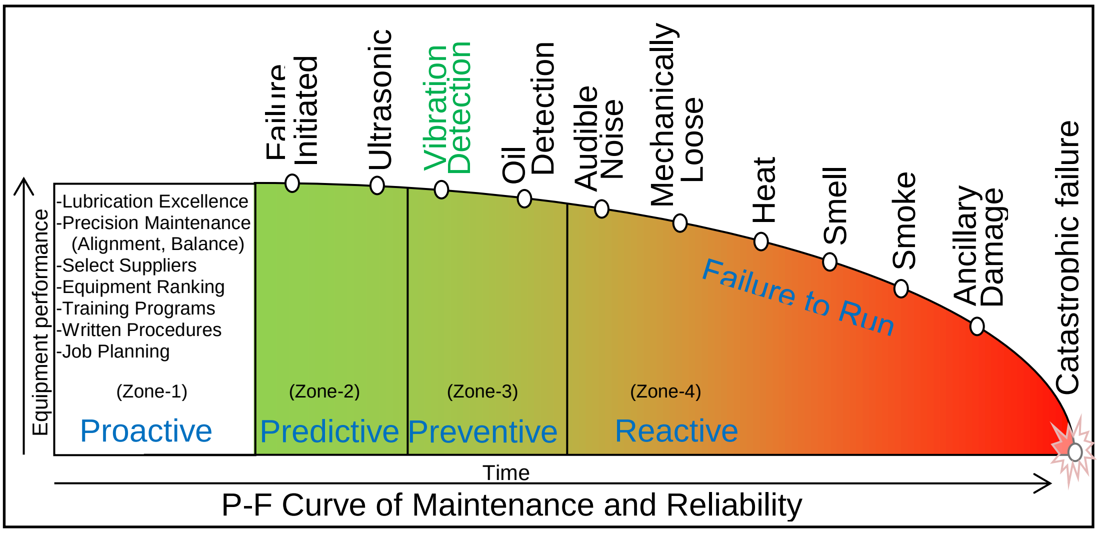

Figure 1. Potential Failure (P-F) curve. Vibration is selected as an early warning signal among the symptoms appear at different stages of lifetime and degree of failure.

Vibration in trains can be a matter of comfort and the cause of accidents too. Serious vibration could cause fatigue [29], cracks in wheels and other parts of the machine resulting in accidents. Thus, vibration is not only used for early warning of failure, but also for lifetime predictions based on historical vibration data [30].

With logged in-service with Radio Frequency Identification (RFID) [31], [32] of the health condition of all wheels in a fleet, statistical intelligent functions are possible. In the model of failure analysis, with a large population, the failure rate will follow the “bathtub” curve [33], [12] known as reliability hazard functions [34]. Of course, for a complex and repairable system such as a train, the bathtub curve is a bit more complex [35], [36] with local variations. With a long-term historical trend of the health conditions monitored and screened of all trains, decision-making support for prioritizing the maintenance schedule is facilitated. Consequently, maintenance efficiency is increased, railway safety is improved and the lifetime of the asset is lengthened.

1.2 Rationale

Railway safety and reliability is important not only in Hong Kong but in all countries including the United Kingdom. A real railway maintenance case occurred on the south coast of England as shown in the news item [37], "When old trains are better than new" – the BBC News website on 18 March, 2002. It portrayed the reliability characteristics of the life cycle of a fleet by Mr. James Abbott, the editor of a British monthly magazine, Modern Railways (MR). The item reported the dilemma facing the modern rail transport industry.

Online available: http://news.bbc.co.uk/2/hi/uk_news/1878933.stm

Similar to most metropolises in the word, the railway system in Hong Kong was the largest market share within public transportation, with 1.9 billion of total patronage per year, 48.1% of the transportation market share. The service quality is up to 99.7% and 99.9% relating to on time and delivery respectively [38]. Any delay or accident will affect massive numbers of people and economic activities seriously [12]. Thus, a highly efficient condition monitoring system is necessary to retain such high quality services.

1.3 Objectives

Currently, railway condition monitoring has reached a bottleneck because most of the existing systems utilize electronic types of sensors with which signal distortion is inevitable due to environmental disturbances like EMI. Therefore, for large-scale and long distance measurement, signal conditioning such as (1) amplification, (2) filtering and (3) signal repeating [39] may be necessary. In addition, all these functions are implemented in the form of hardware and have to be duplicated at short distances. Thus, the setup is very costly and the data integrity is very limited. Consequently, modern information technologies are difficult to apply.

At the same time, railway transportation is increasingly important because of its high usage and its market share, causing the safety and reliability to become more critical. The objective of this study is to investigate and develop a feasible FBG solution, to overcome the environmental disturbances problem so that large-scale measurement is possible and information technologies can be applied to enhance railway condition monitoring.

FBG is a sensing element locates in a single mode optical fiber. It basically measures the two physical phenomena of temperature [40] and strain [41], [42] only. All other functions are evolutions depending on the mechanical designs and algorithms. Therefore, both data collection and information technology are important for the further development of FBG sensing technology. Consequently, the application of FBG to railway condition monitoring is a win-win situation. It not only increases railway safety and reliability but also extends the limits of FBG sensing technology.

1.4 Scope of Works

To break through the railway condition monitoring bottleneck, FBG is proposed alongside modern intelligent technologies to gain the necessary synergy. Indeed, different FBG-based sensors including the (1) Track Settlement Level Sensor [43], (2) Axle Counting Sensor [44], (3) Weight Balance Sensor and (4) Vibration Index (VI) Sensor [20] for railways have been developed during this research and papers published, describing the experiments made, and the algorithms, simulations and analyses performed and verified.

To reach the goal of synergy, a Smart Railway Health-Condition Monitoring (SRHM) system has been developed to connect the above FBG sensors as a network [45], and to the wavelength interrogating equipment, computer, networking and a database in the server. A software platform and tools have also been developed to extract useful information using modern technologies such as Big Data [46], signal processing [47], and Data Mining [48], to enable the system to be compatible with different sensor algorithms. Data manipulation such as backup, long-distance transfer, and remote monitoring are also included in the system. With this system, testing and development can be carried out continuously while the railway system is in-service.

During the research, the VI sensor was selected for further analysis in the SRHM system, as a real-life case study. In a full year of trial testing, data for a fleet of trains have been logged and analyzed. The massive quantity of vibration data was then correlated to the OOR of train wheels. The historical data was then modelled employing the Weibull distribution as a failure analysis method. As a result, a 3A-Warning system for VI values was derived enabling technical staff to recognize the magnitude of the vibration amplitude for simplicity. A Decision-making support System (DSS) [49]–[51] to help prioritize the maintenance schedule was thereby proposed.

Using the historical data, similar vibration research by others, were compared with the SRHM results. The findings were used to further improve the wheel re-profiling [21] by establishing a balanced regime. Consequently, the lifetime of the wheels should be maximized while using the minimum of resources.

1.5 Thesis Organization

This thesis includes 10 chapters. After the Introduction, Objectives and Contributions in Chapter 1, Chapter 2 reviews the maintenance strategies used in the railway industry and their next generation of intelligent condition monitoring. Chapter 3 reviews the optical fiber sensing technologies.

Chapter 4 introduces the FBG-based *Track Settlement Level Sensor*. The principle, structure and testing method are elaborated. Results at different temperatures and the errors are discussed. New materials such as anti-freeze liquid, together with 80 μm optical fiber are proposed. Calculated results and actual sensitivities are also compared.

Chapter 5 describes a FBG-based *Axle Counting Sensor*. This chapter introduces the development, experimental arrangements and testing of an Axle counting sensor. It also reviews the disadvantages of the traditional Track Circuit and proposes the FBG type sensor as an alternative. The test results at three locations are at 100% accuracy with no error found. Algorithms for finding the peaks in the signal are proposed.

Chapter 6 describes a FBG-based *Weight Balance (WB) Sensor* and train *Vibration Index (VI) Sensor* measurement by FBG. The research is on the calculation of dynamic weight and the balance of the wheels on the same axle. The experiment arrangements, data acquisition and analysis approaches are also described. An experiment showcased wheel re-profiling in a car with high inter-axle vibration signal. The result shows the FBG sensor can distinguish the OOR values of different train wheels.

Chapter 7 presents the SRHM System and the VI Sensor. The system includes a modular software sub-system and the fusion of all the above sensors. VI is one of the sensor types in the system selected for case study. The sensor network arrangement, the structure of the system, the principles and advantages are described. Calculation of the VI, the VI interpretation and the related historical data are discussed. In addition, the 3A-Warning system, Accept, Alert and Alarm are derived. The methods of information extraction are introduced as a type of Data Mining technology.

Chapter 8 includes analyses using information and data extracted from the SRHM system. The historical VI values are modelled by employing Weibull reliability analysis, and facilitating a DSS in prioritizing the maintenance schedule. Referring to similar research, a balanced regime of wheel re-profiling is proposed for maximizing the lifetime of wheels with minimized efforts.

Chapter 9 discusses Future Developments. It proposes a few desirable improvements to the SRHM system. Additional sensors, more information and deeper intelligence levels are the directions for further and sustainable development.

Chapter 10, Conclusions, summarizes the development of the above FBG sensors and the SRHM system.

1.6 Publications Contributed

During the study period, the author published 6 papers; 2 conference papers and 4 journal papers.

1.6.1 Conference Papers

(1) C. C. Lai, H. Y. Au, K. M. Chung, W. H. Chung, S.Y. Liu, H. Y. Tam, Y. Q. Ni, "Optical sensor networks for structural health monitoring of Canton tower," APVC2011 The 14th Asia Pacific Vibration Conference, 2011.

(2) H. Y. Tam, H. Y. Au, K. M. Chung, W. Y. Liao, W. H. Chung, S. Y. Liu, C. C. Lai, Y. Q. Ni, "Distribution optical sensor system on the 610-m Guangzhou New TV Tower," Optical Fiber Communication Conference and Exposition (OFC/NFOEC), 2011 and the National Fiber Optic Engineers Conference, 2011, Pages: 1 – 3.

1.6.2 Journal Papers

(1) C. L. Wei, C. C. Lai, S. Y. Liu, W. H. Chung, T. K. Ho, S. L. Ho, A. McCusker, J. Kam, K. Y. Lee, "A fiber Bragg grating sensor system for train axle counting," IEEE Sensors J., vol. 10, no. 12, pp. 1905–1912, Dec. 2010.

(2) C. C. Lai, C. P. Kam, C. C. Leung, K. Y. Lee, Y. M. Tam, S. L. Ho, H. Y. Tam, S. Y. Liu "Development of a Fiber-Optic Sensing System for Train Vibration and Train Weight Measurements in Hong Kong," Hindawi Publishing Corporation, Journal of Sensors, Volume 2012.

(3) K. L. Yu, C. C. Lai, C. Q. Wu, Y. Zhao, C. Lu, H. Y. Tam, "A High-Frequency Accelerometer Based on Distributed Bragg Reflector Fiber Laser," IEEE Photonics Technology Letters, 2014, Volume: 26, Issue: 14, Pages: 1418 – 1421.

(4) C. C. Lai, H. Y. Au, S. Y. Liu, S. L. Ho, H. Y. Tam "Development of Level Sensors Based on Fiber Bragg Grating for Railway Track Differential Settlement Measurement," IEEE Sensors Journal, VOL. 16, NO. 16, August 15, 2016.

Chapter 2 **Literature Review**

2.1 Introduction

This chapter introduces the background information and technologies involved. They include the three major areas include (1) practices in the railway industry [1], (2) information technology [13] and (3) maintenance strategies [12]. The factors of vibration, the next generation of railway condition monitoring, Big Data and Decision-making support are also discussed. The background to optical fiber sensing is described in Chapter 3 separately.

2.2 Train Wheel Out-Of-Roundness

Train vibration is the key phenomenon studied in this research and relates to the Out-Of-Roundness (OOR) of a wheel. OOR is usually in the form of a spot, flat or polygon along the wheel tyre [52]. Measuring methods involve dial-gauges and lasers [53]. The FBG method used in this research is included in the issued paper [20] in Chapter 4. OOR was developed during the normal operation of a train in-service running on the track. The initiation of OOR could have multiple reasons such as friction between wheel and track, vibration at wheel/rail interactions [52], and the start and stop motions on journeys. OOR causes vibration and vibration causes OOR [54] in a vicious circle relationship. Thus, once OOR is initiated, it develops with increasing speed.

The concept of OOR and the measurement method are illustrated in Figure 2 for easy understanding. Figure 2 (a), a sketch [55] of OOR, shows the changes of the outline of a wheel before and after wheel re-profiling and the targeted re-profiling depth.

Figure 2 (b) is the arrangement [55] for OOR measurement with three Linear Variable Differential Transformer (LVDT) [56] probes contacting the wheel tyre horizontally. Each probe measures along a line of the tyre as the wheel turns slowly. The readings are recorded by computer nearby. Figure 2 (c) is a photograph [52] of an OOR on a wheel tyre on 16 mm depth. Several imperfections clearly appear on the upper side as can be seen.

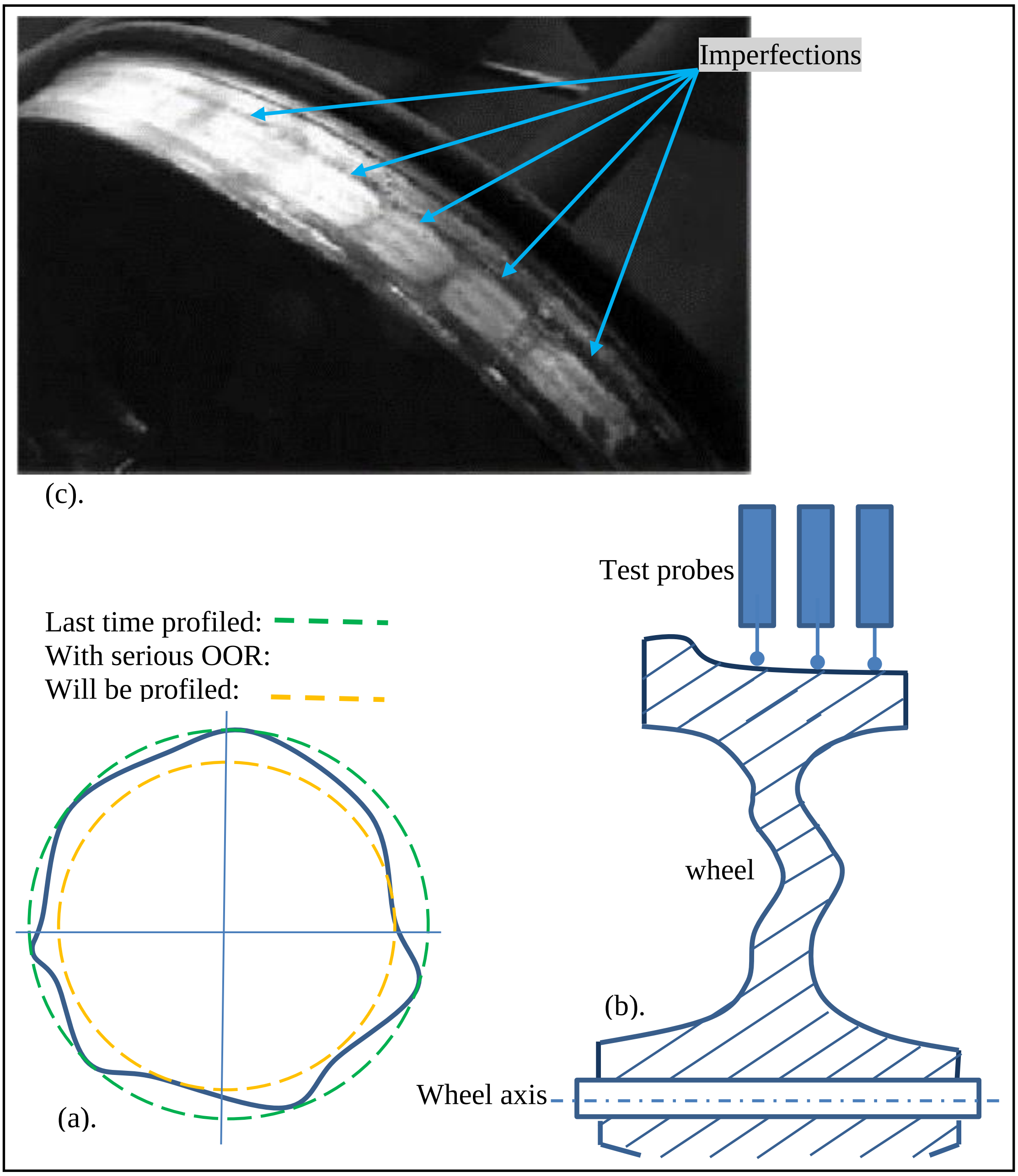

Figure 2. (a) Sketch OOR shows the change of wheel shape before and after wheel re-profiling. (b) Setup of OOR measurement. (c) Photo of OOR on wheel tyre.

Other than vibration, OOR creates acoustic noise, aggravated degradation and discomfort of the passengers, and eventually, a safety risk when vibration becomes serious. Hence, investigations based on measurement and subsequent solutions to reduce OOR, are important, as mentioned in previous publications [52], [53]. According to [53], measurement could be performed in the depot during routine preventive maintenance procedures, or when the train is running on the track during operation. The former method is basically handled manually with dial-gauges, while the latter is automatic with measurements taken every time the train passes through a testing point. Thus, OOR information is updated daily. For this reason, different automatic methods have been developed for measuring OOR [53].

Currently, the solution adopted to reduce OOR is wheel re-profiling [52]. This aims to remove the surface layer imperfections on the wheel tyre using a lathe in the depot. The surface is then very smooth. Unfortunately, once running on the track, OOR is initiated straight away, and the vicious circle restarts. Besides, the stiffness of the tyre material is a variable factor affecting the development of OOR, as revealed in the literature [54], but this variable is outside the scope of this study. The repeated cycle of OOR development and wheel re-profiling reduces wheel life. This is a common problem that railway enterprises always face.

In the Netherlands, the Dutch Railways and Lloyd’s Register Rail Europe have the same difficulty. A solution on wheel re-profiling to lengthen lifetimes has been investigated [54]. In the paper, two regimes were compared, (a) profiling the wheels when OOR becomes serious enough, regardless of mileage; (b) profiling at regular short mileage intervals (70,000 km) where the OOR is still less serious. After years of tests, their findings show that regime (a) results in significantly shortened lifetimes. Regime (b) lengthened lifetimes by 48%, with a 45% decrease in reactive maintenance.

Regime (b) is known as “Scraping”, meaning to profile the wheel in a very thin layer of approximately 1 mm. However, the thickness of material removed from the wheel tyre each time is 6-7 mm in regime (a). Actually, the development rate of OOR in the early stages is close to linear, but the rate increases quickly in later stages. In other words, OOR develops non-linearly over time, and at an increasing rate. This explains why lifetimes shorten when wheel re-profiling only taken place when OOR has become serious.

2.3 The Maintenance Strategy in Railway Industry

The purpose of maintenance is to ensure the machine runs in the normal condition. Maintenance can be broadly classified into the *two strategies* of Predictive/Preventive Maintenance (PM) and Reactive/Corrective Maintenance (CM) [27], [57], [58] as shown in Figure 3. PM is conducted according to either a Time-Based Maintenance (TBM) schedule or following information from a Condition-Based Maintenance (CBM) system before the onset of failure. CM is also known as Reactive Maintenance (RM). It is called Run-to-Failure.

In CM, repair or replacement occurs on breakdowns. Because of the breakdown condition, CM action is usually taken very urgently. This is why related cost in CM is usually higher than for PM. Moreover, maintenance costs are mainly of three types, (1) due to damage and hazard directly caused, (2) repairing and replacing costs, (3) loss of production cost.

PM is designed to reduce these costs. The sub-category, TBM is performed at fixed intervals or is otherwise scheduled. CBM is executed according to inspection results. Performing maintenance work on a fixed time interval by CBM is difficult, as CM takes the higher priority, and any planned schedule is easily overtaken by the unplanned CM tasks. A CBM system, however, does allow flexibility in scheduling suitable times, due to the early warning of failure, enabling maintenance work to be finished at a convenient time. This reduces costs and smooths the demand for labor.

The Proactive Maintenance of Figure 3, is prepared for during the design stage. For example, embedding sensors during fabrication for symptom detection. Although this is not a formal type of maintenance strategy, such Proactive Maintenance is very useful in terms of early warning.

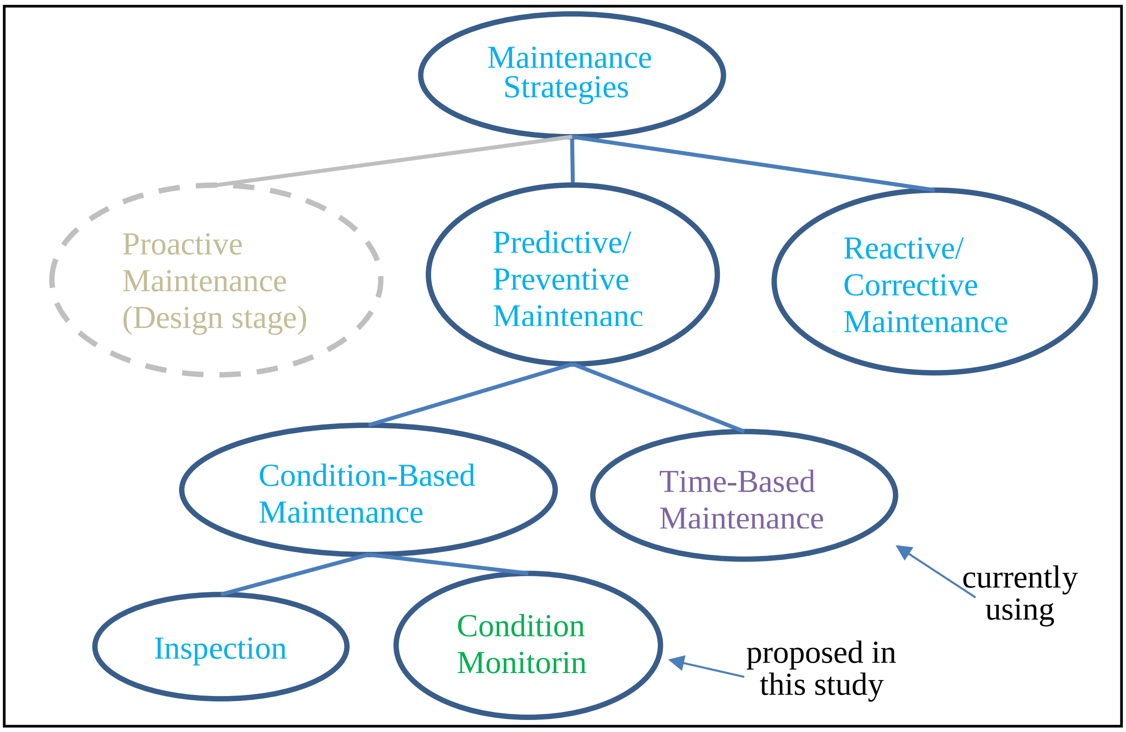

Figure 3. Types of maintenance strategies. Condition Monitoring Maintenance is a kind of predictive method and is recommended more by industry.

Currently, TBM is the commonly adopted maintenance strategy in the railway industry [8]. This strategy allocates resources evenly to all assets whether they need maintenance or not. Trains with more problems, therefore, may not be discovered and repaired in time. In other words, some of the maintenance cost is "wasted". To understand more about maintenance, a comparison between the strategies [59] is given in Table 1.

Table 1. Comparison of maintenance strategies. Most commonly used in the railway industry is Preventive Maintenance.

	Strategies	Method	Advantage	Drawback
1	Reactive/Corrective maintenance (Run-to-Failure)	Fix it after breakdown (corrective)	Less initial cost	Service stopped, serious accident occurred
2	Scheduled Time-Based Maintenance	Regularly inspection. Repair if about to fail. (correct & preventive)	Balance of cost and failure	Fair initial cost and large labor
3	Scheduled Predictive/ Preventive Maintenance	Perform Lubrication, Repair, overhaul or Replace regularly (preventive)	Balance of cost and failure, less failure rate	High initial cost and large labor
4	Proactive Maintenance Design Change	Re-design it so as to have a longer lifetime (preventive)	Less cost and less failure rate, early warning	Expensive and long time
5	Condition Monitoring based Maintenance	Use sensors, equipment and processing algorithm (preventive)	Just-in-time, prevent accident, less downtime, maintenance on demand, high effective	Fair initial cost and less labor

2.3.1 Machinery Condition Monitoring

The machinery condition monitoring procedure [60] measures the physical condition of a machine, such as in the aerospace [61] and railway industries and then provides appropriate maintenance advice. It is an independent industry with international standards, including ISO13373 [62] and ISO13381 [63]. ISO 13381-1:2015 provides guidance for the development and application of prognosis processes. ISO 13373-1 provides General Guidelines for data processing, communication and presentation. A plumbing system case [64] which followed the failure prognostics procedure in ISO13381 is an example. The standards also apply to the railway industry as guidance.

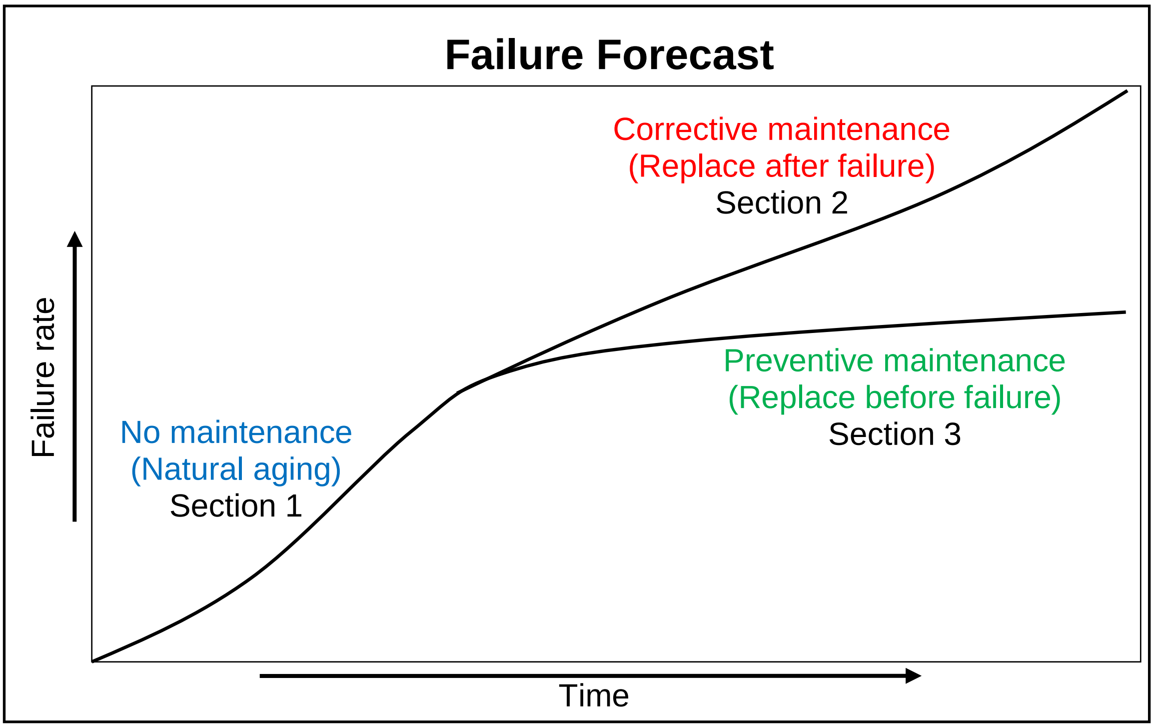

Figure 4. Failure Forecast chart demonstrated that a good maintenance strategy can significantly lower down the failure rate.

According to the previous study, by applying an appropriate maintenance strategy in the earlier lifetime stages, the failure rate can be lowered as shown in Figure 4 Failure Forecast chart [65]. Initially, the failure rate increases sharply, Section 1 of the curve, because of natural aging with no maintenance strategy applied. In Section 2, the failure rate slows down slightly on applying the Corrective Maintenance strategy. In Section 3, the curve slows down significantly on applying a Preventive Maintenance strategy such as Condition Monitoring Maintenance [66]. Consequently, by running the correct maintenance strategy, the lifetime of the production item can be maximized.

2.3.2 Condition Monitoring Market in Machinery and Railway

The market for Machine Condition Monitoring (MCM) is a fast growing industry especially in the global equipment market. Market size will expand from USD 1.5 B in 2015 to 2.45 B in 2020 as revealed in [67]. Thus, an increasing number of international enterprises will participate in the industry. Most of the main players in the MCM equipment market are famous world equipment suppliers such as B&K Sound & Vibration SKF (Sweden), and FLIR(U.S.) [67]. Some of them already have total solutions in specific markets. For example, SKF is an expert in railway condition monitoring [68]. Some are targeting the railway sector [69]–[71].

<u>Railway Condition Monitoring (RCM) Market Sector</u>

Governments, such as the European Union (UN) invest in the railway condition monitoring market. The project sum is usually huge such as the "*Wireless Railway Condition Monitoring project in European Union"* of up to €100s of millions, and *"I-RAIL"* in Europe up to €1,474,500 budget [71]. In addition, China is the largest participant [72] [73] so far. Three typical commercially available examples [69], [70], [71] are listed in Table 2.

Table 2. List of commercially available railway condition monitoring system

Company	Model	Country	Function
Strukton Rail	POSS®	Dutch	Preventive Maintenance and Fault Diagnosis System for point machine
Knorr-Bremse	Comoran®	Germany	Bogie monitoring and diagnostics
D2S & Heverlee (BE)	I-RAIL	European rail network	An Intelligent On-line High-Speed Rail Condition Monitoring System Deployed via Passenger and Freight Trains

2.4 Factors of Vibrations in a Railway

Vibration is one of the focuses of this study. One of the main sources of vibration is the OOR [52] of wheels. Vibration is influenced by different components including the suspension system, the wheels and tracks etc. [74] as shown in Table 3. Vibration is not only a problem affecting the safety as it is also a kind of pollution. Noise and vibration pollution in urban areas are restricted by laws in some countries [75], [76].

Table 3. Factors of vibration induced by trains.

Factors	Influence
Vehicle suspension	Higher vibration for high stiffness in the vertical direction.
Wheels condition	Wheel roughness and flat spots are the major cause of vibration.
Track surface	Rough track is the cause of vibration.
Track support system	Track support system is the major components of ground-borne vibration. The vibration levels are higher for tracks on rigid concrete floor.
Speed	Higher speeds result in higher vibration levels (as intuitively expected)
Track structure	The heavier the track structure, the lower the vibration levels.
Depth of vibration source	Vibration characteristic is significantly different between underground and at the ground surface.

The Frequency of occurrence and amplitude are two of the criteria used to evaluate the significance of vibration. For vibration amplitude, the causes derive from different factors and the most significant amplitude ones are summarized in Table 3. For the frequency of occurrence, no conclusive explanation has been found. The reason may be that most railway systems include all the relevant factors and their responses are dependent on different conditions as indicated in the literature [77].

2.5 Next Generation of Railway Condition Monitoring Systems

Keeping information up-to-date, is to know more about new developments and even points towards the future research needed on the next generation of railway condition monitoring. According to one study [78], future research will be mainly based on intelligent and large-scale systems. The most common functions and features will include fully automated, intelligent, wireless, multi-technologies, network based, track records of historical data, as well as cross systems. The systems will be employed on high-speed railways, driverless trains and cross-country railways. The new technologies involved in the next generation of railway condition monitoring systems [73], [79] include:

1. Wireless sensor networks [80], [81],
2. Artificial intelligence [82],
3. Internet/data sharing/Big Data/information system [83], [84],
4. Ontology-driven data integration [85], [86],
5. Event driven monitoring [87].

2.6 Big Data

Big Data [88] in information science is essential for use in intelligent applications. In this study, Big Data was employed in a real case study [89]. The definition of Big Data usually relates to either the 3Vs or 5Vs versions. Some information scientists defined Big Data in information systems as possessing the three characteristics:

Volume, Velocity and Variety known as 3Vs at the early development stage of Big Data. Some experts later added: Veracity and Value whence it becomes 5Vs [50], [90]. Their detailed descriptions and the links to the information in our SRHM are listed as follows:

(1) **Volume:** This is the quantity of data. The data volume should be huge enough to enable a change of phenomenon to be observed and monitored. In this study, the data amount is vast because the sensors log to Network-Attached Storage (NAS) with a sampling rate of 2000 Hz continuously for 24 hours a day and 7 days a week. The data volume is at the level of Giga bytes/day, huge enough for the application of Big Data technology.

(2) **Variety:** This relates to the types of data sources. The sources of data in this study include FBG, RFID, accurate time stamp and information about the train such as speed, number of cars and train direction etc. Four pairs of FBG sensors are for cross-checking the left and right hand rails. A RFID reader verifies the identities of trains and cars. This study attempted to utilize all these data sources in extracting the most useful information using Data Mining and Big Data technologies. Therefore, the variety of data sources at this moment is enough for this application.

(3) **Velocity:** This is the speed of data collection. The sampling rate during data acquisition should be high enough to capture any change of phenomenon. In this study, the sampling rate of FBG sensors was 2000 Hz, as above. The RFID data was collected in real-time and the processing was also in real-time. This is fast enough to facilitate the Big Data application. In addition, the total

volume of data is increasing, as historical data and results were also used in the algorithms in this study. In addition, the number of sensor is also increasing.

(4) **Veracity:** This represents the integrity, or quality, of data. The integrity of data is measured in terms of useful data and unwanted noise. That is, how accurate are the transducers employed in sensing the signal of the phenomenon. This involves different types of variation such as the locations where transducers are installed, interference by environmental disturbances and the sensitivities of the transducers etc. In this study, the manual entry of data was seldom used. Most data derived from sensors and were collected automatically. Consequently, the error rate should be very low.

(5) **Value:** This is the usefulness of the information extracted as it benefits society. The useful information extracted in this study included the Vibration Index (VI), Weight Balance (WB), track settlement level and axle counting. By applying historical VI values, the benefit is to facilitate management decision-making support [91]. Therefore, the SHRM system of this study fits the "value" requirement in Big Data.

With a specific algorithm, Big Data can be used to infer valuable output for the benefit of society. When high quality Big Data is available, a smart algorithm becomes more important in achieving high quality processing. Thus, in an artificial intelligence age, the human role in designing algorithms becomes more important. So, the purpose of designing the SHRM system is to benefit humans in a more intelligent way.

2.7 Decision-Making Support System

Decision-making [92], [93] is to strike a balance between the pros and cons among a list of factors to be considered in making a final decision. A Decision-Tree [94] is an example. The factors consist of items of meaningful information. Based on this theory, a Decision-making Support System (DSS) [8], [51] was developed as an information technology tool, as a series of standardized procedures to be followed. The output provides useful information for decision makers. Furthermore, a larger scale version, a Group Decision Support System (GDSS) is already used by a group of organizations. The accuracy of the final decision relies on information integrity and timing. Cases of DSS in railway [95] and other transportation systems [96] are available such as the Model of the Environment and Temperature of the Roads (METRo), which is used in Canada for forecasting the availability of a section of road in relation to the materials, machines and labor needed to complete road maintenance works [97], [98]. On the other hand, a DSS might not recommend a final decision but provide information useful to a strategy framework only [99]. Some researchers have inferred DSS benefits as follows [51], [92]:

(1) Time saving,

(2) Enhance effectiveness,

(3) Improve interpersonal communication,

(4) Cost reduction,

(5) Increase decision maker satisfaction,

(6) Increase organization control.

2.8 Chapter Summary

One of the causes of vibration is the OOR of a train wheel. Thus, vibration can be used to measure OOR, which begins to occur as soon as its use on the track re-commences. OOR development occurs linearly with time at first, then grows at an increasing rate. Thus, to maintain OOR at less than serious level, is one way of maximizing wheel lifetimes. Condition monitoring is a more recommended PM strategy than CM strategy because it provides an early warning and is highly efficient. PM is also more flexible for maintenance scheduling processes as the information is available in the computer at any time. Condition monitoring is very much practiced, and guided, through international standards, and is growing at a fast pace. Some condition monitoring practitioners are international companies and even governments. The factors causing vibration are various. The more significant are listed, but their frequency of occurrence is undefined as they differ for different cases. The next generation of railway condition monitoring will be based on large-scale data sets, multiple technologies and artificial intelligence technologies. The Big Data 3V and 5V systems are defined and mapped to the real-case data of this research. Finally, DSSs and their applications in railway and other transportation systems are introduced.

Chapter 3 **Optical Fiber Sensors**

3.1 Introduction

The optical fiber sensor, measuring physical phenomena such as strain and temperature, is the core technology used in this study. The Fiber Bragg Grating (FBG), among various types of optical sensor, was adopted in this study due to its high spatial resolution and sampling rate. This chapter explains optical fiber sensors in detail.

3.2 Fiber Bragg Grating

FBG technology, invented by Kenneth Hill in 1978 [1], [41], creates a grating in a section of fiber. The typical sensing element length is approximately 10 mm. Since no additional materials are fixed to the fiber during the grating inscribing process, the fiber remains the same size and the grating cannot be identified by the naked eye. The working principle, strengths and drawbacks, and fabrication details [100] of FBG are explained below.

3.2.1 Working Principle of Fiber Bragg Grating

Figure 5 illustrates the working principle of the FBG. All sensors [5], [20], [43], [44], [101], [102] introduced in this study are based on FBG sensing technology. The structure of a FBG is a periodic modification of the refractive index in the core of a single-mode optical fiber. It is usually fabricated by the phase mask technique where a short section of optical fiber is illuminated by a 248nm Ultra-Violet (UV) laser source under a phase mask [103]. FBG reflects optical signals with a wavelength of $\lambda_B = 2n\Lambda$ (green in Figure 5), which is the well-known Bragg condition [1], where λ_B is the Bragg wavelength, n is the refractive index of the core material, and Λ is the pitch of the grating. The unit of a FBG readout is in nm which is also the unit of wavelength. The maximum strain tolerated is up to 10000 μ strain. The maximum operating temperature is up to hundreds of degree Celsius. The FBG Bragg wavelength changes width thermal and mechanical (strain) perturbations altering the refractive index and the pitch of the FBG. As such, if the user only requires strain changes in the application, thermal compensation is necessary to cancel the temperature effect. For measuring temperature, however, strain must be kept steady. In general, the sensitivities of the above two critical factors must be made clear in all FBG applications. The strain sensitivity of a FBG is approximately 1.2 pm/με while the thermal sensitivity is around 10 pm/K [6], [104].

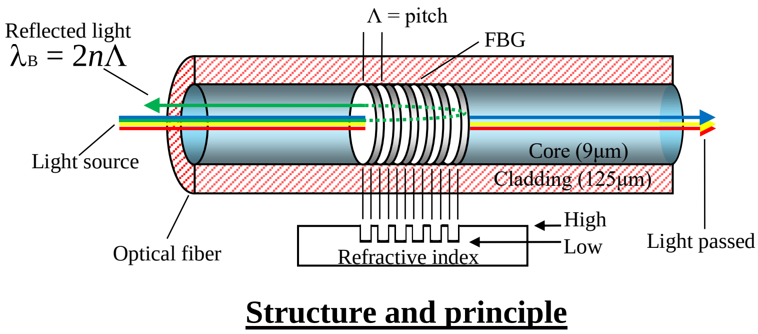

Figure 5. The structure of a FBG. Grating experiences periodic change in refractive index in the core. Light with wavelength (green) the same as the pitch of the grating will be reflected back to the source, while others pass through.

3.2.2 Fabrication of Fiber Bragg Grating

Before inscribing a FBG in a fiber, preparation work is required to increase the photosensitivity of silica in the fiber, permitting grating inscription of higher reflectivity. The preparation starts by loading the fiber in a chamber filled with Hydrogen (H_2) under 100 atmospheres of pressure for two weeks at room temperature. Afterwards, the fiber is kept at low temperature to retain the Hydrogen for later use.

The fabrication of a FBG is to create a grating in the core of an optical fiber. The process is to shine an UV [100] laser beam on a fiber, when a fringes pattern will be created due to the configuration of Convex Lens, Concave Lens, Phase Mask and UV beam. The energy of the UV beam requires adjustment to be high enough to create a permanent fringe pattern on the material of both the core and cladding of the fiber. This pattern is the so-called ‘grating’. The depth of the pattern can be adjusted by tuning the power of the UV laser beam. The wavelength of the grating can be adjusted by employing Phase Masks [1] different pitches.

The apparatus is commercially available nowadays. The fiber used is a standard telecommunications single-mode fiber (Corning-SMF28) [105]. The wavelength demodulation device (interrogator), FBG sensor, and programming and processing software are available from international suppliers [106], [107].

3.2.3 FBG in Single Mode and Multimode Fiber

Even though existing studies were mainly focused on FBG in single-mode fiber (SMF), FBG can also be inscribed in multimode fiber (MMF) that possesses some advantages [108], [109]. However, the FBG in MMF is less popular because it gives multiple peaks in the reflection spectrum as a result of the multiple propagation modes of MMF, this makes demodulation and processing of the reflected signal more difficult and complicated [110]. In addition, the effective bandwidth of FBG in MMF is wider than those with SMF. Thus, fewer gratings can be multiplexed in a fiber with a same measurement wavelength range.

In recent years, more studies on FBG in MMF have been conducted. Better measurement results have been demonstrated by using the FBG written in graded-index MMF [111], than those in step-index [108]. The availability of low cost and high power light sources and photonics components nowadays also permits both sensing and power transfer functions to be incorporated in large core MMF that has an embedded FBG [109].

3.3 Advantages and Disadvantages of FBG

The FBG was adopted for this study due to its major advantage of being free from EMI and emission interference effects. Table 4 and Table 5 illustrate the advantages and disadvantages of the FBG [1], [4], [40], [105] in comparison with electronic transducers.

Table 4. Advantages of FBG in comparison with electronic transducers

	Factor:	**Description:**
1	Multiplexing	FBGs with different wavelengths can be connected serially in the same fiber
2	High corrosion resistant	The material of optical fiber is affected by corrosive chemical materials such as acids
3	Long transmission distance	Distance from FBG to the demodulation device could be as long as several kilometers without the need of signal conditioning devices such as filter/amplifiers.
4	EMI/RFI immunity	Good EMI/ Radio Frequency Interference (RFI) immunity. Since no electric conductor in the fiber or no electric current flows through
5	Electric isolation	The fiber material is electrically isolated as the material is an electrical insulator and no current flows through the fiber
6	High temperature and pressure resistant	FBG is sensitive to temperature buy the melting point of the fiber material is very high. The fiber is insensitive to pressure.
7	Long-term stability	The durability of the fiber material is over 20 years
8	Size	The diameter of a fiber is extremely small (125μm)

Table 5. Disadvantages of FBG compare to electronic transducers

	Factor:	**Description:**
1	Brittle	Easy to break the bare fiber
2	Difficult to re-connect	Special equipment such as cleaver and splicer
3	Equipment is still expensive	Wavelength interrogation equipment is much more expensive than for electric sensors
4	Sampling rate is relatively low	Sampling rate of data acquisition/demodulation equipment is relatively low, in kHz, while for electronic types is in the order of 100 MHz
5	Relatively expensive when number of sensor is less	Cost effectiveness is low when the number of FBG is small because the equipment dominates the total cost

3.4 Optical Source and Optical Detection System for FBG Sensing

The FBG interrogator used in this study is purchased from Micron Optics [28]. A simplified schematic diagram of the optical source and wavelength detection system of this interrogator for FBG sensing is shown in Figure 6. The upper left corner of Figure 6 presents the wavelength scanning laser source which also called swept laser source [112]. The output of this optical source is split by a coupler and then fed into four measurement channels via circulators. The light reflected from the FBGs is passed to a photodetector via the circulator for converting into electronic signal. The timing information from wavelength scanning, and the reflected signal are synchronized by the timing circuitry so as to re-construct the wavelength of the reflected FBG.

The wavelength scanning laser source is tunable within an 80 nm range from 1510 nm to 1590 nm as shown in Figure 6 (a). The output wavelength is controlled by a voltage signal applied to the internal filter inside the laser cavity. The wavelength is scanned by using a voltage source generating a triangle wave. However, the drawback is that the wavelength positions in the rising and falling edge of the triangle wave are mirrored. As a result, corresponding arrangement is needed for re-constructing the correct order of wavelength.

The output power of this laser source is relatively constant over the entire wavelength scanning range as shown in Figure 6 (b). The benefit of using wavelength scanning laser is that it emits much higher power than in a broadband source. Thus, the power is high enough and can be split into four channels for wavelength division multiplexing (WDM) of more FBGs [112] in a single system.

The spectral response of the signal reflected by the connected FBGs is captured by the photodetector once every cycle, any peaks in this signal represents one FBG is being connected, the wavelength of the FBG can be computed by using both the timing information of the applied triangular wave and the voltage–wavelength response of the scanning laser. The reflected wavelengths from FBGs in a channel is shown in Figure 6 (c). Only the wavelengths identical with the Bragg wavelengths of the FBGs are reflected while the rest are being transmitted to the fiber end.

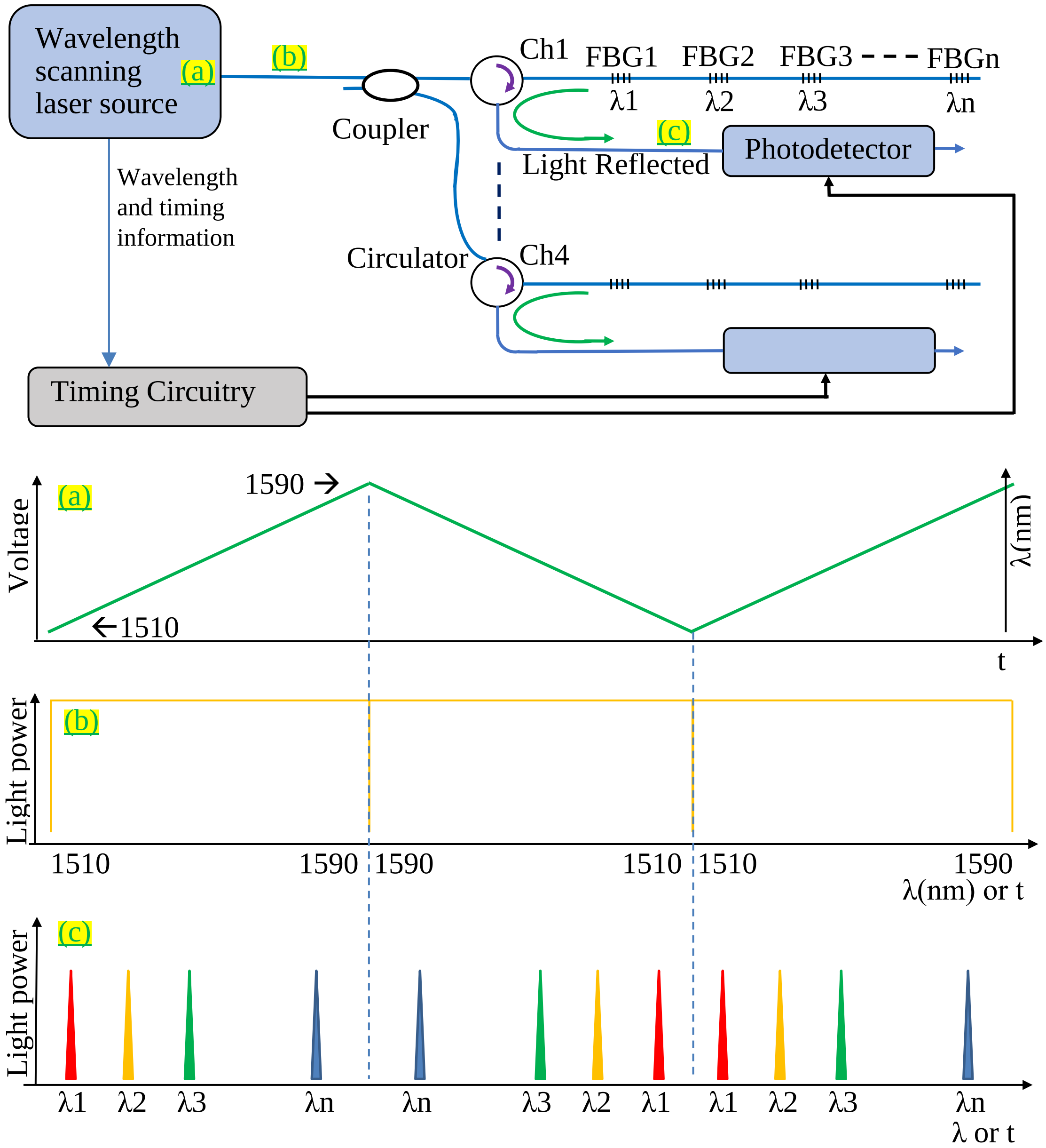

Figure 6. The light source and optical detection system for FBG sensing. (a) the output wavelength of a wavelength scanning laser source with a triangle wave controlled voltage input. (b) the output power of the scanning laser source. (c) the spectral response of the reflected signal from all the FBGs connecting one measurement channel.

3.5 Distributed Sensing Technique

Other than the FBG, the distributed sensing technique [113], [114] is also popular in structural health monitoring industry, it is particular useful for measurements of mega scale objects and with slow response time situations, such as measuring of deformations and temperatures of dams, bridges and high-rise buildings. In distributed sensing, the sensor consists of the whole fiber, and therefore, unlike the FBG, this technique does not require any preprocessing of the fiber itself, such as an Ultraviolet (UV) light inscription to turn the fiber into a sensor. The sensing ability is distributed and continuous along the entire fiber length. The measurement length of a fiber can be up to as much as 100 kilometers. The spatial resolution depends on the pulse width of the laser source injected into the fiber. The shorter pulse width injected, the finer resolution can be achieved. Since the power scattered back to the input end for measurement is usually extremely low even with very high amplitude laser pulse is injected, multiple times of measurement are carried out to improve the measurement accuracy.

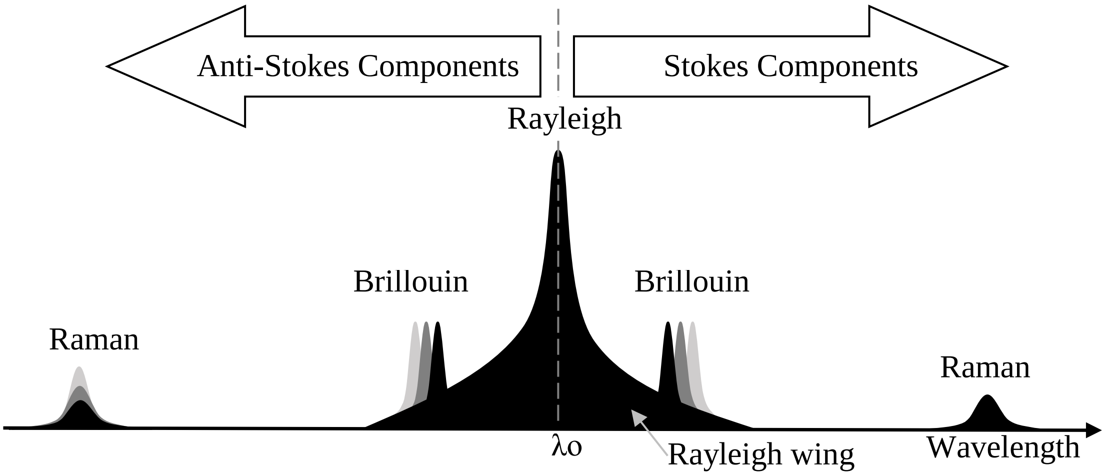

Figure 7. The spectrum of backscattering in an optical fiber due to injecting a short laser pulse. Three scattering phenomena namely Rayleigh, Brillouin and Raman are produced because of the temperature, strain and impurity of the material in the fiber. For Stokes components, the wavelength shift is shorter than the injected pulse, while for anti-Stokes components, the wavelength shift is longer than the injected wave.

For distributed fiber sensing or measurement, a very short laser pulse is injected at one end of the fiber, and the returned light which is the "echo" along the entire length is received and analyzed. The operation is similar to that of the Optical Time-Domain Reflectometer (OTDR), which is used for testing the continuity of optical fiber in the communications industry. The major difference is that the OTDR only focuses on amplitude versus time but is not sensitive to wavelength. The working principles of the distributed sensing technique are based on related scattering. The following section explains the principles and their advantages and limitations.

<u>Rayleigh sensing</u>

The strongest amplitude is Rayleigh scattering, as shown in the middle of Figure 7. Rayleigh scattering occurs due to the variation of material densities and the impure composition of materials in the fiber. The wavelength in Rayleigh scattering is identical to that of the injected laser pulse, but it has Rayleigh wings including lower and higher wavelengths shifting with much lower amplitudes. Having the highest amplitude of scattering, the Rayleigh component determines the main slope of the decaying intensity curve in the received “echo”. Therefore, Rayleigh is often used to locate discontinuities and inhomogeneous properties along the fiber in OTDR testing. The variation of strain or temperature causes spectral shifts in the local Rayleigh backscatter pattern can be measured by swept wavelength interferometry (SWI) [115], which detects the local wavelength deviation in frequency/wavelength domain by dividing the fiber length into small windows. These spectral shifts can be calibrated to indicate the temperature or strain distributed along the fiber.

Brillouin sensing

Based on Brillouin scattering, two types of sensing method have been developed. They are spontaneous Brillouin Optical Time Domain Reflectometry (BOTDR) and stimulated Brillouin Optical Time Domain Analysis (BOTDA) [116].

In BOTDR, a short laser pulse is first injected into the fiber. Then the returned Doppler shift of the diffracted light, which is caused by acoustic waves generated by atom vibrations in the material of the fiber is measured. These atomic vibrations are influenced by material density and are related to strain and temperature. The bulk vibrations travel at about 6 km/sec. The travelling wave changes the local glass densities and indexes of refraction when moving in the fiber, which acts like a moving Bragg grating [117]. The method of extracting the wavelength shift is to suppress the unwanted peaks, such as Rayleigh and Raman by a filter, then to locate the Brillouin peaks. Since the demodulation method is inherited from traditional OTDR, the result has similar characteristics such as low spatial resolution and long interrogation distance.

In BOTDA, the working principle is to inject a short laser pulse (known as a pump wave) and a continuous wave (known as a probe wave) from the opposite direction into the fiber, and then to measure their frequency difference (known as the beat frequency). In the fiber, once the beat frequency has the same wavelength as the Brillouin frequency shift in the optical fiber, a strong interaction between the two beams occurs, enhancing the occurrence of acoustic waves (phonons) generation. This phenomenon of strong interaction is also known as stimulated Brillouin scattering.

Raman sensing

When a light source is injected into a fiber, most of the photons become scattered by Rayleigh backscattering. The small ratio of photons that interchange their energy with the material of the fiber will then generate new photons in this interaction. The wavelengths of the newly generated photons will be determined by the absorption and desorption of the quantum energy in the atomic bonds of the silica material in the fiber. Consequently, some newly generated photons exhibit higher wavelengths (Stokes Components) while the others exhibit lower wavelengths (Anti-Stokes Components). This wavelength shifted component is known as Raman Scattering.

When a section of the material is heated up, the heat in the material, the anti-Stokes component has a higher amplitude than the Stokes component. The ratio between the amplitudes of the peaks (anti-Stokes and Stokes component) provides an indication of the material temperature according to the arrival time of the reflected signal.

Therefore, Raman scattering is not affected by material strain. This working principle is adopted in commercially available instruments for temperature measurement along optical fiber.

A common application of Raman sensing is for water leakage detection in the dams of lakes or long water pipes, using the rationale that water carries away heat when leakage occurs. The spatial resolution depends on the width of the laser pulse injected in the fiber. By measuring the time locations of the two Raman scattering peaks, the physical location of the material where temperature changes exist can be determined. Since the spatial resolution is greater than 1m, the measuring range is up to 50 km in length and the temperature resolution is up to 0.1°C.

Table 6. Comparison of various optical fiber sensing techniques

	FBG	BOTDR	BOTDA	Rayleigh	Raman
Spatial Resolution	Depends on grating length 2 to 10 mm	Depends on pulse width 10 cm	Depends on pulse width 10 cm	Depends on pulse width 1-2 cm [118]	Depends on pulse width 1 m
Length Range	50 km	100 km	100 km	100 km [119]	50 km
Acquisition Time	5 kHz	20 minute	5 minute	10 Second	10 Second
Strain Accuracy	±1 μ ε	±30 μ ε	±10 μ ε	±1 μ ε	N.A.
Temperature Accuracy	±0.1°C	±0.2°C [120]	±1-2°C	±0.1°C	±0.1°C
System Complexity	Less complex Wavelength scan for multiplexing	Complex Pulsed laser sources	More complex Pulsed and CW laser sources	Complex Pulsed laser source	Less Complex Pulsed laser source
Meaningful phenomenon	Wavelength	Doppler shift wavelength	Beat Wavelength	Rayleigh spectral shifts	Ratio of Anti-Stokes and Stokes
Temperature and strain dependent	Yes	No	Yes	Yes	No
Supplier	MicronOptics, Fibersensing, Insensys	Yokogawa, NTT, Sensornet	OZ Optics, Omnisens, Neubrex	LUNA	Omnisens

Table 6 [113], [114] compares the various optical fiber sensing techniques. Two major types of sensing technique, namely single point and distributed sensing, are compared.

The FBG measures both strain and temperature simultaneously, while Raman can measure temperature only and is not distorted by strain. The single point sensing technique has a higher spatial resolution and sampling rate than distributed sensing. Since the sensing element in distributed sensing is the entire fiber, this technique is often applied in measurement relating to large-size objects, where the update rate is comparatively slow due to the long acquisition time. In other words, applications that require faster sampling rates such as vibrations in railway engineering should employ FBG. This is also the reason for choosing FBG as a sensing element in this study.

3.6 Chapter Summary

This chapter is an overview of optical fiber sensing technology. It presents the working principles, properties and applications of FBG and distributed sensors such as Rayleigh, Brillouin and Raman. A comparison between FBG and distributed sensors, justifies the use of FBG in this research. This chapter also introduces fabrication procedures, preparation work and equipment. Graphs and descriptions are provided to explain the optical source and demodulation method for FBG. The advantages and disadvantages of FBG are compared in tabular form. A drawback of FBG is its simultaneous sensitivity to both mechanical strain and temperature. Thus, thermal compensation is required when measuring strain only. Finally, this chapter highlights the characteristics of FBG such as the fact that its maximum strain can be up to 10000 μ strain, its operational temperature can be up to hundreds of degrees Celsius. In addition, its strain and thermal sensitivities are approximately 1.2 pm/με and 10 pm/K respectively.

Chapter 4 **Track Settlement Level Sensor**

4.1 Introduction

In recent years, there has been a rapid boom in railway system development and construction worldwide. Since railway systems usually cover long distances and large areas in varying geographical conditions, track settlement is inevitable to some extent. Track settlement occurs when the ballast and subgrade undergoes non-elastic deformation. Some deformation occurs as a continuous basis, for example, it can be caused by environmental disturbances such as flooding, seismic actions and extreme temperatures, or it occurs every time that a train passes through. In addition, some part of deformation cannot be restored to its original state. The severity of settlement depends on the stiffness of the tracks, as well as the geotechnical performance of the ground under loading [121]. If settlements differ between the left and right hand rails, this is regarded as differential settlement [122].

When serious geotechnical deficiencies occur, differential settlements can be obvious, leading to dynamic reaction in the train-track system, rapid track degradation, low passenger comfort, as well as a high risk of derailment risk [123]. Consequently, settlement condition monitoring is vital for safety and operational efficiency. The measurement of settlement can be difficult because it often occurs in such cases as extreme ambient temperature, inaccessible geographical location, limited electrical power, and there may be excessively long distances between measurement points.

Various methods exist for measuring settlement. For example, traditional soil strain gauges can be located within the ground under test, such that settlement is measured according to the vertical and horizontal strains in the ballast layer [121]. Exploiting Global Positioning System (GPS) devices [124] is also a common approach to measure horizontal and vertical displacements of the ground. However, these methods are not adequate for the requirements of modern technology. Apart from the above, electronic-based [125] settlement sensors are also commonly used whose working principle is to measure the resonant frequency of built-in vibrating wires [126]. These, however, might suffer from serious electromagnet interference (EMI), as they are often used in civil and structural engineering applications and are thus less suitable for railway tracks. The performance of electronic-based sensors can also be severely interfered with by electromagnetic (EM) waves generated by high voltage overhead electrical power lines.

To overcome the above limitations, FBG, an optical fiber sensing element, was used as a settlement level sensor in this study. With reference to the previous studies [127], the FBG provides higher sensitivity and is more suitable for application in a hostile environment. The advantages of FBG include immunity to EMI, resistance to corrosion, is suitable for a wide range of operating temperatures [2], [128], superior multiplexing capabilities, works over long distances, making it a satisfactory sensing element for application in extreme environments. FBG sensors are typically used in condition monitoring of the structure of bridges, railways and buildings [5], [20], [105], [129]. The proposed level sensor is designed to work in a network. Multiple sensors can be cascaded along a single item of fiber and demodulated by a single piece of interrogating equipment. To apply the proposed sensor, a firm, stable, common reference level must be clearly indicated for the distribution of sensor network.

4.2 Theory

The rationale of the liquid level sensor is to produce a wavelength shift in the embedded FBG when there is a change of the liquid level in the sensor body. Figure 8 is a schematic diagram illustrating the sensing mechanism. A liquid-filled sensor body with a low density float is located at the center. The upthrust force on the float caused by the liquid inside is transferred to the fiber connecting the float to the bottom of the tank. The FBG in the fiber will have a wavelength shift with any deviation of liquid level in the tank.

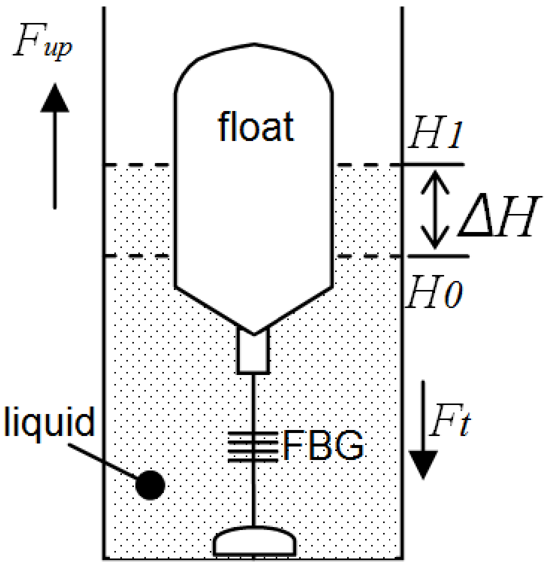

Figure 8. Sensing mechanism of the track settlement level sensor.

The upthrust force (F_{up}) by the float and the tension force (Ft) of the optical fiber in the system is given as:

$$F_{up} = Ft$$
$$\Delta F_{up} = \Delta Ft \qquad (4.1)$$

ΔF_{up} and ΔFt represent the variations of upthrust force and tension force respectively.

The upthrust force variation (ΔF_{up}) on the float caused by the liquid level variation is expressed as:

$$\Delta F_{up} = (\rho_1 - \rho_2) g * \Delta H * A \tag{4.2}$$

where ΔH is the liquid level deviation from the initial liquid level, defined as $H1\text{-}H0$. The densities of the liquid and the float are defined as ρ_1 and ρ_2 respectively. The gravitational acceleration and the cross-sectional area of the float [130] are represented by g and A respectively.

The variation of tension force in the fiber is given as:

$$\Delta Ft = \sigma * a$$

$$\sigma = \Delta Ft / a = E * \varepsilon$$

Thus,

$$\Delta Ft = E\varepsilon a \tag{4.3}$$

where σ, a, E and ε are respectively, the stress in the fiber material, the cross-sectional area of the fiber, Young's modulus of the fiber material, and the strain in the fiber under tension.

The relationship between the strain and the wavelength of FBG [100], [131] is expressed by:

$$\Delta\lambda_B = 0.76 * \varepsilon * \lambda_B$$

Hence,

$$\varepsilon = \frac{\Delta\lambda_B}{0.76\lambda_B} \tag{4.4}$$

Substituting equation (4.2), (4.3), (4.4) into (4.1), the relationship between the variation of liquid level and the wavelength variation is given by the equation:

$$(\rho_1 - \rho_2)_g * \Delta H * A = \left(E\left(\frac{\Delta\lambda_B}{0.76\lambda_B}\right)a\right)$$

$$\Delta H = \frac{\left(Ea\left(\frac{\Delta\lambda B}{0.76\lambda B}\right)\right)}{((\rho 1 - \rho 2)gA)} \tag{4.5}$$

Therefore, the sensitivity of the sensor expressed in (4.5) can be re-written as:

Sensitivity: $$\frac{\Delta\lambda B}{\Delta H} = \frac{0.76\lambda B}{Ea} * \ (\rho 1 - \rho 2)gA \tag{4.6}$$

4.3 The Structure of the Sensor

A stainless steel container forms the main structure of the settlement level sensor as illustrated in Figure 9. The tip of the main structure is an air vent and a liquid inlet is at the bottom. A tank of large volume is connected to the sensors via a flexible tube, providing a reference liquid level for all sensors in the system. Any changes in the liquid level inside the sensor will cause liquid to flow in or out through the flexible tube. An optical fiber outlet, located near the bottom, is connected to the interrogator [132] for wavelength measurement. A screw is fixed at the tip to secure the position of the float in the body during transportation. To avoid breaking the fiber during transportation, the lower part of the float is fastened to a T-shaped sub-assembly which is mounted on the mechanical stopper. The mechanical stopper, at the tip of the float, is to guard against the vertical movement of the float within the limit during normal operation.

As shown in Figure 9, the V-groove at the center of the T-shaped sub-assembly provides a better contact and alignment when mounted on the fiber. The sensing FBG is written in the middle of the fiber and is re-coated back with an acrylic jacket after inscription. The coatings at the two ends of the FBG are stripped and glued at the V-groove of the float and the bottom part of the sensor. Consequently, the tension force between the float and the bottom is fully transferred to the fiber.

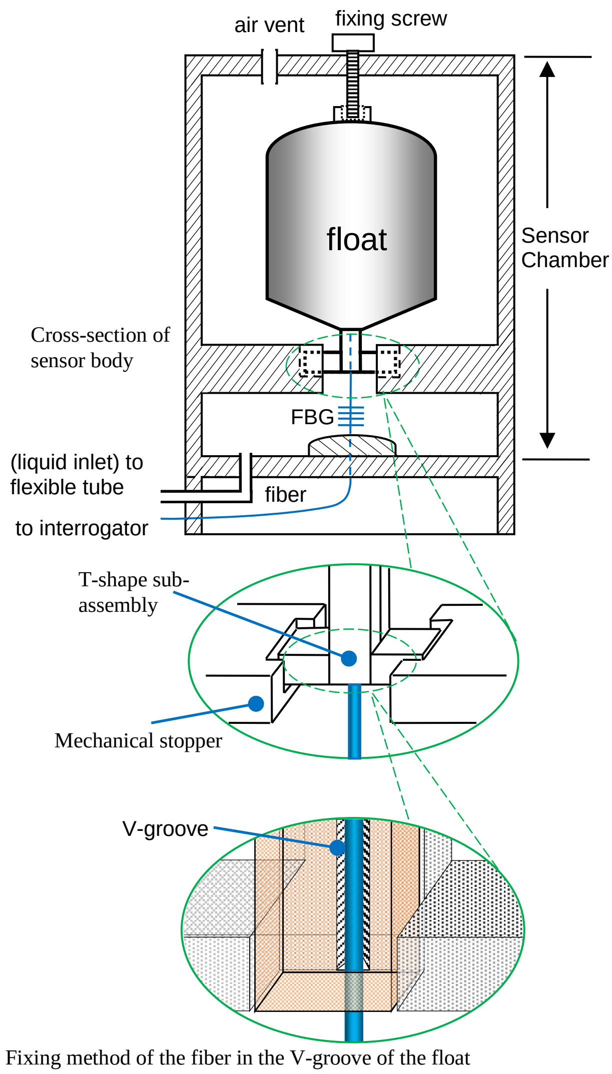

Figure 9. Schematic diagram of the structure for the level sensor.

The optical fiber employed in this study is a 1310-Hp-80 fiber from Nufern [133] with diameters of 9 μm at the core and 80 μm for the cladding. That core diameter is compatible with the ordinary single-mode fiber used in communication. Hence, splicing it to a standard fiber does not introduce high insertion loss to the sensor.

Furthermore, since the diameter of the cladding (80 μm) is smaller than the conventional size (125 μm), a higher strain can be induced by the same force in the fiber, as introduced in Formula (4.3).

A photograph of the settlement level sensor is shown in Figure 10. Its height is 230 mm and its diameter is 85 mm, with a cylindrical shape for the stainless body. The standard of stainless steel utilized in the sensor is of SS316 grade, having the properties of high mechanical strength, high creep resistance, as well as excellent mechanical and corrosion-resistance at sub-zero temperatures [134]. This standard is considered suitable because the sensor is designed to be used in harsh environments where temperatures range between -30°C and 80°C. To avoid the liquid inside the sensor from freezing at low temperature, an anti-freeze coolant with a melting point lower than the ice-point is employed, which is compliant with the ASTM-6210 [135] standard.

For clear realization of the conditions inside the sensor, a liquid level observing window is equipped on the body as shown in Figure 10. This window is convenient for liquid level adjustment during installation. To enable the full expected range to be maintained, the liquid level should be adjusted to the optimum level at the reference position. This position varies for different applications and depends on the trend of the settlement level under measurement. In order to avoid leakage and achieve the best shielding protection with the highest reliability, the various parts of the gauge and the flexible tubes used in this study are suitable for a wide range of operation temperatures and pressures, and were also waterproof and corrosion resistant [136].

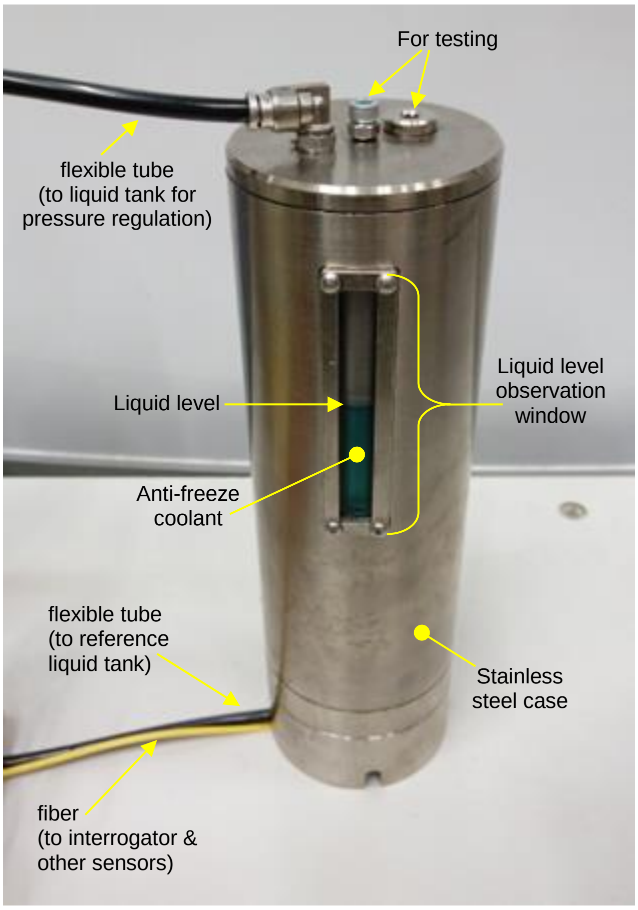

Figure 10. Photograph of the track settlement level sensor

The density difference between the liquid (anti-freeze coolant) and the float (ρ_1-ρ_2) is 800 kg/m^3 and the cross-sectional area (A) of the float is 4.42*10^{-3} m^2 (diameter of 70 mm). The FBG has a Bragg wavelength (λ_B) of 1550 nm, while the Young's modulus (E) and the cross-sectional area (a) of the fiber material (silica) are 73 GPa [131] and 5.026*10^{-9} m^2 (fiber diameter of 80 μm) respectively. With the above figures, the sensitivity designed for this sensor is ~0.1 nm/mm as written in Formula (4.6).

4.4 Results and Discussion

The experimental arrangement, for evaluating sensor performance, is depicted in Figure 11. A large tank is filled with anti-freeze coolant liquid, there are two settlement level test sensors (sensor #1 and sensor #2), two independent vertical movement translation stages, a FBG interrogation system outside the chamber, and a temperature controlled chamber. Within the chamber, the tank is connected to the two level sensors through a flexible tube and a T-joint. The optical fiber from the sensor is connected to the interrogation system, placed outside the chamber, for wavelength measurement. Since FBG intrinsically senses both temperature and strain at the same time but does not distinguish between them, an additional FBG is used for temperature compensation in the chamber and is also connected to the interrogator. In order to balance atmospheric pressure, the tips of the liquid tank and the sensors are connected via flexible tubes, providing a path for airflow.

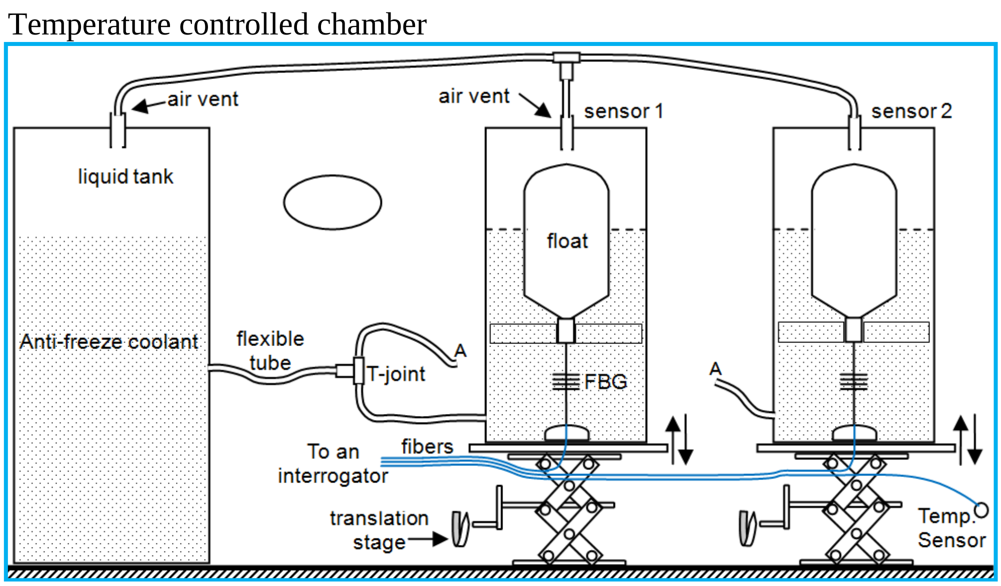

Figure 11. Experimental configuration for performance evaluation.

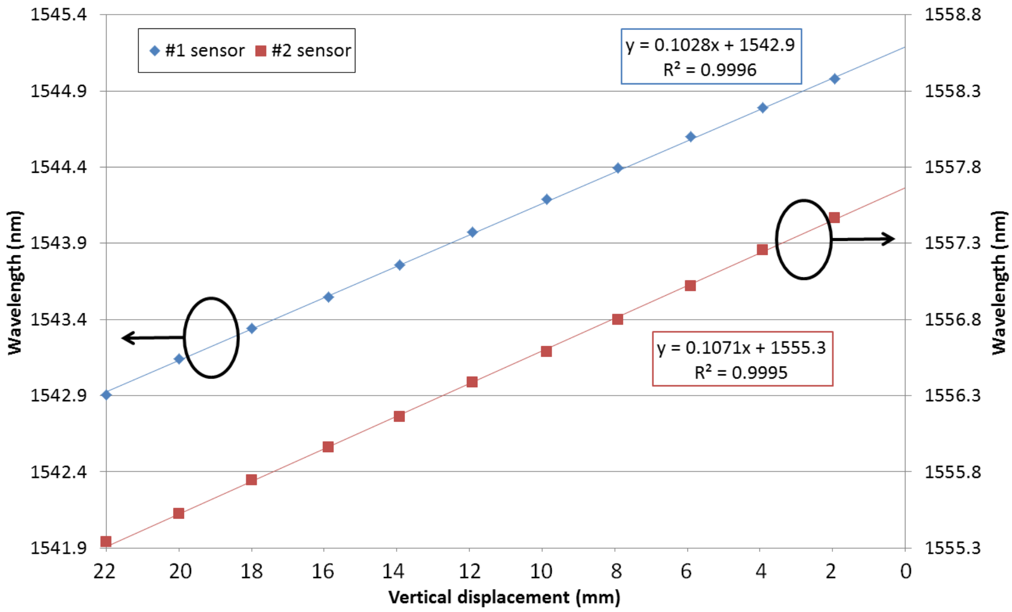

Figure 12. Measured wavelengths of the two sensors at different vertical displacements

The experimental arrangement had two purposes. First, to evaluate the performance of the level sensor, and second to study the feasibility of constructing a network of multiple sensors for settlement measurement over a wide area. In the experiment, the range of 0 to 22 mm for vertical displacement was examined based on 2 mm steps, controlled by a translation stage.

The experimental results, deriving from the two sensors, giving vertical displacement against the corresponding wavelengths are shown are Figure 12. The wavelengths of sensor #1 and sensor #2 were 1542.9 nm and 1555.3 nm respectively. Both sensors worked linearly with wavelengths decreasing as vertical displacements moved upwards. According to the measurement, the experimental sensitivities of sensor #1 and sensor #2 were 0.103 nm/mm and 0.107 nm/mm respectively. These values are very close to the designed value of 0.100 nm/mm. The minor differences between the measured and design sensitivities can be attributed to density deviations between the floats and the liquid, as well as machining error in the metal parts.

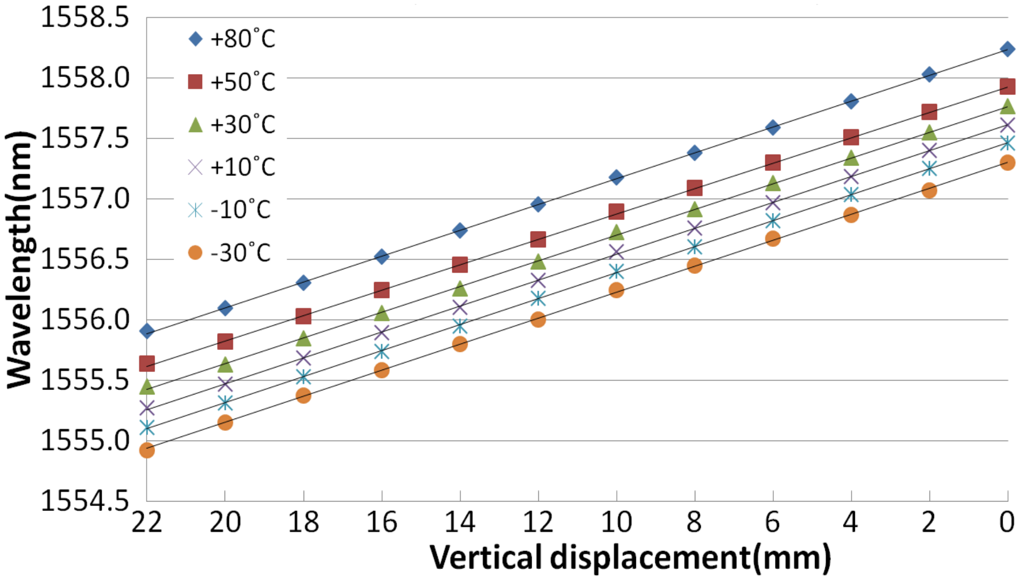

Figure 13. Vertical displacements at different temperatures (-30°C, -10°C, 10°C, 30°C, 50°C and 80°C).

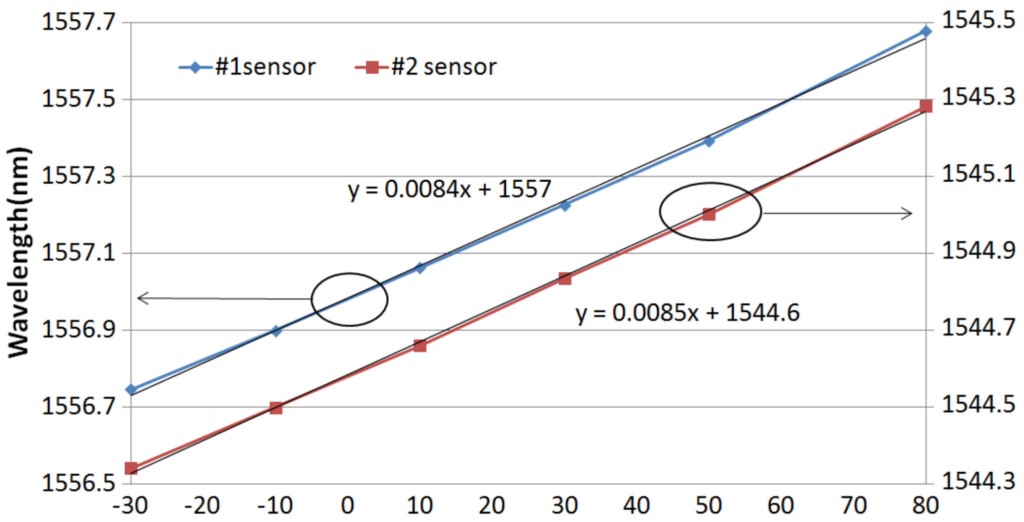

Figure 14. Temperature characteristics of the sensors.

To investigate the temperature characteristics, sensor #2 was selected for the experiment at different temperatures (-30°C, -10°C, 10°C, 30°C, 50°C and 80°C), and the results are depicted in Figure 13. The readings were then plotted and fitted into straight lines with slopes between 0.105~0.107.

The wavelengths at different temperatures for both sensors, whose vertical displacement was fixed at the 12 mm position, are shown in Figure 20. The curves indicate that the sensor temperature effect is limited and can be counted as linear [1], [106], as an embedded FBG temperature sensor was installed inside the sensor body for compensation processes. As shown in the graph, the temperature coefficients are 0.0084 nm/°C and 0.0085 nm/°C respectively after best-fitting the linear curves.

The deviations between wavelengths at different temperatures and different vertical displacements are shown in Figure 15. The range variation is around ±0.03 nm, corresponding to vertical displacement changes of approximately ±0.3 mm. Therefore, the deviation percentage in this sensor is around ±1.3% for a 22 mm of measurement range. From the graph, it can be seen that the deviation of vertical displacement is more serious at the extreme temperatures (-30°C, 50°C and 80°C) than at normal temperature (-10°C to 30°C), for a range of around 0 to -0.025 nm (~0 to -1.1%). To perform differential settlement measurement over a large area, a sensor network can be established by cascading multiple sensors into a single and long distance fiber. The experimental results indicate that the characteristics of individual sensors are not interfered with by other cascades in the same sensor network.

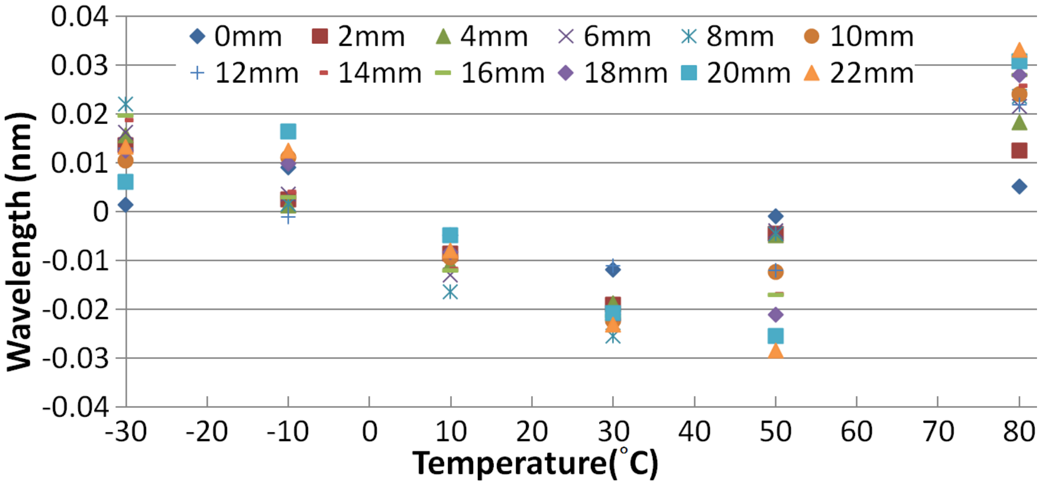

Figure 15. Variation of wavelengths at different temperatures.

4.5 The Maximum Range, Resolution and Environmental Disturbances

This prototype demonstrates the working principle and feasibility of this level sensor to be used for practical applications. The factors that determine the range of vertical displacement of the settlement level sensor are the tensile strength of the fiber used for FBG inscription and the upthrust force induced by the float of the sensor designed. The sensitivity of this sensor can be modified by varying the size of the float or using optical fiber with different diameters. The resolution of level sensing system on the other hand is limited by both the sensor sensitivity and the resolution of the interrogation system used for conducting the measurement.

The noise caused by environmental disturbances can include the vibration produced by the passage of the train, and the ambient temperature. For the vibration, the measurement noise measured by the sensor induced by passing train could be easily identified and can be classified as invalid data. For the ambient temperature, the temperature effect has been considered during sensor development. Actually, the effect is shown to be very limited of approximately ±0.3 mm equivalent to ±1.3% for a 22 mm of measurement range as discussed in Section 4.4 of this chapter. On the other hand, with the built-in temperature compensation sensor, further improvement of the accuracy can be achieved. Besides, most of the noise caused by environmental disturbances are of relatively higher frequency as compared with the change of settlement. Thereby, frequency filtering may also be useful for removing the related noise.

4.6 Chapter Summary

This chapter introduces a FBG-based level sensor for the monitoring of differential settlement of a railway track. The vertical displacement of the sensor, which is relative to liquid level changes inside the sensor, alters the tension force within the embedded FBG. Experimental results show high linearity between vertical displacement and wavelength shift of the FBG. An 80 μm-diameter optical fiber is used with the aims of enhancing the overall sensitivity and reducing the physical size of the sensor. The sensitivities of the two assembled sensors are 0.103 nm/mm and 0.107 nm/mm respectively, both of them very close to the designed value of 0.100 nm/mm. The temperature effect on the sensor was measured as 0.008 nm/°C. This can be compensated for by adding an embedded temperature measuring FBG within the sensor, or else by use of an external temperature sensor. The sensor design also incorporates several measures to facilitate sensor operation in extreme environmental conditions. The sensor gives a measurement error of ~±1.3% within its operational range of -30°C to 80°C. For differential settlement measurement over a long railway track, multiple units of there settlement level sensors, which require no power supply, can be multiplexed to form a sensing network, thus providing the advantages of higher simplicity, cost-effectiveness and reliability in relation to conventional electronic based counterparts. Apart from the sensor, a system for continuous condition monitoring in the sensor is also proposed. The use of historical data for intelligence management is also recommended as worthy of future study.

Chapter 5 **Fiber Bragg Grating Based Axle Counter**

5.1 Introduction

This chapter introduces a FBG-based [137] axle counting sensor [138]. Axle counting on a railway is to detect the presence/absence of a train in a block of the track for signaling purpose, so as to ensure the block ahead is clear and enable automatic train operation. Otherwise, manual operation is used instead, with a relatively lower speed for safety reasons. The method is to count the number of axles entering and leaving a signaling block. This maintains a crucial role [139] in railway operation, because an effective fail-safe signaling system is essential to ensure the safety and reliability of a railway system, because drivers may not be always able to clearly see obstacles (e.g. a train) ahead while running at high-speed, in bad weather or at night.

5.1.1 Track Circuit

A Track Circuit [140]–[142], regarded as a type of signal, is a section installed on the tracks which tells drivers of the presence of obstacles or of another train. With accurate signaling information, drivers can operate the trains at normal speed while ensuring travel safety.

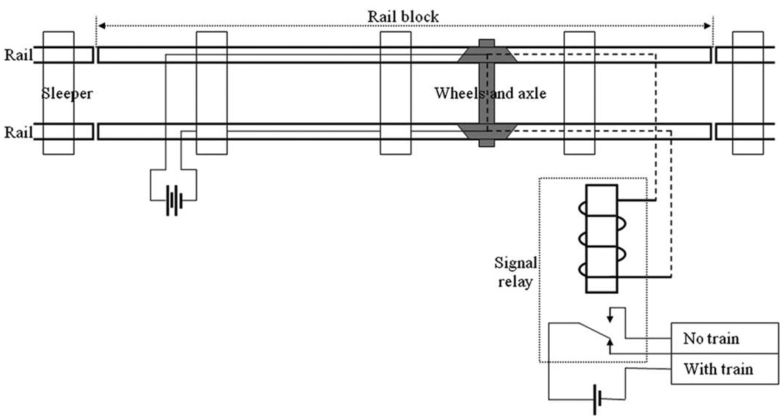

Figure 16. Schematic of a Track Circuit.

As shown in Figure 16, a Track Circuit includes an electrical circuit with a power source at one end of a section of the track [140], [141]. The working principle of a traditional Track Circuit is explained below. When a train is present on the track, a pair of wheels on the same axle are in contact with the two rails to complete the circuit. A complete circuit enables current flows through an electrical relay and therefore a switch to “With train” status. Otherwise, the status is that of “No train”. Drivers can easily appreciate the condition of the track section ahead by reading the signs displayed by the system.

5.1.2 Electronic Axle Counter

An alternative signaling device is the Electronic Axle Counter (EAC) [139] as shown in Figure 17. Traditional EAC consists of two pairs of electric coils, the transmitters and receivers. To install the device, the coils are mounted on the rail by drilling holes and fixed using screws into the rail. To a certain extent, this installation damages the rail. The working principle of an EAC is to detect the presence/absence of a metallic obstacle by which blocks the magnetic flux flowing between the transmitters and receivers.

However, both the Track Circuit and EAC solutions have limitations. For example, they are easily interfered with by EM wave and environmental disturbances such as the presence of lightning, they are also bulky and difficult to install. To overcome these limitations, a FBG-based [143] axle counter is proposed in this research. The FBG sensor possesses many advantages over electronic sensors and has high potentials of being used in condition monitoring. The working principle of the FBG sensor is to measure the deformation of the track due to the weight of trains acting on the rail and which could be used as an indication of the presence of a train. A train usually weighs tens of tonnes, whereas other moving objects in nature are seldom so heavy. As compared to the conventional axle counting system, this is the novelty of using FBG as sensing elements for axle counting.

Furthermore, compared to the traditional Track Circuits and EAC signaling equipment, the FBG is less likely to be interfered by environmental disturbances and is thus more accurate. Due to the easy installation process and low cost of FBG, redundant sensors can also be installed nearby to confirm the signals and thereby improve the system reliability. For example, measuring the axle loads on both left and right hand rails, their arrival times and weight are generally very similar and hence one can positively confirm the correct arrival of the train if the left and right rails are both indicating there is an axle on the rail. Besides, EMI in electronic type signaling equipment may cause errors not only in the sensing phase but also in signal transmission. As such, the FBG is absolutely safe even in stormy weather [104].

Figure 17. Electronic axle counter formed by two pairs of transmitter and receiver installed in a rail closely. The inset exhibits converter equipment connecting the axle counter at the trackside.

5.2 Setup and Experiment for FBG Axle Counter

Since the rationale is to measure rail deformation caused by the weight of a train, the most sensitive position of the rail must be clearly identified before sensor installation. As such, for this purpose, a finite element simulation by ANSYS Multiphysics software [144] and an onsite experiment have been conducted.

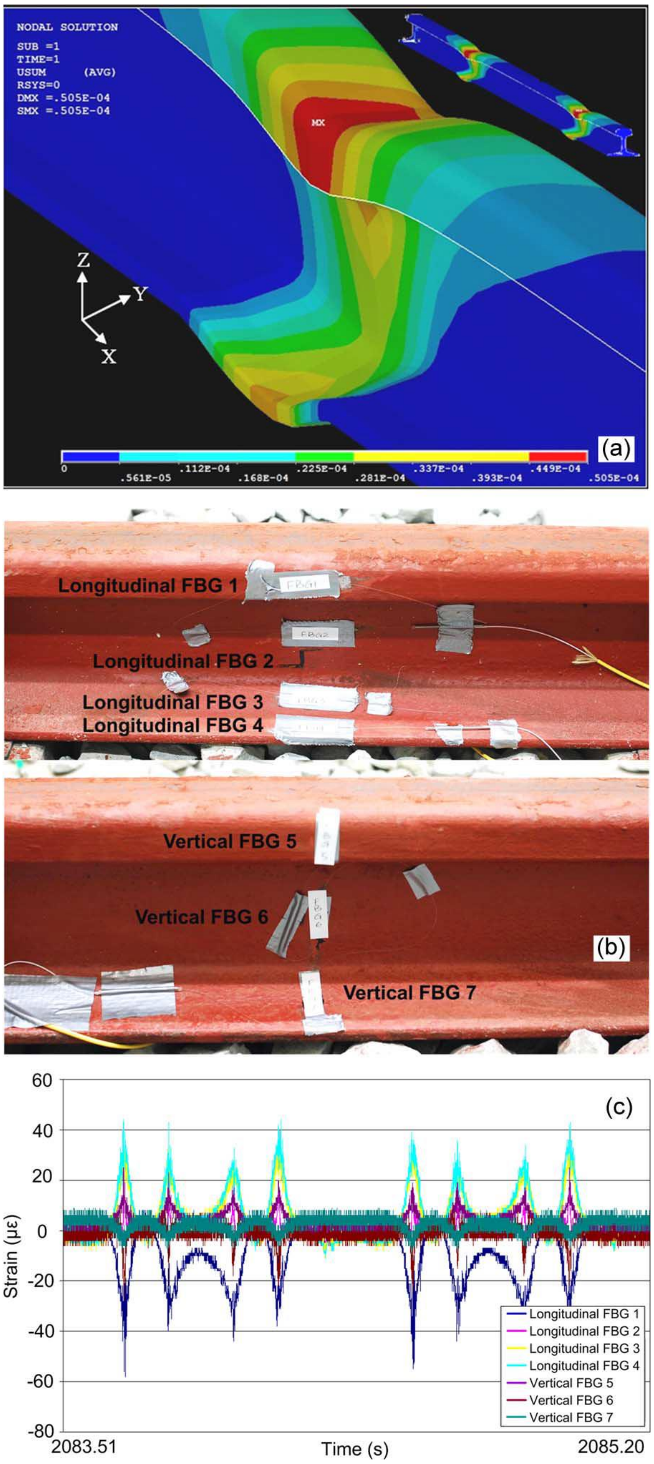

Figure 18. (a) Finite Element Simulation of deformation in a rail under load. (b) Upper rail shows four longitudinal FBGs installed at one side of the rail and the lower shows three FBGs installed vertically in another rail. (c) Strain response of the seven FBGs when a wheel passes the testing point for four times.

As shown in Figure 18 (a) and Figure 18 (c), both results confirmed that maximum deformation occurs at the head of the rail. The rail model UIC54, which is made of steel with a Young's modulus of 207 GPa and Poisson ratio 0.29, was adopted in the simulation as a reference. This simulation assumes that the load is provided by a train weighing 48 tonnes with eight wheels standing on the rails. The experiment assumed a train of similar weight approached the sensing points slowly, at 5 km/h, to simulate a static load. In addition, to avoid unwanted mistakes, the train passed the sensing points on four occasions. The deformation signals from the seven FBGs were recorded by the system and stacked in Figure 18 (c).

In the experiment, the seven FBGs were mounted at different positions as indicated in Figure 18 (b). The results show that no matter what the longitudinal (upper rail) or vertical (lower rail) alignments, the sensitivities of the FBGs were of the same order, i.e. the highest sensitivity was at the head of the rail (FBG1 and FBG5), the second highest at the foot (FBG4 and FBG7) and the lowest in the middle (FBG2 and FBG3). The above results align with the simulation result of Figure 18 (a) and are clearly shown in Figure 18 (c). Despite its highest sensitivity, the head position was not selected because of contact with the wheels and destruction of the sensor. The second highest location, at the root, was therefore selected.

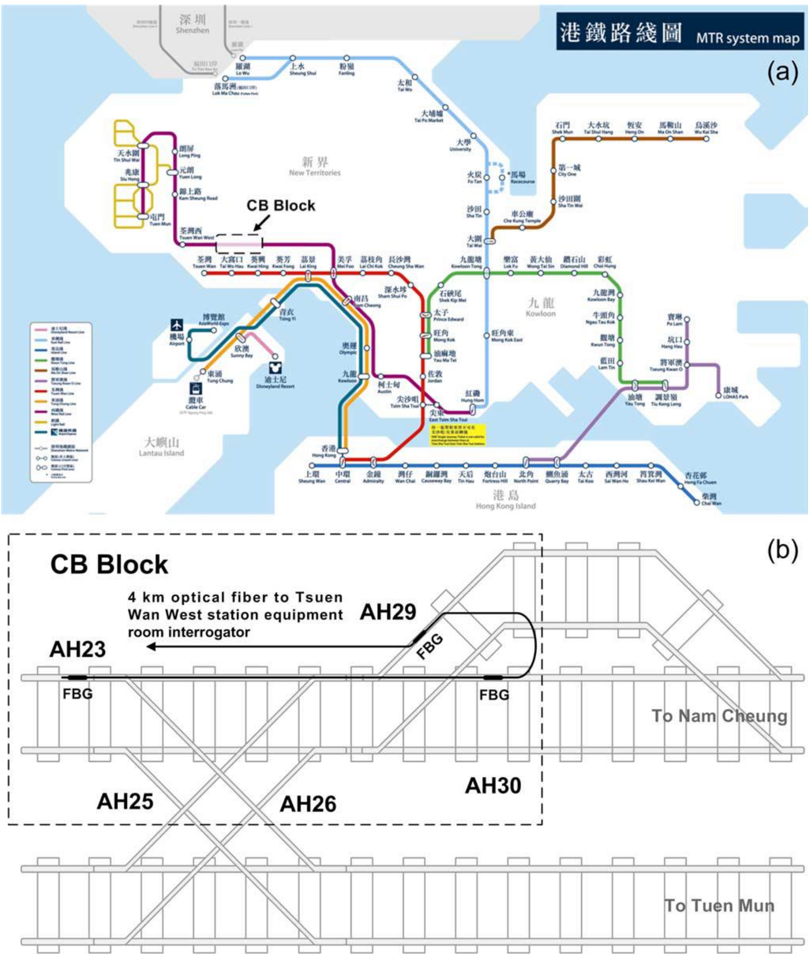

Figure 19. (a) The route map of the West Rail line; (b) Schematic of FBG sensor locations in the CB block.

A test was also carried out with the proposed FBG system operating alongside an existing electronic type axle counter system for performance verification. The installation of FBGs is shown in Figure 19. The line used for the test was the West Rail Line in Hong Kong as shown in Figure 19 (a) [145]. The signalling block tested, covering nine stations, was 30.5 km long, and located between the two districts of North-West New Territories (Tuen Mun) and the city center (Nam Cheong in Kowloon). The fleet comprises 22 trains, each with seven cars and 220 m long. The maximum train capacity is 2,345 persons. The track allows a maximum speed of 130 km/h. The overhead pantograph provides a 25 kV/50 Hz power source for the train. The track-forms on this line include a Low Vibration Track (LVT) inside the tunnel sections and a Floating Slab Track (FST) on the viaduct sections. The existing UIC60 track model was adopted.

The CB block was selected for testing the FBG axle counting system and a schematic of this signalling block is shown in Figure 19 (b). This block contains two junctions and five boundary points, namely AH23, AH25, AH26, AH29, and AH30, which are all supported by the traditional axle counting systems. FBGs were installed only at the three most frequently used entries, of AH23, AH29, and AH30. All FBGs were connected by a single model fiber to an interrogator [28] [146], which was located in the Signal Equipment Room at the Tsuen Wan West station, 4 km distant from the sensors. The distances between AH23 and AH29, AH23 and AH30, and AH29 and AH30 are 1500 m, 1200 m and 600 m respectively.

5.3 Methodology

Data logging, started in a computer was performed real-time with an interrogator to demodulate the wavelength. Sophisticated software has been developed to execute the algorithms and detect the axles. The Bragg wavelengths of the FBGs are in the range of 1535 nm to 1575 nm. Figure 20 (a) shows a measured waveform of 28 peaks corresponding to 28 axles, derived from a train of 7 cars. The wavelength swing is about 0.3 nm induced by 300 $\mu\varepsilon$. Figure 20 (b) gives the strain of the first six peaks in the waveform with noise and high frequencies clearly shown. After a 10Hz filtering, the noise is removed as indicated in Figure 20 (c). In order to achieve high accuracy, this data validation process is necessary before counting the number of axle.

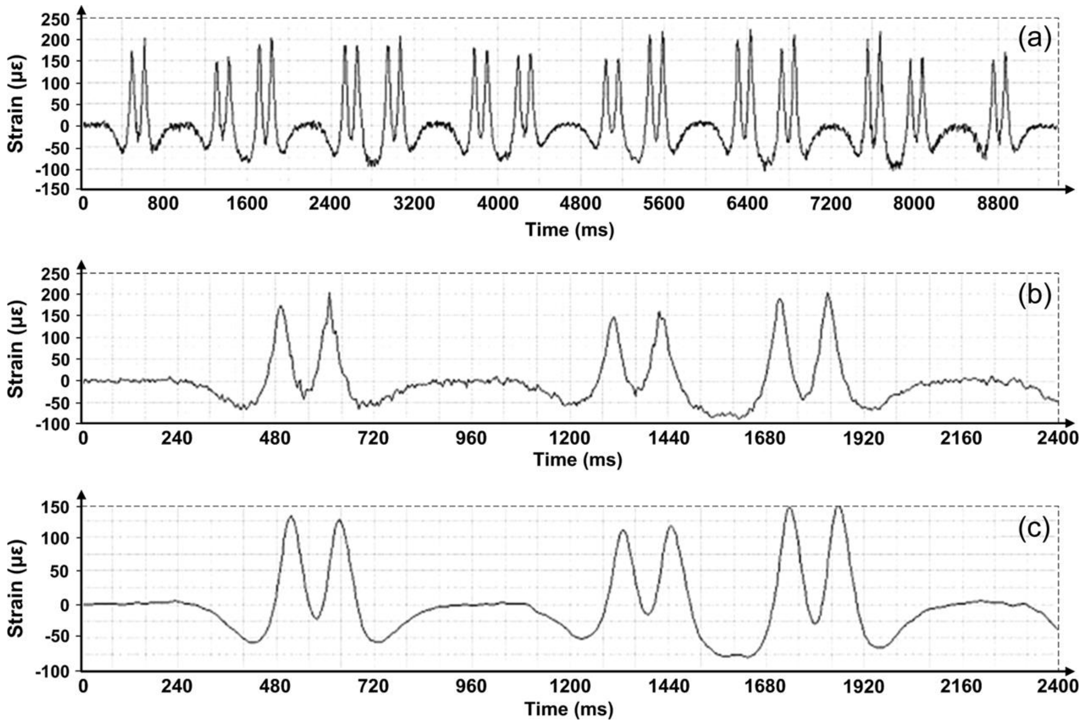

Figure 20. Detected strain in the rail (a) 28 wheels of the passage of a train, (b) the first six wheels of the train, (c) the signal after low-pass-filtered.

Axle counting refers to counting the number of peaks in the deformation waveform of the rail, therefore an accurate detection of peaks by the algorithms is crucial. X-Crossing, as shown in Figure 21(a), is an algorithm developed in this study. A peak is defined by the presence of a rising edge followed by a falling edge, at least a minimum time interval (T) apart.

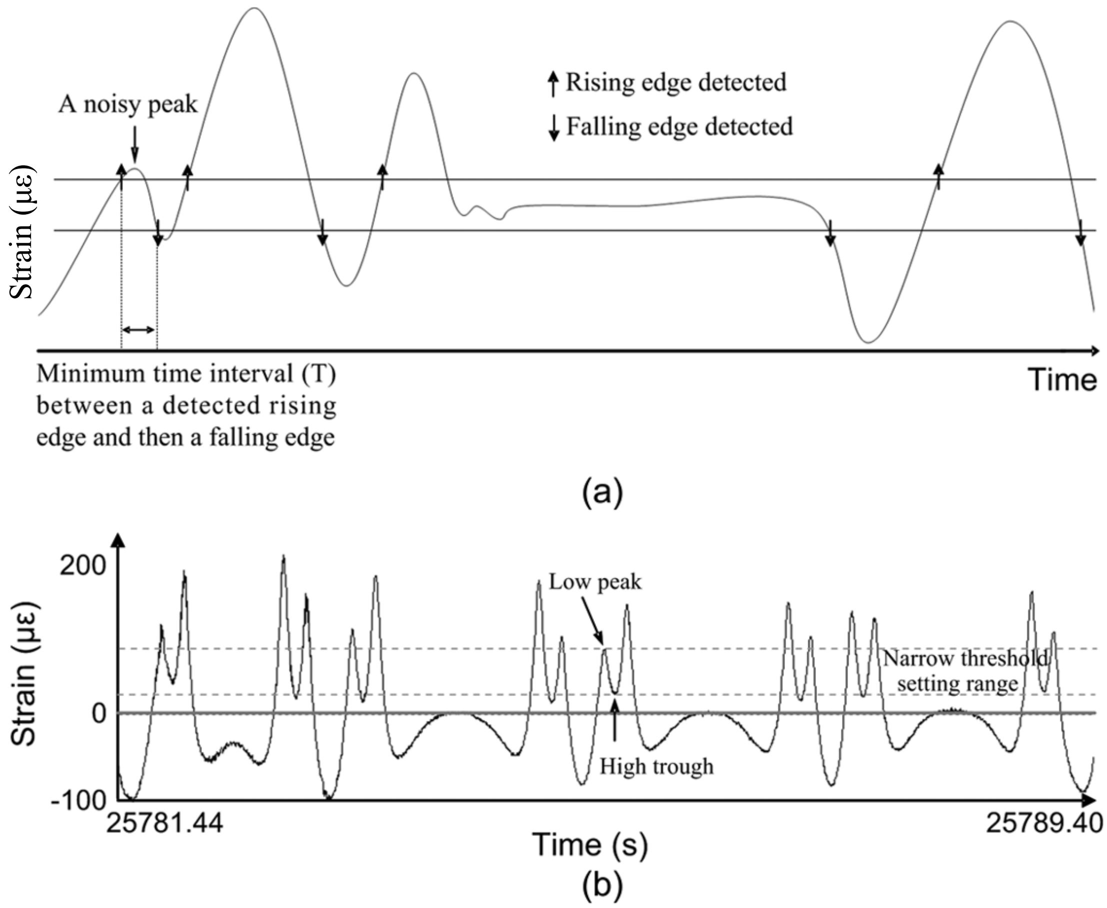

Figure 21. (a) The X-crossing method and the minimum time interval setting; (b) a narrow threshold for X-crossing.

The mathematical expressions relevant to the X-Crossing method are given below:

Rising edge = $Y_F = \wedge\, (x_{i-1} < x_i < x_{i+1})$ (5.1)

Falling edge = $Y_R = \wedge\, (x_{j-1} > x_j > x_{j+1})$ (5.2)

Peak = $P = (Y_F \wedge Y_R) \wedge ((x_j - x_i) > T)$ (5.3)

where *i, j* = 0, 1,2…n-1, and *T* is the minimum interval between the rising and falling edges.

The mathematical expressions for rising and falling edge detections are given in Formulae (5.1) and (5.2) respectively, while the peak is shown in Formula (5.3).

The X-Crossing method was developed at the beginning of the study. For the first 45 days, this method obtained a satisfactory result for 252,000 axles (9000 trains) counted at the testing point AH23, notwithstanding that 13 trains were mistakenly counted. However, as shown in Figure 21 (a), the processing of the result was affected by low frequency noisy peaks caused by wheel imperfections or other engineering trains which repair the track at night. In addition, it is not reasonable to adopt a fixed threshold for all peaks because some low peaks may have relatively high troughs at the same time. As such, as shown in Figure 21 (b), the signal range allowed for the threshold has been narrowed to limit the possibility of drawing a line, especially when low value peaks and troughs occur simultaneously in the waveform. For the rest of the research, different approaches were used to further improve the results.

D-Crossing, as shown in Formula (5.4), is one of these different approaches taken. The first-derivative (Y_i) of the D-crossing method helps to solve the problems of constant high strain waveforms and local variations, as shown in the middle part of Figure 22(a). In fact, the method can be regarded as continuous detection of the changes of signal between a preceding data point (x_{i-1}) and the next data point (x_{i+1}).

$$Y_i = ((x_{i+1} - x_{i-1})/2dt \qquad (5.4)$$

Where i = 0, 1, 2…n-1.

In order to remove local variations, before feeding the signal into Formula (5.4), the low-pass-filtered original data (as shown in Figure 22(a)) should have the lower part of the signal cut by a threshold (as shown in Figure 22(b)). As shown in Figure 22(c). after performing the first-derivative, the output waveform with high strain is now removed, which was caused by a train stopping, with a noisy peak. In addition, the first four peaks in Figure 22(b), which were originally coupled with only positive half cycles, now have both positive and negative cycles as shown in Figure 22(c), thus facilitating easy detection.

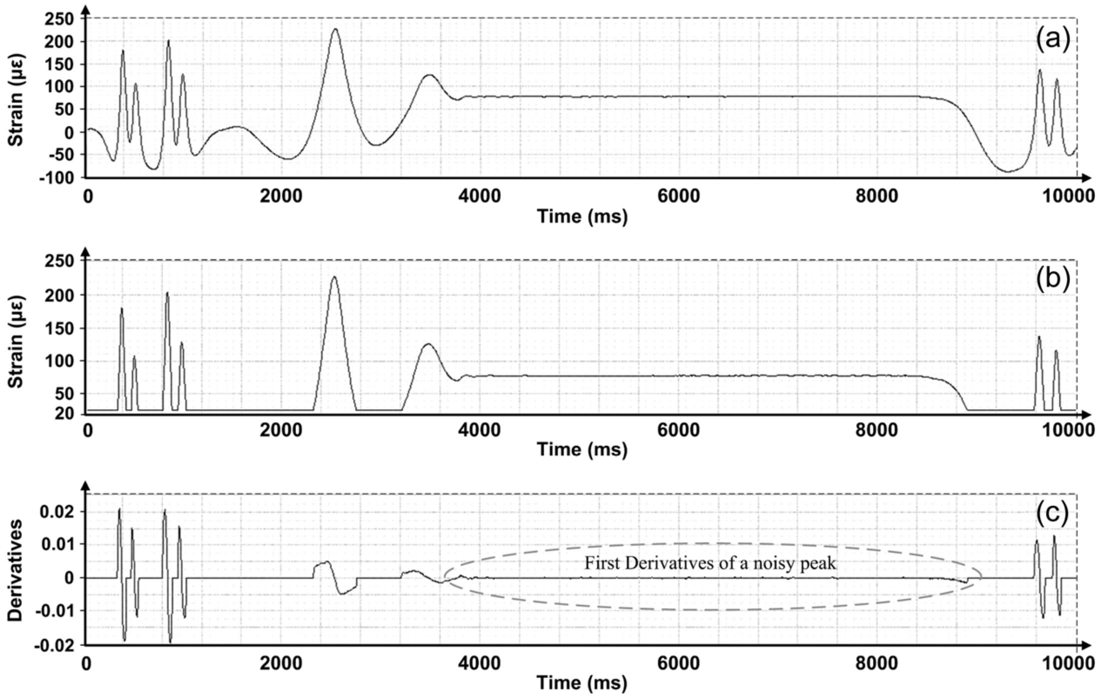

Figure 22. (a) A constant high strain level caused by the train stopped at the sensing with low-pass-filtered, (b) remove the local peaks by threshold setting, (c) waveform after first derivatives of the signal.

To evaluate the performance of the D-Crossing method, data of the 9,000 trains, which included errors produced by the13 trains in the X-Crossing, were loaded to the D-Crossing again. In general, the result was satisfactory –most of the axles being correctly counted, with only one train mistaken, which can be attributed to the two peaks and valleys in the middle of the waveform as shown in Figure 22(c). Fortunately, these noisy peaks can be tackled by the X-Crossing method. Eventually, both algorithms were run on the system concurrently, all axles were correctly counted and the testing continued for the following six months.

5.4 Results and Discussion

The FBG-based axle counting system installed in the CB block is operating fully automatically, in-service, on a non-stop basis. The results are in real-time and allow the researchers to examine the success of the algorithm. The X-Crossing and D-Crossing algorithms, developed in the study, have their own strengths and weaknesses. The algorithms complement each other well and the final results are satisfactory. Regarding algorithm selection, in general, the X-Crossing is used when the signal is clean with little noise, whereas the D-Crossing is adopted when noise signals are detected, for example, a train stops at the sensing point. In addition, since a train can move and change its direction, an additional FBG should be installed nearby to identify direction.

After five months of operation, data on 1,680,448 axles (60,016 trains) have been processed by the system. These data were obtained from the three FBGs located at AH23, AH29 and AH30; which monitored 840,224 axles (30,008 trains), 280 axles (10 trains) and 839,944 axles (29,998 trains) respectively. The outcome was that no axle was wrongly counted. In other words, the test accuracy was 100%.

To validate the result, the existing electronic type axle-counter system was operated as an image. Both systems counted the same numbers of counting and thus the counting result is reliable. Apart from its high accuracy, simple equipment and sensor installation is another advantage of the FBG axle counting system. Its installation requires no electronic parts, but only a single set of equipment to connect the three entries with FBGs installed on the rails. The traditional system, however, contains three individual systems at each entry and is therefore more complicated than the FBG type. In addition, the FBG system allows the addition of further counting points by adding a fiber to the end of the existing fiber without needing extra equipment. The only concern is the processing power of the computer. Based on the above, it has been demonstrated that the FBG system provides an alternative solution for axle counting with the advantages of expandability, high accuracy and low cost.

5.5 Chapter Summary

This chapter begins with an introduction of two traditional types of axle counting systems, namely the Track Circuit and EAC, and their limitations. One major limitation of the conventional systems is that they are easily interfered with by EM waves. To tackle the problem, this study validated a FBG-based axle counting sensor as an alternative solution. The rationale of the proposed approach is to measure the weight of a train by FBG sensors. The optical fiber sensing eliminates any interference produced by EM wave due to lightning or other high voltage apparatus. A FBG-based axle counter can be fabricated by mounting a FBG on the rail and counting the number of peaks as the trains pass through. An on-site test was conducted on the West Rail line in Hong Kong. The X-Crossing algorithm was initially adopted but defects were found when counting signals for a train stopped with continuous high strain values. To overcome the problem, the D-Crossing algorithm was developed, with only one mistake, which can be overcome by then using the X-Crossing method. The testing result shows that no axle was wrongly counted after the processing of 1,680,448 axles over five months. The result validates the feasibility of the FBG type axle counting sensor and proves its potential advantages of higher accuracy, lower cost and higher flexibility in system expansion.

Chapter 6 **Train Weight Balance and Vibration Index**

6.1 Introduction

This chapter introduces a FBG-based sensor system for the measurement of train weight and Vibration Index (VI). The measurement of train weight and its balance on the track can support derailment risk monitoring, while the measurement of vibration can support Out-of-Roundness (OOR) monitoring based on a condition monitoring [11] system. A comfortable in-service line and railway safety have always been vital to train passengers. Train derailments can lead to serious accidents and losses of life and assets. To enhance railway safety and minimize the risk of train derailment, previous studies have devoted considerable efforts to developing train monitoring methods. Despite this, much of the existing literature discusses electronic sensors which are easily interfered with by EM waves in noisy environments. For example, the overhead power lines of the railway system can be a source of noise, seriously interfering with traditional electronic sensors, and causing faults. There is a need to develop more reliable and accurate train monitoring methods.

The sensor employed in this study is the optical fiber sensor, because it is EMI-free, reliable, of low cost, durable and produces zero EM wave emissions, and is thus more appropriate for use in railways than the traditional sensors. Detailed information is given in Chapter 3 and more in-depth explanation is provided in this chapter. The optical sensor used in this research is the FBG [4], [138], [147]. To verify the theory, a test on a train loaded with sandbags has been carried out for weight balance measurements. Wheel re-profiling was also carried out to prove the relationship between the wheel OOR [52] and vibration.

6.2 The Arrangement of FBG Sensors Network

A FBG-based sensor network was established for both weight balance and vibration measurement purposes as shown in Figure 23. The installation is located near the Siu Ho Wan depot (SHD) between Yam O and Tung Chung stations on the Tung Chung line in Hong Kong. The sensors were installed on a track 2.5 km in length. Eight FBG sensors with different wavelengths were mounted on both the up track and down track, connecting two separated optical fibers to an interrogator and a computer located inside the depot, 3 km away.

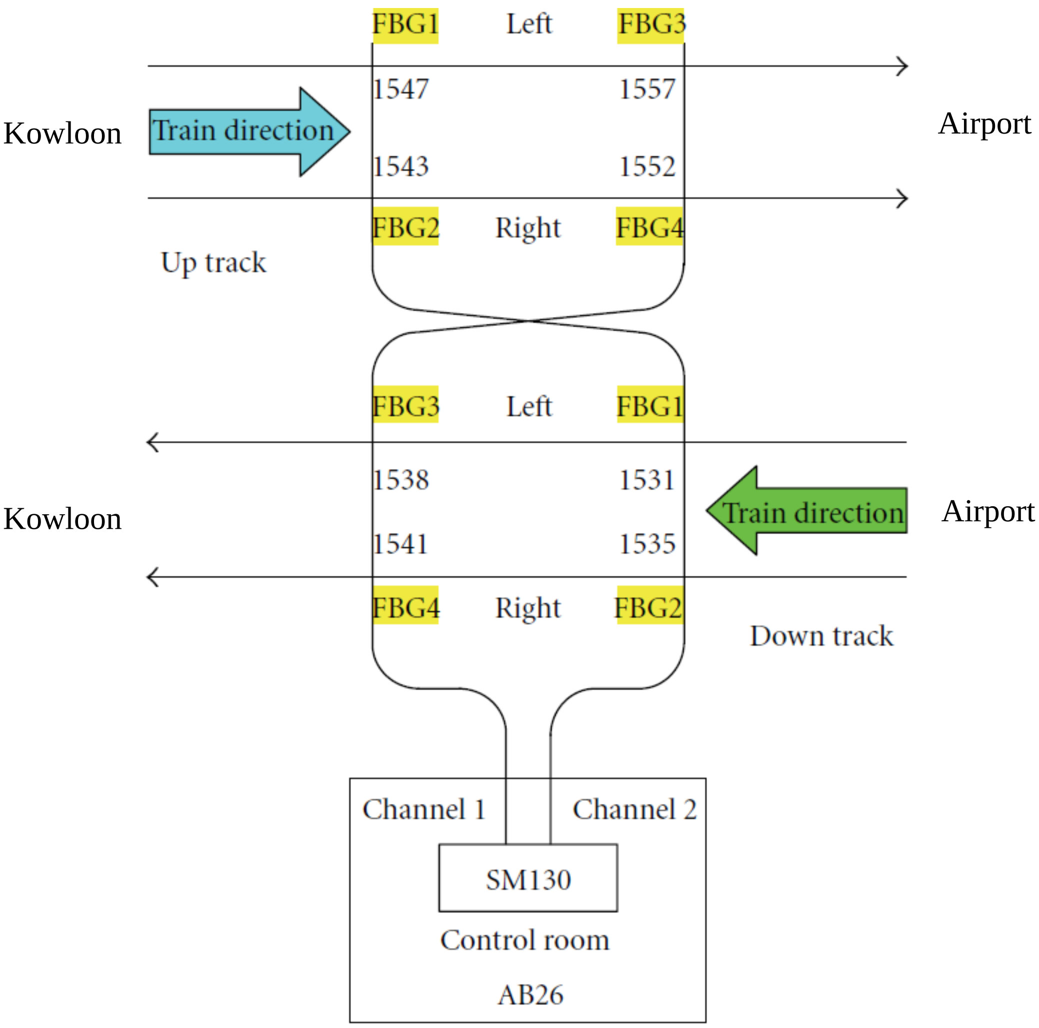

Figure 23. Schematic of FBG sensor network for railway condition monitoring. Sensor group 1543, 1547, 1552 and 1557 in nm are installed on the up track, while sensor group 1531, 1535, 1538 and 1540 in nm are installed on the down track.

In the sensor network configuration, each fiber connects four FBGs in a group, notwithstanding that two only are sufficient. The extra two serve as backup for system double-checking and data integrity purposes. In order to achieve multiplexing, the wavelength of a fiber has to be unique. The other end of the fiber is run back to the control room as spare. If the fiber breaks, the FBG signal can still be received by connecting the other end to the interrogator to resume the system immediately and automatically, without too much interruption. This configuration applied to all systems in the research study.

6.3 Weight Balance for Derailment Risk Monitoring

The FBG produced waveforms suitable for weight measurement [148] are shown in Figure 24. The train under test passes through the down track section of the Tung Chung service line. This particular waveform was generated by train “TCL 08” and measured by a FBG on the down track. In fact, the measurement is a change of rail strain, so it can be converted into weight by calibration based on the known weight of each car. To calibrate the system, the static weight of each axle is equated to the amplitude of the FBG signal, when the train is moving very slowly over the track. The ratio (i.e. weight-of-axle/amplitude-of-the-FBG-signal) is then used to convert the dynamic amplitude of each FBG signal to axle weight.

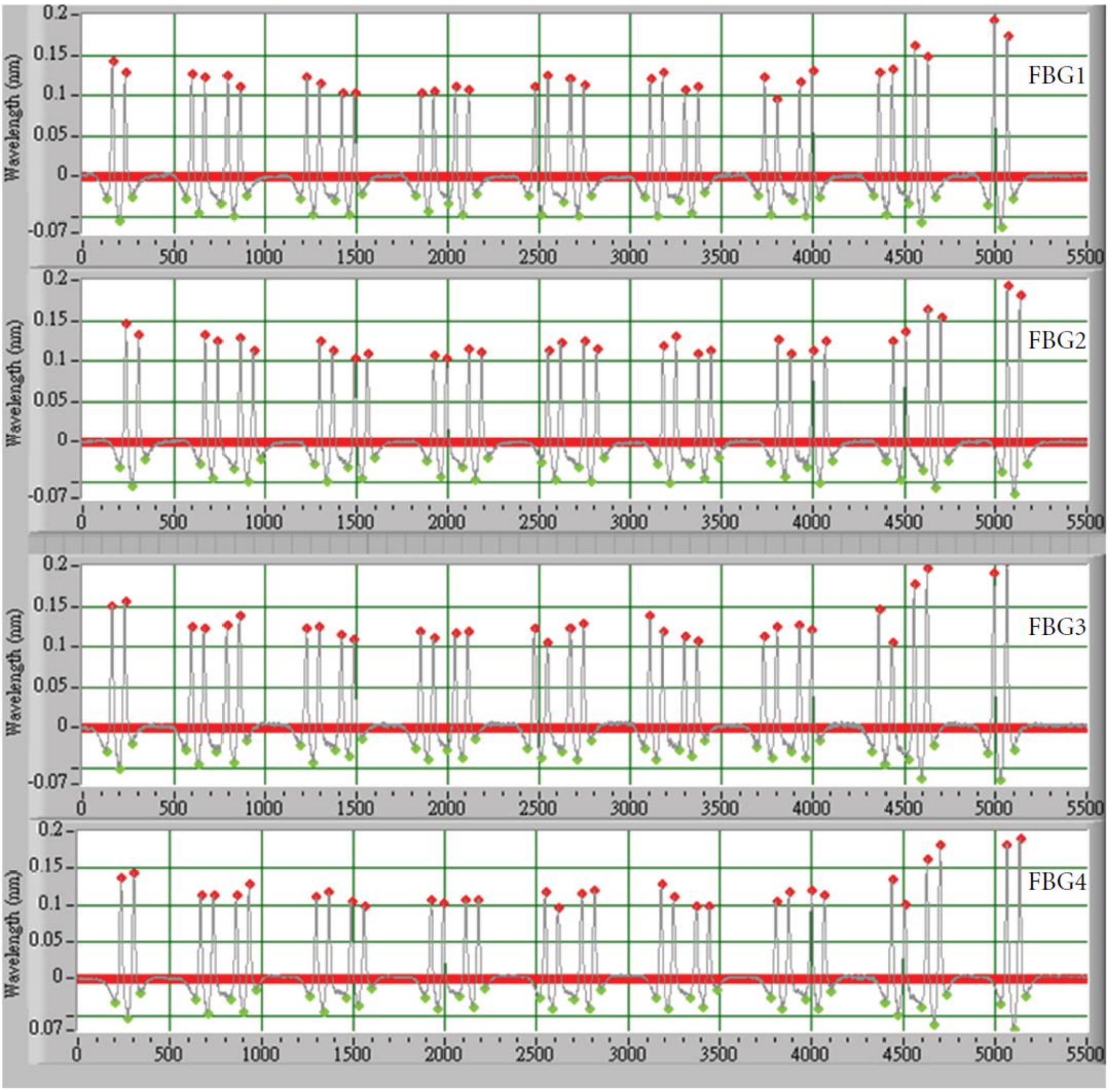

Figure 24. Wavelengths of the train under test for weight measurement.

The measured wavelengths are then correlated to the weights. This process is automatically run by an application program in the computer. First, the waveform has to be processed to filter out the noise before peak detection. Afterwards, the values of the peaks and valleys can be found, as denoted by the red dots in Figure 24 which relate to the dynamic loads. Four approaches were proposed for evaluating performance and identifying the best candidate. The graphical indication is shown in Figure 25 and their mathematical expressions are presented in equations (6.1) to (6.4) below the figure.

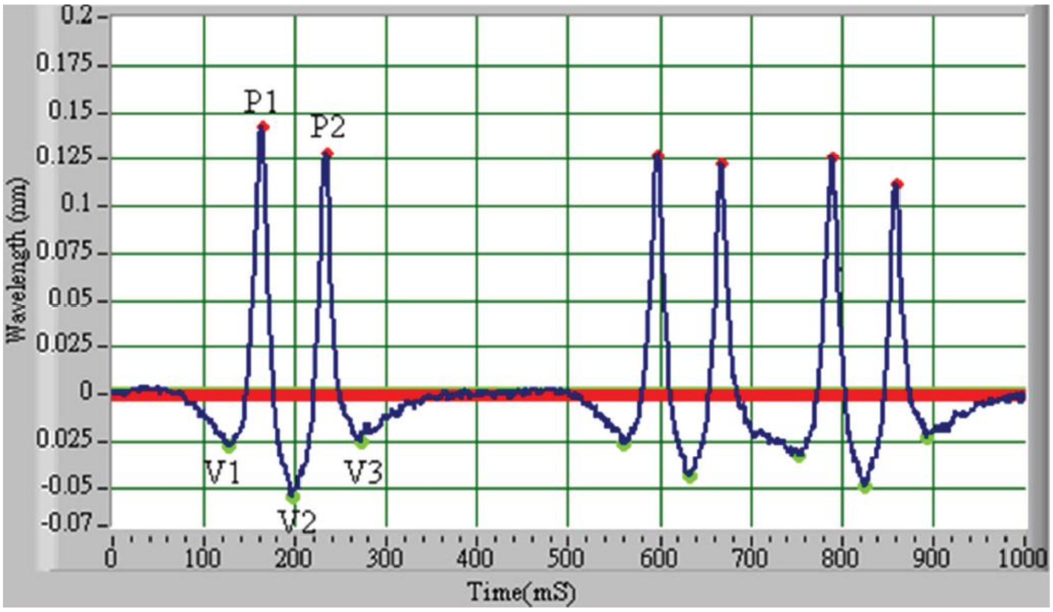

Figure 25. Waveform of dynamic load with two peaks in an axle labelled.

Approach 1: $W1 = (P1 - V1); W2 = (P2 - V2)$, (6.1)

Approach 2: $W1 = (P1 - V2); W2 = (P2 - V3)$, (6.2)

Approach 3: $W1 = (P1 - (V1 + V2)/2); W2 = (P2 - (V2 + V3)/2)$, (6.3)

Approach 4: $W1 = P1; W2 = P2$. (6.4)

where $W1$ and $W2$ are defined as the respective weights of axles 1 and 2 of the same bogie; $P1$ and $P2$ are the signal peaks excited by the load being applied to the corresponding axles; $V1$, $V2$, and $V3$ are the respective valleys, which are generated when the train car moves along the rail.

The results of the four approaches were then examined to evaluate the performance in relating dynamic weight to FBG signal. The results are shown in Table 7. The average error obtained from the four FBGs was 10.39%. The best scenario is Approach 4 which obtained the lowest error of less than 10%. Normally, the dynamic weight of a train is considered to be 10% higher than its static weight, thus the results are considered to be in excellent agreement with the static weight. Consequently, Approach 4 is selected as an algorithm for dynamic weight measurement in condition monitoring.

Table 7. The results of the four approaches.

Error %	Approach 1	Approach 2	Approach 3	Approach 4
FBG 1, 2	11.51	12.51	14.39	12.48
FBG 3, 4	11.53	13.10	12.59	9.94

Up rail

Error %	Approach 1	Approach 2	Approach 3	Approach 4
FBG 1, 2	14.43	14.37	12.00	9.40
FBG 3, 4	12.36	12.82	12.34	9.74

Down rail

Derailment monitoring is possible with dynamic weight measurement, if weight balance is also assessed. Assessing the possibility of derailment is an important safety assessment, especially in negotiating curves and track twists. The likelihood of derailment depends on the condition of the tracks and of the vehicle. The former refers to deviation from train maintenance limits and their geometries, while the latter refers to the condition of the vehicle suspension system together with its wheel re-profiles. Checking of both conditions during off-traffic hours is necessary, unless an in-service [11] condition monitoring system is employed.

6.4 Results and Discussion for Weight Balance and Derailment Risk

Derailment [14] occurs when the wheel of a train leaves the rail. Derailment can be caused by a twisted track which is related to the combination of horizontal guiding force and the reduction of vertical loading on the leading wheel. Figure 26 shows a schematic of derailment while Formula (6.5) presents its mathematical expression.

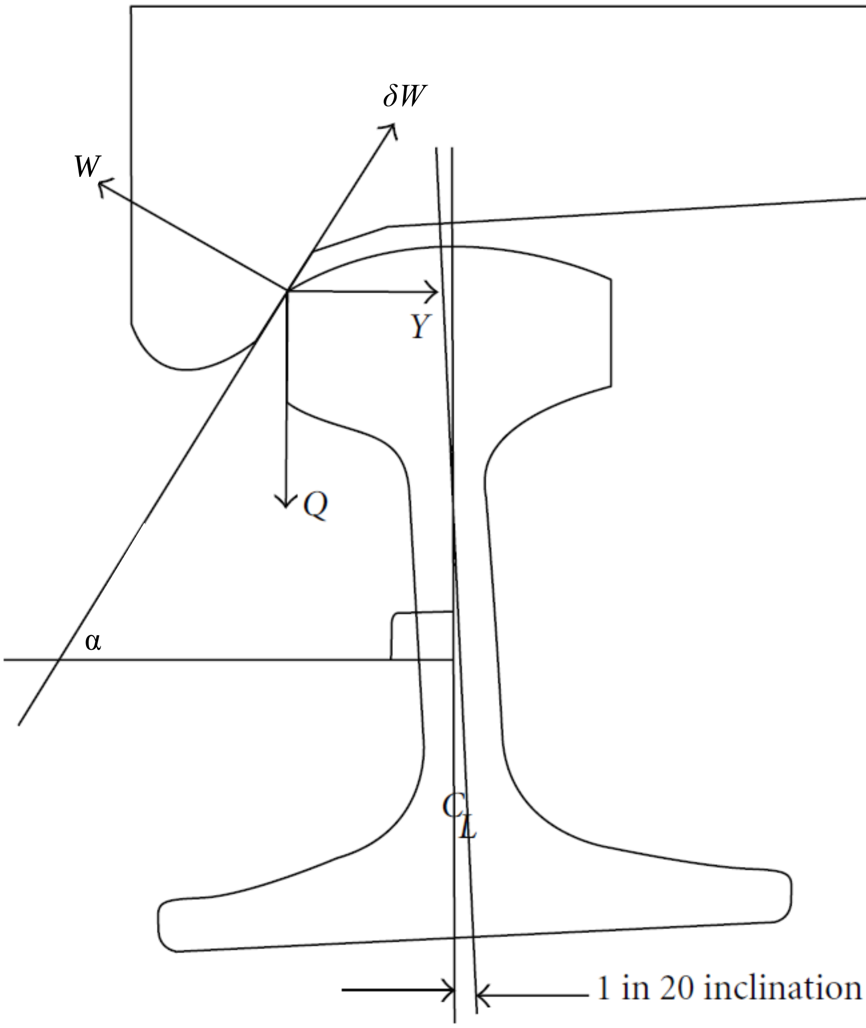

Figure 26. Schematic of Nadal limit for derailment at wheel/rail interface.

$$\text{Nadal limit} = \frac{Y}{Q} = \frac{(\tan\alpha\ -\ \delta)}{(1 + \tan\alpha)} \tag{6.5}$$

where

Y is the lateral force at wheel angle, *Q* is the vertical load on the wheel, α is the wheel angle at the plane of contact, *δ* is the frictional coefficient at the angle/rail contact point with *δW* as the frictional force [149].

When a force acts between wheel and rail, *W*, and *δW* as the reaction and frictional forces on the wheel flange are balanced by the *Q* and *Y* acting on the rail. The force vectors at the interface may lead to a situation when *δW* is too big for friction to bear and cause the guiding wheel to slide/climb over the rail, and cause a derailment. For safety reasons, a warning threshold, which is known as the Nadal limit (Y/Q) [150], [151] by the industry, has been developed to estimate the risk of derailment; and its detailed description is included in a standard named the Railway Group Standard GM/RT2141 [152]. Since the lateral force (Y) [76] has not been measured in this study, the Nadal limit cannot be identified. Consequently, the Off-loading ratio concept is proposed as an alternative solution for condition monitoring in this study. The Off-loading ratio is the absolute ratio of the difference between the loads on the two rails and their sum as shown in equation 6.6. Theoretically, the loads on the left and right hand rails are supposed to be identical. However, when derailment occurs or tends to occur, the two loads differ substantially, which can be considered as the appearance of a lateral force. Notwithstanding that the theory established is based on tracks in a straight line and thus not strictly applicable to curved tracks.

In negotiating curved and twisted tracks, a lateral force is inevitably present on the train wheels. Therefore, the wheel-sets have to be designed to operate within the Nadal limit even with adequate vertical loads. The force transferred between wheel-sets is important and has to be kept within the limit of 60% of the original load transferred as shown in Formula (6.7),

Off-loading ratio $$\frac{\Delta Q}{Q} = \frac{|(Q1 - Q2)|}{(Q1 + Q2)} \tag{6.6}$$

where $Q1$ and $Q2$ are the vertical loads from the two wheels in the same axle added to the rails.

Consequently, Formula (6.7) shows that the Off-loading ratio can be calculated from the dynamic weight as sensed by the FBGs [148] installed on the rails. It can be used as an important derailment factor in condition monitoring. Besides, the Off-loading ratio $\Delta Q/Q$, concerns only the relative ratio of the loadings, but not the absolute value of the weight. Therefore, any temperature effect is cancelled as the weight is measured at the same time.

6.5 Results and Discussion for Vibration Index

The FBG sensor network described in the previous section has been adopted as a means of train vibration measurement. The vibration waveform evaluated by a train giving a strong signal, is measured with a FBG, as shown in Figure 27. The cause of the vibration is investigated by comparing the noisy signal, as shown in Figure 27 (a), to a normal train healthy signal, as indicated in Figure 27 (b). According to Figure 27 (a), vibration is more significant in Car 6 and Car 8 (from the left hand side) as they produce noisier signals than the adjacent cars. Engineers would be alerted by the noisy signal in this case to pay special attention to the wheels of this train. Eventually, engineers would call for a checkup and measure the OOR [52] of the wheels, so as to also examine the relationship between wheel imperfection and the consequent vibration.

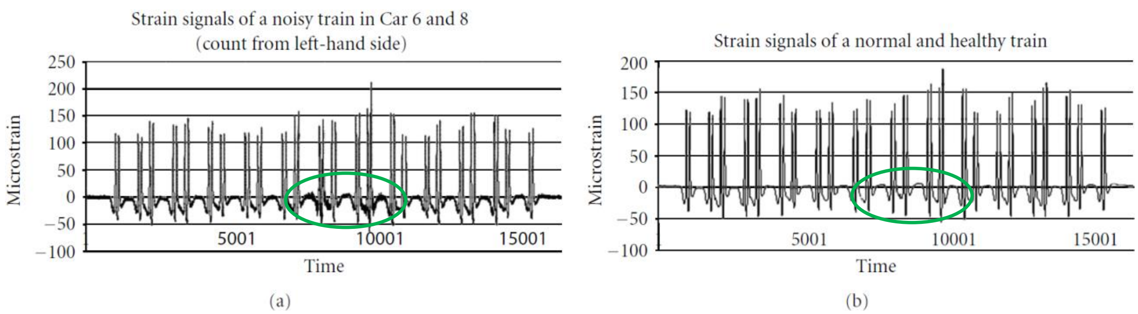

Figure 27. Strain measured by FBG mounted on the rails. (a) The FBG waveform of a train with noisy signal. (b) The waveform of a normal and healthy train.

Wheel imperfection is expressed in terms of roundness. It is a defect caused by flange pitting and wheel flats, producing what are known as polygonal wheels [52]. Wheel imperfections may cause uneven strains on the rail due to periodic impact forces. This interaction between wheel and track is the cause of vibrations. Wheel re-profiling [54], therefore, to reduce the OOR can be a solution. Deeper description is given in Chapter 2 Literature Review and thus is not discussed in detail here.

To prove that there is a correlation between vibration and wheel imperfection, a test on the re-profiling of noisy wheels was carried out. The wheel re-profiling was conducted at the depot. All eight wheels on the four axles of a car were removed and turned in a lathe as is normal maintenance work. A thin layer of material is removed from the wheel tyre during the re-profiling process until the wheels are round enough and smooth. The OOR readings are recorded using a dial gauge, before and after wheel re-profiling. In addition, wheel re-profiling was carried out on one of the two noisy cars, while the wheels of other noisy cars were kept unchanged as a control.

The test showed the correlation between OOR and vibration. Engineers attempt to relate inter-axial vibrations to wheel OOR mathematically, so that the imperfection of a wheel can be determined indirectly by measuring the inter-axial vibrations. Inter-axial vibration is the vibration on a rail between two bogies in a car. The vibration can be determined simply by measuring the dynamic strain on the rail. As such, in the first stage of the study, a mathematical expression was derived as a kind of index for reference purposes, based on the experience and knowledge of researchers. As more information becomes available later, the formula should be revised appropriately. The graphical expression for VI is shown in Figure 28, while its mathematical expression is provided below the figure.

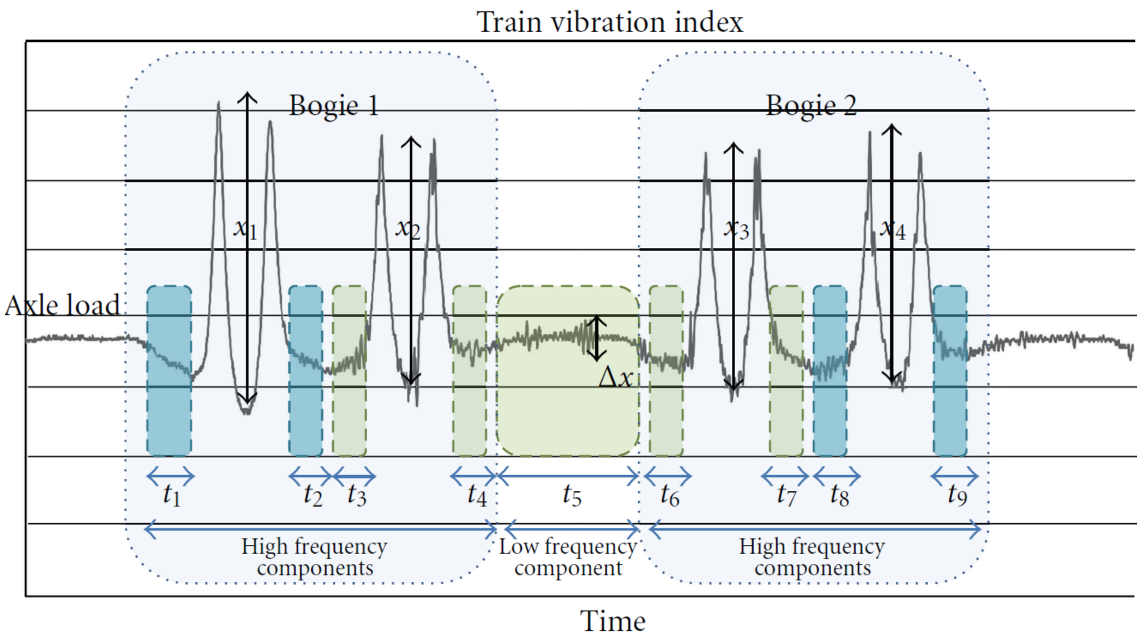

Figure 28. Wheel Out-Of-Roundness versus Vibration Index.

$$\text{Vibration Index (VI)} = \sum_{n=1\ldots9}^{n} K_n\, f\,(\Delta X_n\,/X_n\,,t_n\,) \tag{6.7}$$

where ΔX_n, X_n and t_n are the dynamic strain, the maximum strain, and the time duration respectively for the function f, where function f describes the overall vibration in the period of time t_n, and K_n is a weighting factor applying as appropriate to each component.

The weighting factor K_n concerns the mechanical conditions of the passing train, such as vibration in the traction system and the braking system. It has a unique value for each component and these values are used to normalize the final vibration amplitudes of a train. Consequently, they differ in the Motor Car and the Trailer Car, for instance. The values of K_n will be calibrated once sufficient data has been collected. This weighting factor is set to 1 at the early stage of the investigation and to be replaced by a calibrated value once available.

The Vibration Index (VI) for a car (with two bogies, i.e. four axles) is provided by Formula (6.7), indicating the changes of mechanical strain, which is dimensionless. VI is relative to car weight because a heavier car causes stronger vibrations for the same wheel OOR. The term X_n reflects this factor and cancels the effect of train weight.

Since wheels and track are close and make good contact during the periods t_1 to t_4 and t_6 to t_9 , they are expected to be the high frequency components. In contrast, when the wheel/rail interaction occurs far from the sensor, only the lower frequency components are measured, such as in the period t_5 as shown above.

From the measured data, it is seen that strong correlation exits between the OOR and vibration. Figure 29 shows the VI values obtained from a noisy train. The local vibrations, such as those in Car 6 and Car 8 (counting from the left) of Figure 29, have VI values higher than 1.5, while those for other cars are 1.1 or below. The wheels of Car 6 were re-profiled to correct the OOR, while the wheels of Car 8 were left alone to serve as a control. OOR values after re-profiling are between 0.05 and 0.07 mm.

The FBG wavelength after wheel re-profiling, reflects the strain pattern of the train as shown in Figure 30. The vibration in Car 6 has been reduced to a normal level after wheel turning, while the vibration in Car 8 persists. By comparing Figure 29 to Figure 31, the VI of Car 8 (unturned wheels) remains high at around 1.9, while the index for Car 6 (re-profiled wheels) is substantially reduced from 1.8 to 0.8. This result proves that the FBG strain sensor is effective for distinguishing wheel OOR by measuring the vibration in the rail.

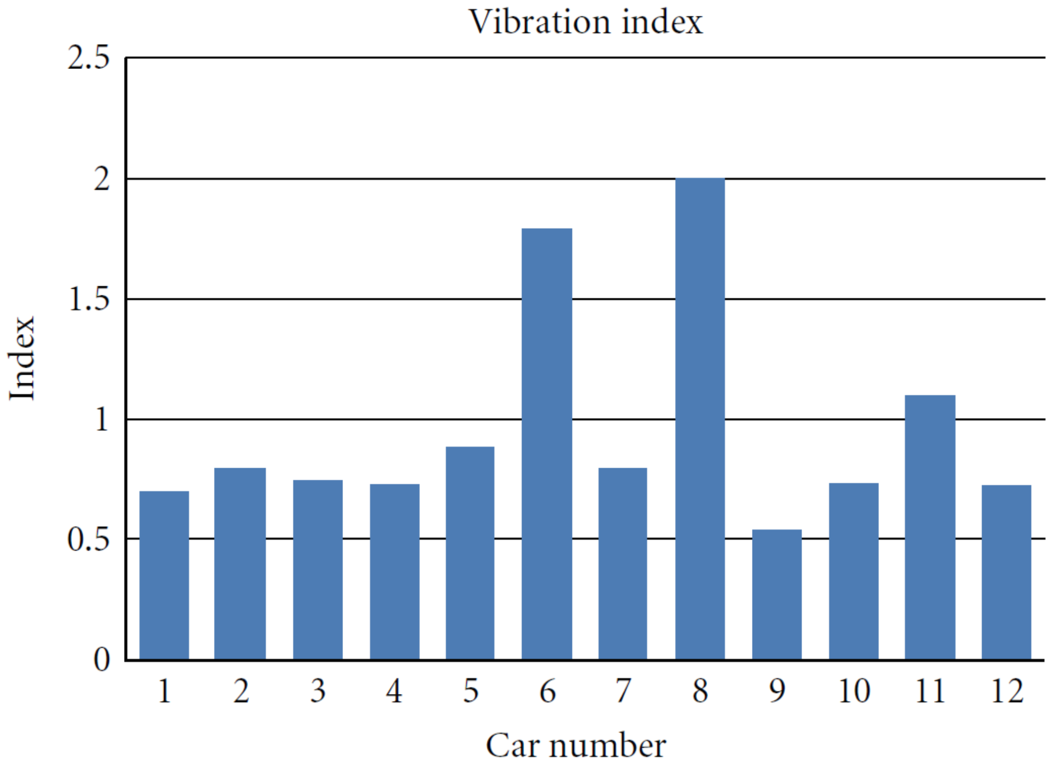

Figure 29. Vibration index of a noisy train with Car 6 and Car 8 higher than the others.

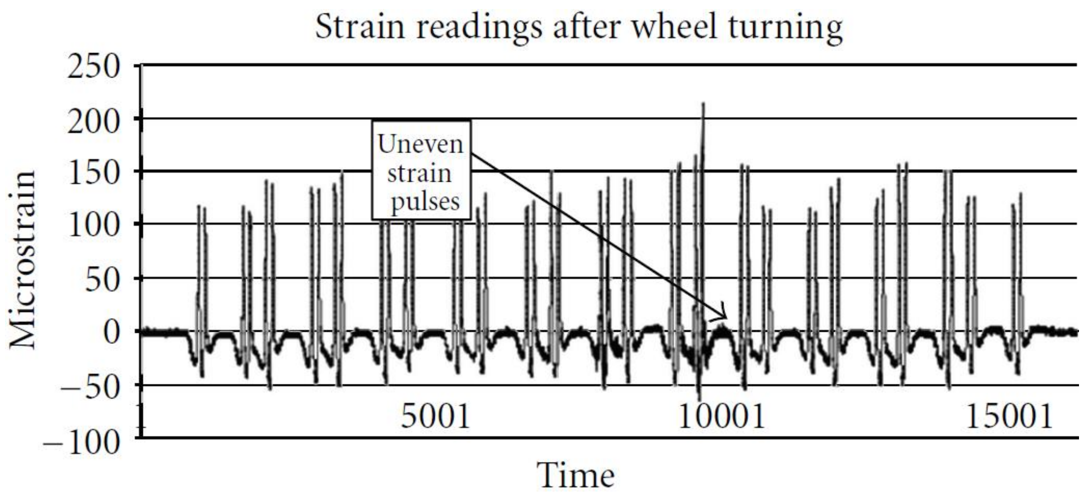

Figure 30. The vibration in Car 6 is reduced to a normal level after wheel re-profiling, while Car 8 remains unchanged and keeps noisy.

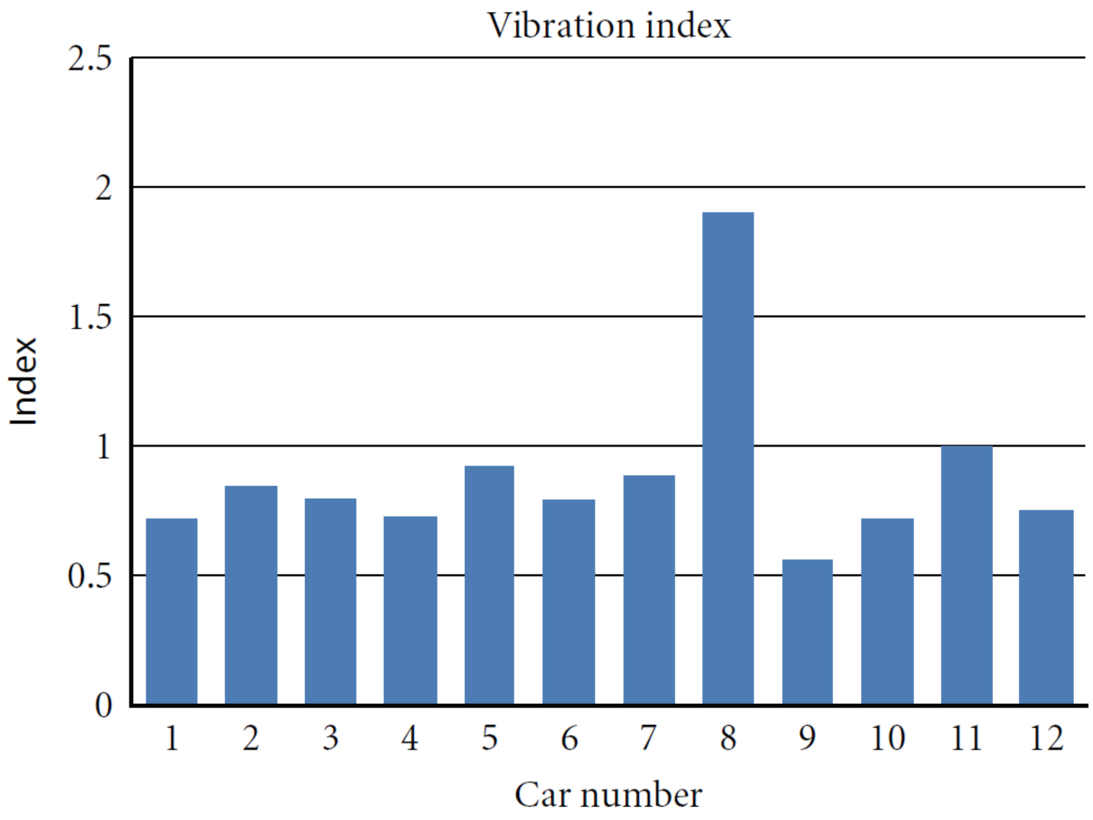

Figure 31. Vibration index after wheel re-profiling, Car 6 reduced while Car 8 remains high.

6.6 Chapter Summary

In this chapter, it explained how the dynamic weight of a train and the vibration induced by the OOR of the wheel are measured by FBG sensors. The sensor network arrangement and experiments to acquire test data are reported using charts and graphs. Mathematical expressions for the calculation of VI and dynamic weight are given. Four approaches for verifying and determining the best algorithm for dynamic weight calculation were proposed and evaluated. The best approach was identified, with the highest accuracy, with only 10% error, among the four proposed approaches. A test to identify the correlation existing between the vibration and OOR in train wheel is presented. The result shows that the relationship is strong and can be used for real-time condition monitoring to determine the OOR of the wheels at any time. The Off-loading ratio is proposed as a replacement for the Nadal limit which, though useful in condition monitoring for derailment estimation for a straight track it is not applicable to a curved track.

Chapter 7 **Smart Railway Health-Condition System**

7.1 Introduction

A Smart Railway Health-condition Monitoring (SRHM) system, for use in this research, is introduced as a case study for long-term and real-life condition monitoring with a VI sensor. The SRHM system was installed on trackside functions at a platform and foundation for the development of railway applications. The arrangement includes a FBG sensor network, RFID tags [31], [32] on trains, and the modular software system is shown in Figure 32. Since the SRHM is aimed at long-term condition monitoring for the entire fleet with many more objectives than an one-time test, the data in terms of volume, variety and accumulated information are massive in quantity. Thus, the Big Data concept with its sophisticated algorithms and processing power was employed to serve these goals.

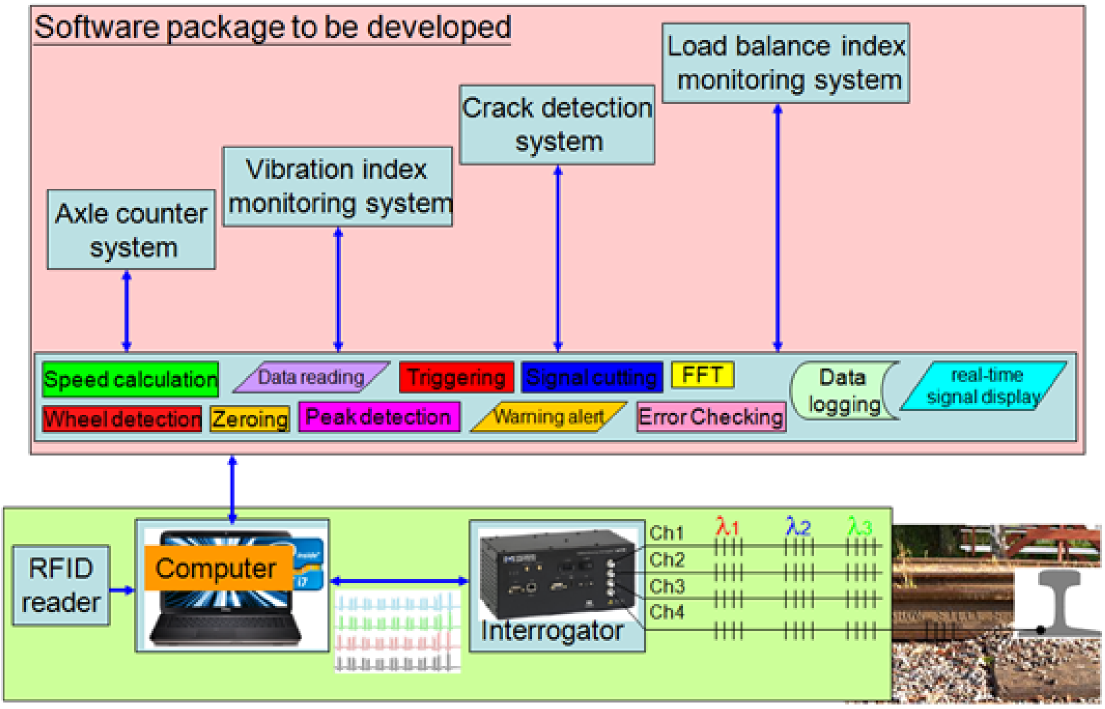

Figure 32. SRHM System with modular program for different sensors and algorithms. RFID and FBG sensor network are connected to form a system.

The sensor network was installed on the track with RFID by its side while the interrogator and processing system were remotely located in a depot or station. The functions of the modular program not only included the sensors algorithms, but also included the signal processing and Data Mining [17], [154] tools such as filtering and peak detection. These functions speed up the research activities and enable more research work to be done. Some modular programs are presented as flowcharts in Appendix F.

7.1.1 Critical Components for Railway Condition Monitoring

Monitoring the health condition of a railway system can be realized by monitoring the critical components such as track/rail, wheels and bearings. These components are critical because they are the most significant causes of potential derailment accidents resulting in human casualties. Relevant research and statistics surveys reported are dominated by these three components [155] as shown in Figure 33. This reveals that these three components contribute 28%, 7% and 6% respectively to all relevant accidents. That means most of the causes of derailments are related to just a few critical components. Therefore, as long as the defects in these critical components can be identified by the condition monitoring system properly, most accidents could be reduced or even avoided.

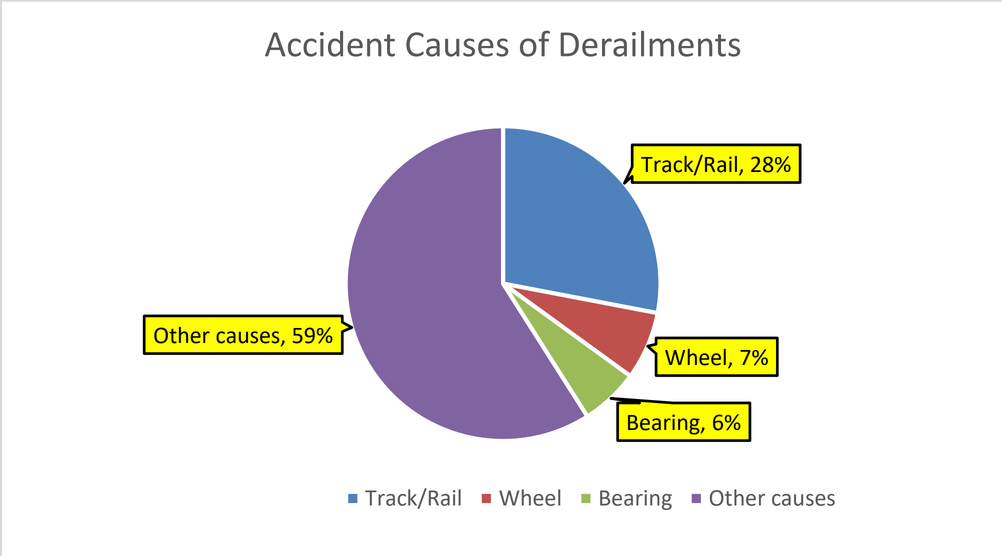

Figure 33. Distribution of accident causes of derailments. Three critical components, Track/Rail, Wheel and Bearing contribute 41% of the occurrences.

Apart from track/rail, wheels and bearings, the gearbox is also a critical component for condition monitoring in railway. Although this component is not the direct root cause of derailments, its failure also leads to significant economic losses and longer repair times. Thus, the gearbox is also discussed in this chapter.

Since the critical components are the dominant cause of railway incidents, researches on the correlation between sensor-based measurement and health conditions have been conducted. There are different criteria for monitoring critical components and each criterion would require different techniques. The criteria selected for discussion here are due to their ubiquities. Below are the detailed descriptions of the sensor-based measurement techniques that are commonly utilized in health condition monitoring.

Track/rail deficiencies commonly include rail cracking, deformation (symmetricity) and corrugation. Cracks on rail may directly cause train derailments. Wheel or rail deformation and rail corrugation can cause serious vibration and even resonance which can damage the train structure. Ultrasound or acoustics techniques that employ piezoelectric transducers and accompany with signal processing are usually used to monitor track/rail.

For wheels, OOR causes vibration to the train, it is one of the common defects and its severity usually grows with mileage. Displacement techniques are employed for measuring depth (also height) of the OOR on the wheel tyre. Displacement measurement is performed offline that uses dial gauges, whereas the vibration measuring technique is performed in-service by using accelerometer, strain gauge or FBG sensors.

For Bearings and Gearboxes, the defects, measurement techniques, signal processing methods and transducers used are very similar to each other. Cracks and pitting of the material are the symptoms to be monitored. Oil analysis [156], vibration, sound, temperature and even motor current are commonly used as measurement parameters. Oil analysis is used to be carried out offline in the past but can now be done in real-time with embedded sensors [157] Both time domain and frequency domain analyses are suitable and can be applied in combination to increase inspection accuracy. Transducers, including accelerometer, strain gauge, FBG, temperature transducers can be used to conduct this analysis.

Table 8. Sensor-based measurements for health conditions of critical components in railway system.

	Track/Rail	Wheel	Bearing	Gearbox
Defect:	Crack, deformation (symmetricity) [158] , Corrugation [159]	Out-of-round [52], [53]	Balls/Roller pitting, crack [82]	Crack, pitting [17], [160]
Technique:	Ultrasound, Acoustic [161], [162]	Displacement, Vibration [52], [53]	Oil analysis, Vibration, sound, temperature, motor Current [156]	Oil analysis, Vibration, sound, temperature, motor Current [17], [163]
Signal processing:	Time delay of waves in reflection and direct wave [161], [162]	Time domain analysis [53]	Time and Frequency domain analysis [82], [164]	Time and Frequency domain analysis [17], [160]
Transducer:	Piezoelectric transducer	Dial gauge, accelerometer, strain gauge, FBG	accelerometer, strain gauge, FBG, temperature transducer	accelerometer, strain gauge, FBG, temperature transducer

To summarize, health condition monitoring for critical components of a railway can be performed using sensor-based measurements. Defects such as cracks, corrugation, pitting and OOR that indicate the health condition of railway can be measured by different techniques including ultrasound, displacement, oil analysis, vibrations, sound, temperature as well as motor current as summarized in Table 8. Transducers include piezoelectric, dial gauges, accelerometers, strain gauges, FBG and temperature sensors can be used in combination to conduct the measurements.

7.1.2 Vibration –Wheel/Rail Interaction

Wheels and tracks are the most significant components contributing to derailments. Thus, monitoring their condition may enable accidents to be reduced. The vibration symptom provides an early warning as seen in the P-F curve [23]–[25] introduced in Chapter 2. Vibration is the result of wheel/rail interaction [76], [165], [166] as a train travels along OOR provides one of the most significant contributions to vibration [20], [52] of the wheel. Consequently, vibrations can be used to detect the OOR condition and conduct reliability analyses [167].

7.1.3 Vibration -Change of Mechanical Strain

The concept of VI proposed in this research, is to provide a value showing the amplitude or the strength of mechanical vibration measured in the rail as shown in Figure 34. This actually represents the change of mechanical strain [41] in the material of the rail. Strain is a physical deformation phenomenon in the material, measured as the change in length per unit of original length. The top and the bottom sections of the rail are the most strain sensitive areas according to computer simulations and experiments [20]. However, the bottom of the rail is not suitable for measurement purposes as the FBG can be damaged if it touches the ground. The top of the rail is obviously also unsuitable. Hence, the lower part of the rail is selected for safety and easy access purpose.

One of the causes of stress in the material is the vibrating wheel loading. Strain can be measured using FBG [4], [6], [41], but alternative solutions are available such as electronic strain gauges [39], mechanical strain gauges [168] and slow light (time delay) in optical fiber [42], [169]. The definition of mechanical strain is given by Formula (7.1):

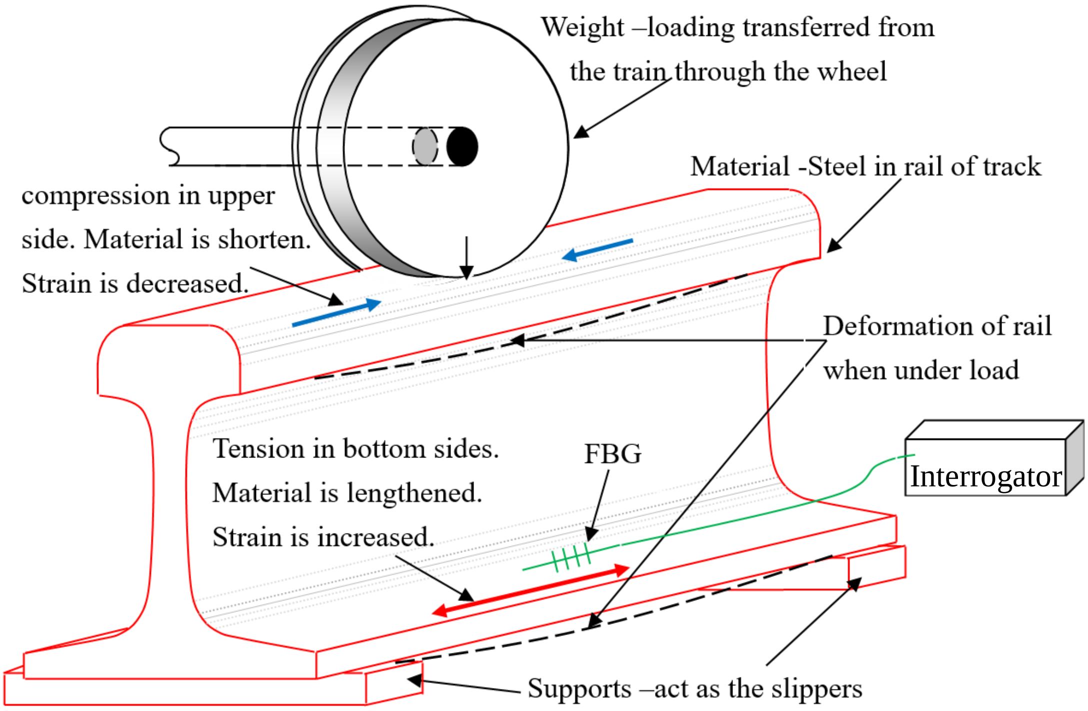

Figure 34. Strain is a measure of deformation. Vibration is a change of strain. FBG sensor is installed on the lower part of a track for vibration measurement.

$$\text{Strain} = \frac{\text{change of length}}{\text{original length}} \tag{7.1}$$

7.2 Signal Processing and Data Validation for Data Mining

Data Mining is the process of extracting useful information from raw data and other information according to the definition in the Cross-Industry Standard Process for Data Mining (CRISP-DM) [170] model. The information extracted can be characterized according to different levels of "depth/complexity" [171]. Data Mining is one component in the information system of Data, Information, Knowledge and Wisdom (DIKW) [172]–[174]. In this study, the information involved concerned only the first three levels of (1) wavelength of sensor as Data [1], (2) VI as Information

[20], (3) the train health condition as Knowledge [154]. Although the DSS provide information to facilitate decision-making, it needs human assistance. Thus, there is not really any wisdom at this stage.

In this study, the useful information was extracted using Data Mining technology including train speeds, number of axles, VI values, and train information. To perform Data Mining most effectively and accurately, the ranges of the different types of parameters should be wide. In addition, suitable signal processing and data validation processes should be employed to ensure the result is reliable. Signal processing adopted in this project included different techniques which will not be discussed one by one here, but only those commonly used such as filtering, peak/valley detection [175], [176] and frequency analysis.

7.2.1 Signal Filtering

The signal filtering of a vibration waveform is demonstrated in Figure 35, which displays wavelength raw data from four FBGs installed on a track. The upper two waveforms relate to a pair of FBGs installed in the same position on left and right hand rails on a track, as can be seen by their synchronous peaks. The lower two relate to another pair of FBGs with a delay which relates to the distance between two axles in a bogie. All four waveforms look noisy and need signal processing before peak detection. More raw data waveforms for train wheels deriving from the four pairs of FBGs are plotted in Appendix E for reference.

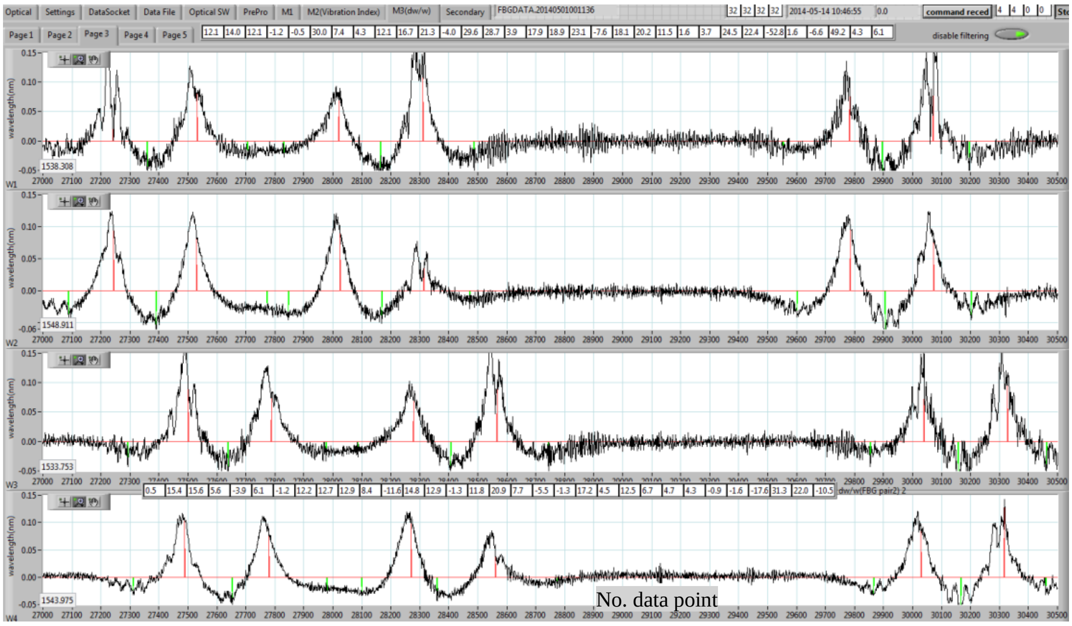

Figure 35. Noisy raw data of wavelength from FBG sensors.

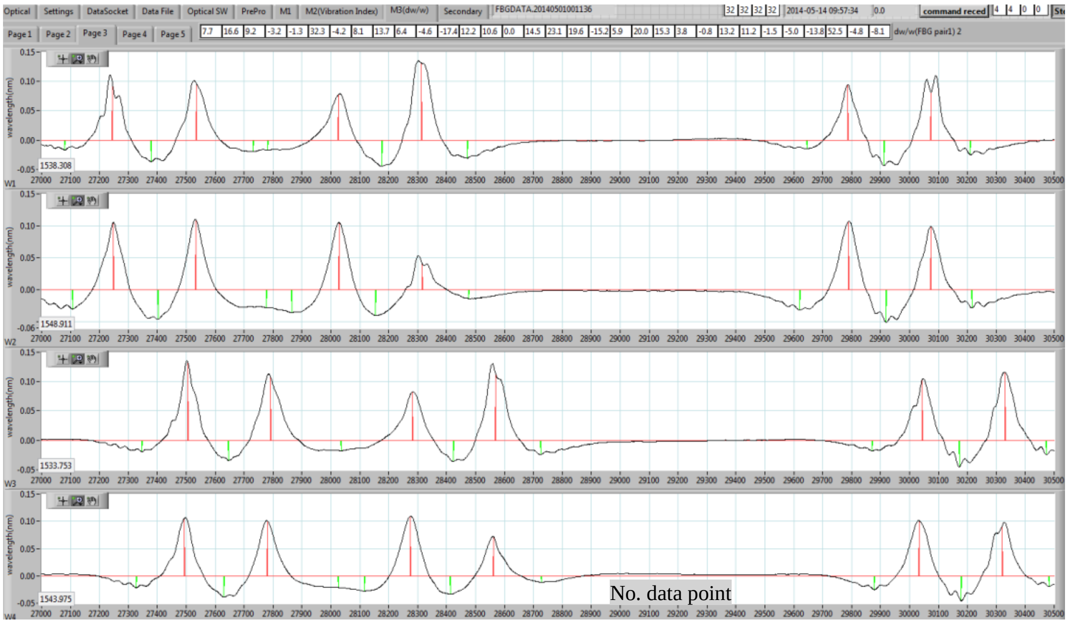

Figure 36. After signal processing, the filtered raw data become smoother.

Signal filtering suppresses unwanted frequency components while letting other components pass through. It is used to remove high frequency noise so that the low frequency peaks generated by the wheels can be detected more easily. To do so, a 30 Hz Low Pass Filter (LPF) was designed for the system. After filtering, the waveform is smoother as shown in Figure 36. Filtering is one of the steps of data "cleaning" [177].

7.2.2 Frequency Response of the Vibration Index

The signal frequency spectrum can also be investigated, although the VI calculation covering all frequency spectrums obtained by Fast Fourier Transform (FFT) is shown in Figure 37. The high amplitude response spectrum is at the low frequency side at around 50Hz to 250Hz.

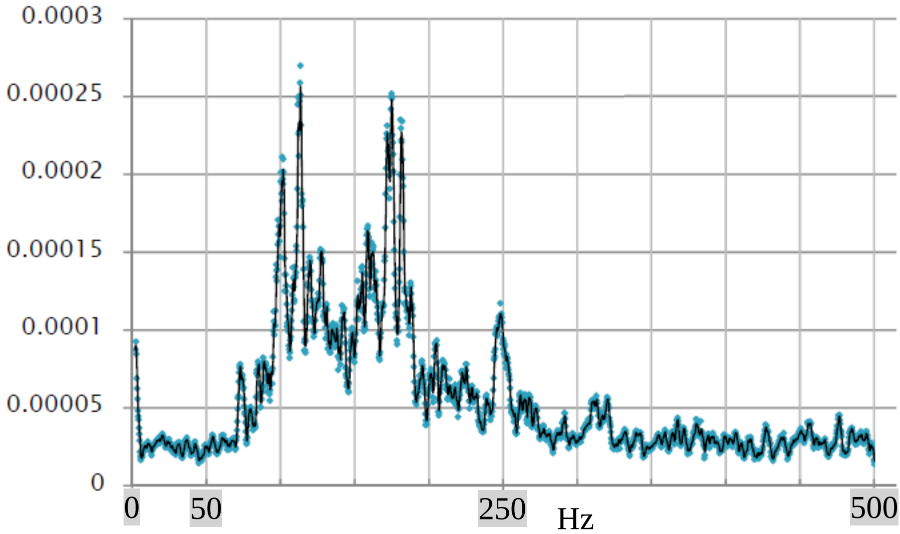

Figure 37. Frequency domain presentation of vibration at wheel/rail interaction. The amplitude is relatively high before wheel re-profiling.

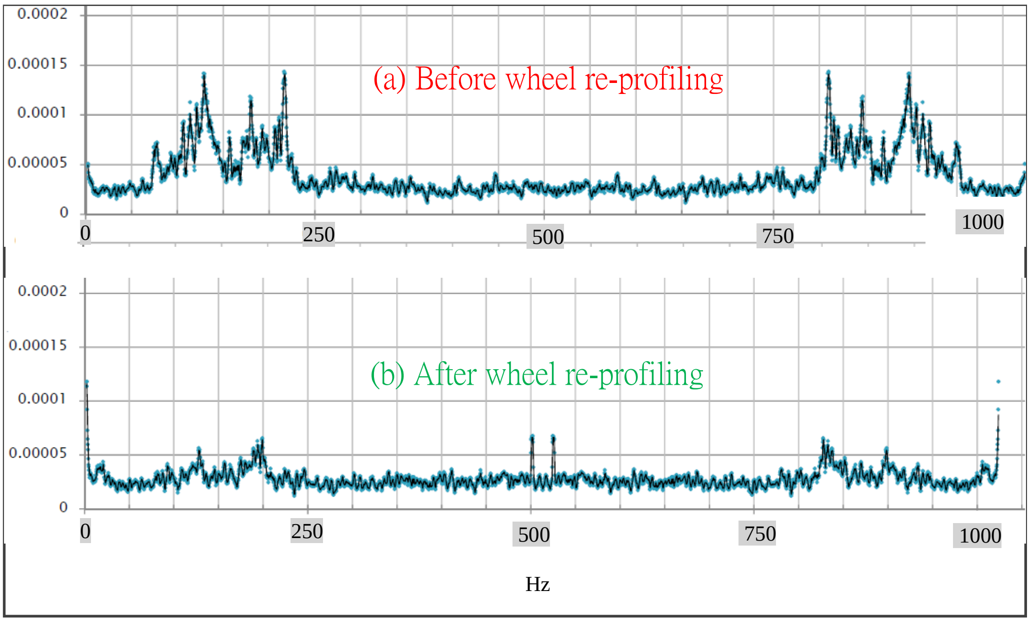

Figure 38. Frequency domain of raw data in vibration due to wheel/rail interaction. Frequency content (a) higher amplitude before wheel re-profiling (b) lower amplitude after wheel re-profiling.

After wheel re-profiling, the overall amplitude dropped significantly with no obvious shift in frequency as in Figure 38. That means a frequency shift cannot be used to determine the cause of the vibration in this case such as the OOR. This is also the reason why the VI calculation covers all frequencies in the spectrum. Figure 38 (a) shows the frequency spectrum before wheel re-profiling with relatively high amplitudes, while Figure 38 (b) shows that after wheel re-profiling, all the frequency components of high amplitude dropped significantly to lower level amplitudes.

7.2.3 Peak and Valley Detection

Peak detection correctly identifies peaks so that the inter-axle area can be identified for vibration calculation. After data cleaning, peaks/valleys detection [44] is enabled. Peak detection is performed by one of the modular programs [44] in the system. A successful output with 32 peaks (red spots on top) and 32 valleys (green spots at the bottom) in the waveform is shown in Figure 39. The number of peaks and valleys are correctly detected and matches the number of wheel axles.

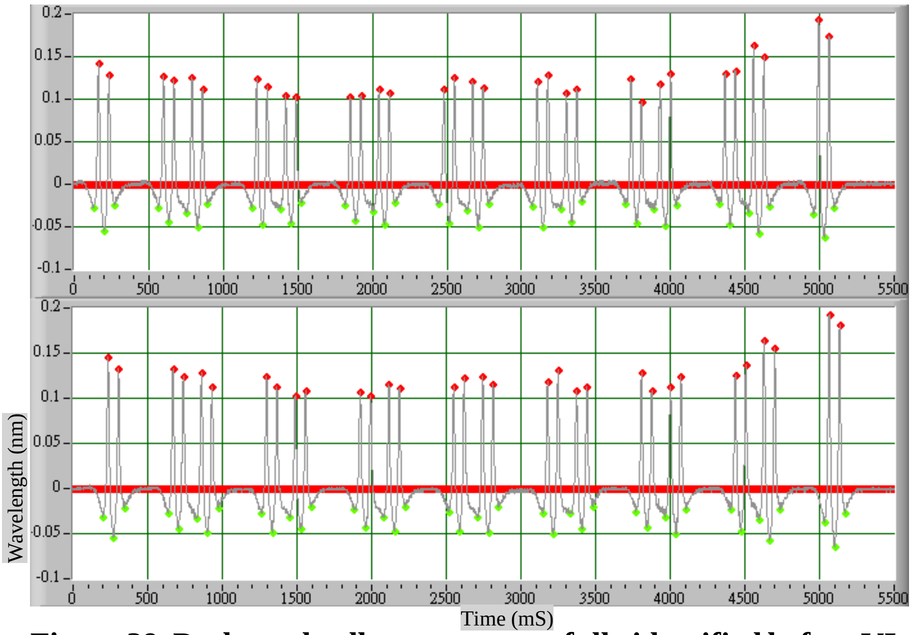

Figure 39. Peaks and valleys are successfully identified before VI calculation. The upper and lower windows show the waveforms caused by the wheels on the left and right hand rails.

7.2.4 Data Validation

Data validation is a process checking the accuracy and quality of data before its utilization [178]. The properties of data and the relationships between data are useful information relating to the performance of data validation. Train RFID data is useful for data validation as it provides deeper information about the train such as the number of wheels, function of a train (e.g. engineering train, passenger train) and the speed of travel. Actually, all trains have RFID tags installed in each car, called Electric-Multiple-Units (EMU), for adjusting the combinations and length of a train in the old days [179]. Luckily, adjusting is not needed today as the length is fixed. The RFID tags used here are of the active type with a built-in battery enabling faster response and larger transmission distance [180].

The parameters to be used for data validation in this project include (1) train speed, (2) number of wheels, (3) peak amplitude, and (4) time of travel. Furthermore, mutual comparisons between adjacent sensors and the output waveforms are also parameters for data validation. Appendix B lists the waveforms of all four pairs of FBGs for reference.

7.3 Data Ming for Railway Condition Monitoring

In this research, the outputs of Data Mining provide information meaningful to people, as described in Chapter 2. They are easy to understand and used by humans. As this project relates to railways, all findings are related to railway parameters including settlement level, train weight and axle counts as introduced in previous chapters. In addition, the train speed, the attendance of a train for service, and the VI extracted in Data Ming processes are described below.

7.3.1 Condition Monitoring Parameter –Train Speed

Train speed is a common but important factor which must be monitored. Train speed relates to the type of a train, such as passenger train or engineering train. Speed rises and falls at different parts of a journey. In addition, the speeds of all wheels are supposed to be the same. These rules can be used to build a condition monitoring expert system to increase system reliability via the Data Mining technique. Extracting train speeds is relatively simple and straightforward by finding the time delay between peaks in the waveforms generated by wheels. The time delay is then correlated to the actual distance between sensors as shown in **Error! Reference source not found.** a nd the mathematical expression is for train speed shown in formula (7.2). The calculated result is consistent with the normal operating speed of 70 km/h.

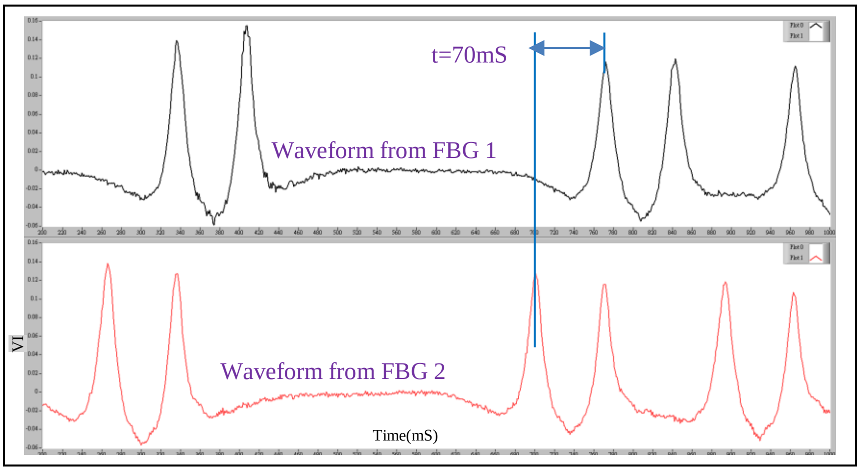

Figure 40. Time delay between two peaks in waveforms of FBG 1 and FBG 2. Speeds of wheels in a train are found automatically by the system.

The formula for the speeds of all wheels in a train is expressed as follows:

$$\text{Velocity} = D/T \tag{7.2}$$

V = 1.5m/70mS

=21.43m/s

Speed = 21.43*3600

= 77.15km/h

Where D is the distance between two sensors in meters and T is the time delay in seconds.

7.3.2 Condition Monitoring Parameter –Maintenance Schedules

With enough data and techniques, some more meaningful and useful information can be extracted easily. Maintenance schedules can be monitored by the SRHM as shown in Figure 41. Maintenance work took around 7 days from 3rd Oct to 10th Oct. As a result, the VI values dropped from high to low as shown.

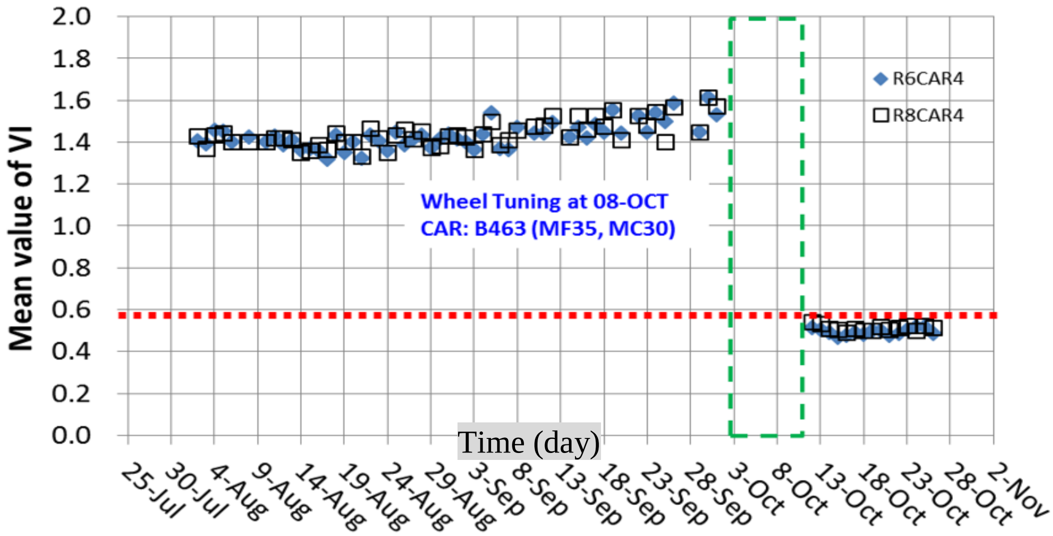

Figure 41. Maintain schedule of a train was monitored by the SRHM system with a 7-days gap VI values. The VI values dropped after maintenance.

7.3.3 Condition Monitoring Parameter -Vibration Index

A previous VI version is introduced in Formula (6.7) in Chapter 6. The reason for a new version here, the Formula (7.3) is because more simplicity is needed for a large volume of data and faster calculation as a Big Data project. In addition, the significance of the coefficients such as weighting factors in Formula (6.7) are still not clear at the moment. Therefore, a much simpler version is proposed. After enough data has been collected, Formula (6.7) will be loaded for calculation and verification later, as a means of calibration to determine these coefficients.

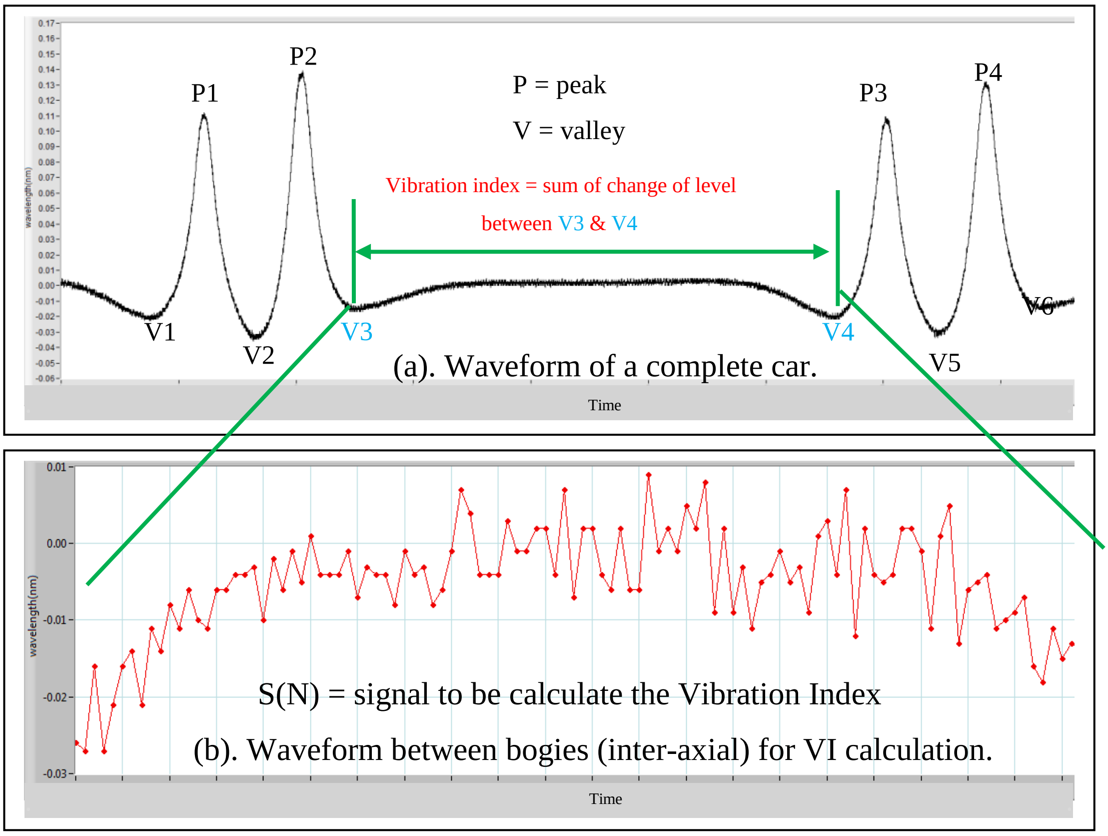

Figure 42. (a) is a waveform of a car and (b) is a section of waveform extracted for calculation of VI.

$$VI = \sum |S_n - S_{n+1}| * 1000 \qquad (7.3)$$

Where: n is the index of samples in the signal, Sn is the nth sample of the signal.

A simpler vibration calculation version is indicated in Figure 42 (a) with a waveform of a car showing the peaks of the four axles in the two bogies clearly identified. The waveform between bogies (inter-axial) [44] is extracted for VI calculation as shown in Figure 42 (b). Actually, the peaks and valleys help in identifying the inter-axial waveform where the signal exists of interest for vibration monitoring. However, peaks and troughs can cause errors too. The formula (7.3) for calculating VI actually gives the variation between data points, which can be interpreted as the energy of the vibration. This formula also covers all frequencies below the sampling frequency of the data acquisition system. For consistency in calculation, the sampling rate has to be the same, that is 1 kHz. If the sampling rate is higher, a scaling down is necessary.

Furthermore, although vibration can be measured by accelerometer, the size of the accelerometer makes it dangerous for installation on the track. As the purpose of VI is to monitor the health condition of trains, an index number is sufficient at the moment.

During this research, the VI values for the complete train is calculated immediately the train leaves the sensing point. Figure 43 (a) shows the waveforms for a complete train derived from the FBGs on the left and right hand rails, represented by black and red colors respectively. Figure 43 (b) shows the corresponding VI values. The reliability of VI can be checked by observation and by relating the high and low VI values to the noisy and smooth waveforms. The VI values on the left and right hand sides are usually similar, but with significant variation in the case of some pairs. In this train under test, the VI value in the third car at the right hand rail is higher than on the left. This is a sign that health screening is needed during the next maintenance. More SRHM system outputs with VI values and vibration waveforms are listed in Appendix A for reference.

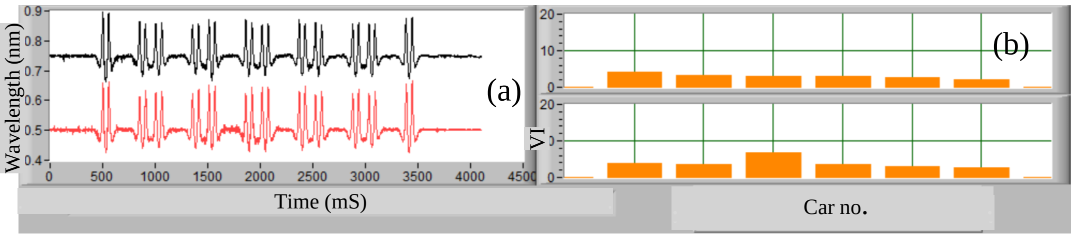

Figure 43. (a) Wavelength waveforms of a complete train with both left and right hand rails. (b) The corresponding VI values.

7.4 Result and Discussion

Nearly a year (360 days) of long-term testing took place, after the SRHM system was established. The real-life data is illustrated in Figure 44. Results are missing between days 56 and 60. The data are related to a 30-train fleet. Detailed discussion and evaluation of these data is given in Chapter 8.

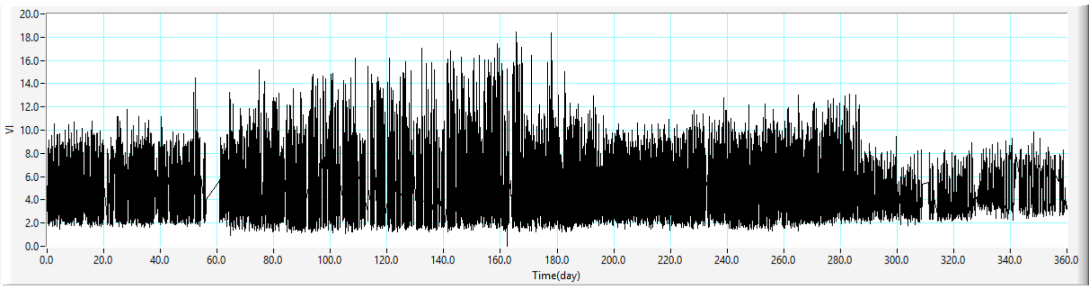

Figure 44. VI values of a real-life testing with 360 days' long-term evaluation.

7.4.1 Long-Term Verification

During this year of investigation, data from all trains passing through the test point were recorded. For these trains which had just finished maintenance, including wheel re-profiling, the VI values dropped from high to low as indicated in Figure 45 and Figure 46. Some wheels were re-profiled more than once within the year. For most of the wheels re-profiled, VI values dropped significantly. To evaluate the performance, the VI values before and after wheel re-profiling have been compared. Among the 33 pairs of wheels, 24 dropped to a low value while the remaining 9 showed no significant changes after wheel re-profiling. The effective success rate is 73%. Hence, the effectiveness was high and convincing at this early stage of the research.

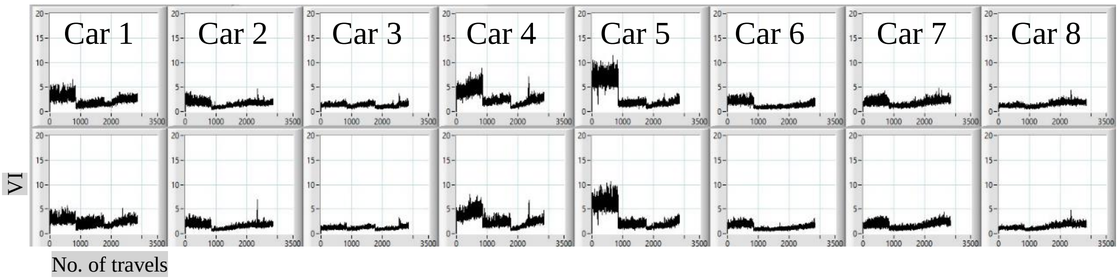

Figure 45. Historical VI values of a train for 280 travels. VI values dropped significantly in Car 1, Car 4 and Car 5, and less significant in Car 2, Car 6 and Car 7 while not significant in Car 3 and Car 8.

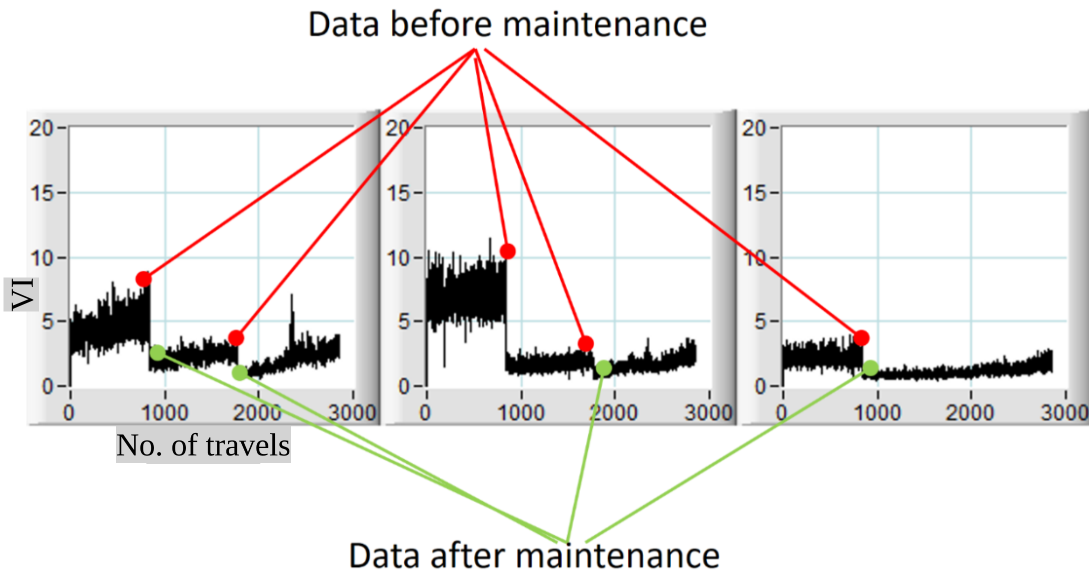

Figure 46. VI values before and after maintenance (wheel re-profiling) of a wheel for 280 travels. The VI values dropped after wheel re-profiling.

7.4.2 Development of Vibration Index

The developments over time of VI values for a wheel are shown in Figure 47. The steady increasing growth rate in formula (7.4) is a sign of concern. If the VI grows at an increasing rate, a high value is reached in a shorter time even though it may be low now. Thus, other than the amplitude, the mileage travelled is also important. Note, the mileages of each train are different depending on their daily usage. The graphs of VI values, showing changes from high to low are shown in Appendix C. The lowest values are showing in Appendix D.

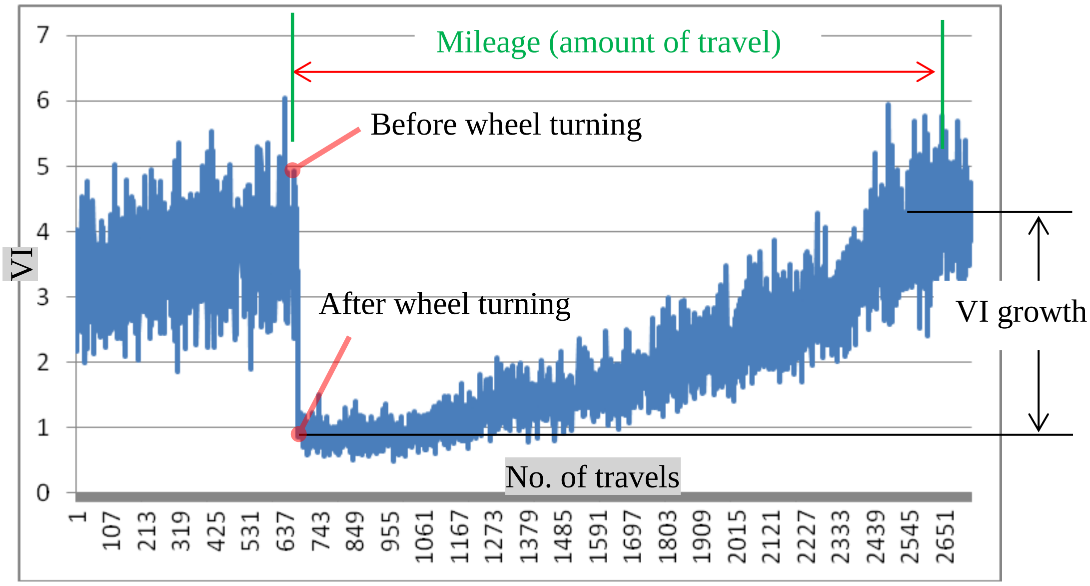

Figure 47. The growth of historical VI values of a train in 265 days.

$$GR = G/Mileage \tag{7.4}$$

where GR is the growth rate of VI in a car, and G is the absolute growth of VI.

According to the failure curve, different mileages could relate to different failure rates and hence failure rate may be affected by vibration amplitude. Thus, both the initial mileage and relative mileage after each wheel re-profiling should be considered for evaluation.

7.4.3 Data and System Integrity

Data and system integrities are defined by their accuracies. During the development of a condition monitoring system, both data and the system may contain errors. Thus, checking accuracies is a way to control errors and improve accuracies. The more the system is understood, the more the properties can be used for integrity checking.

Symmetry is also a property related to data integrity checking. The pair of sensors installed on the left and right hand rails on a track is an example, as shown in Figure 48. The data deriving from a pair of sensors should be very similar. If the data were to fluctuate suddenly on one side but not vary on the other side, this is a signal of data error in one of the FBGs. Pair 2, as in the lower row of Figure 48, shows a few red spots on the upper left hand corner. The other three pairs demonstrate mutually agreed and consistent results.

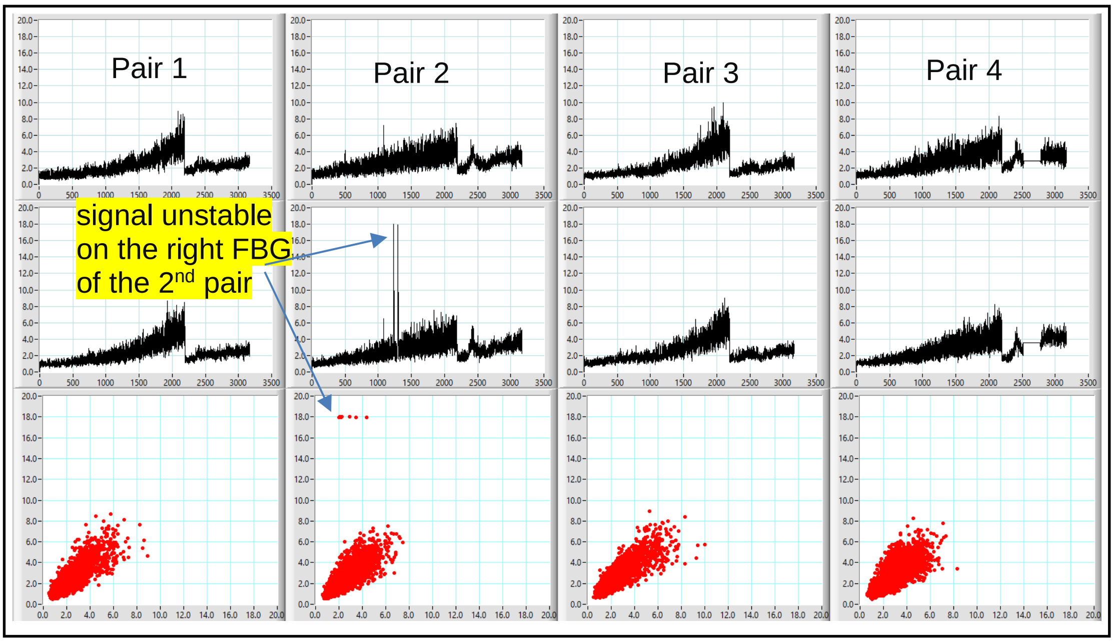

Figure 48. Historical VI (y-axis) vs No. of travels (x-axis) of a car from four pairs of FBG sensors on the upper two rows. Bottom row is their X-Y plot to show their integrities.

The VI values are correlated to the weights of different cars, as in Figure 49 for a typical train. The figure shows that heavier cars usually have higher VI values. A graph displays the VI values for the cars of 30 trains in Figure 50 showing this effect. The relationship can be used as a rule for data integrity checking. The VI values supposedly take similar patterns and are consistent for most of the trains, except for those with wheels newly re-profiled. Where patterns are very different, further inspection may be needed of both the train and the system because the problem could lie with either one.

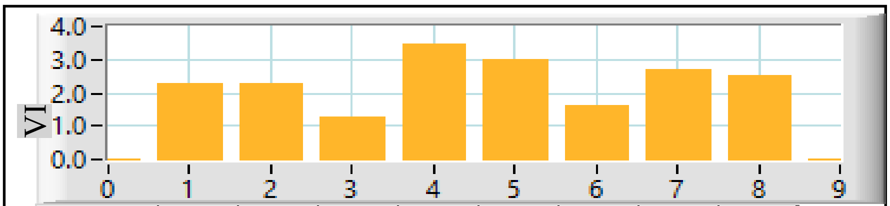

Car no.:	Car 1	Car 2	Car 3	Car 4	Car 5	Car 6	Car 7	Car 8
Function:	Driver	Motor	Trailar	Motor	Motor	Trailar	Motor	Driver
		pan			pan		pan	
Weight(T)	46.1	42.35	36	39.1	42.9	35.75	39.06	63.45
pan=pantograph								

Figure 49. VI values versus the weights of the cars in a train.

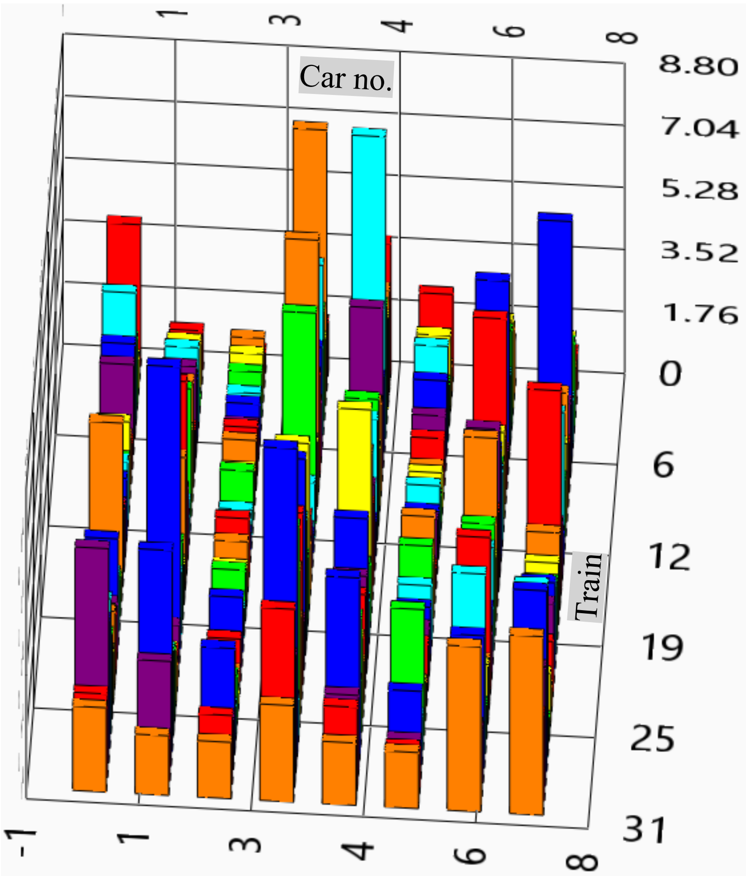

Figure 50. VI values versus the weights of the cars in 30 trains.

7.4.4 The 3A-Warning System (Accept, Alert and Alarm)

For convenience is relating VI values to technical personnel and the public, a simple warning system should be developed. Based on historical VI values for a fleet, a 3A-Warning system, that is Accept, Alert and Alarm is derived below:

Assumption: 90% of maintenance works performed were satisfactory. As the annual report quoted that service quality is 99.7% train punctuality and 99.9% delivery [38], a higher performance rate should be used for estimation of the maintenance quality.

Therefore, if 90% of the population have lower VI values (3.1 or lower) after wheel re-profiling, the train is regarded as "acceptable" as illustrated in Figure 51. The **first line** Alert (orange color) is drawn at a point of 90% of the population **After** wheel re-profiling, with a VI value of 3.2. The **second line** Alarm (red color) is drawn at a point of 90% of the population **Before** wheel re-profiling, with a VI value 6.7.

Hence, in the 3A-Warning system, the VI values are divided into three regions:
Alarm: 6.7 or higher
Alert: 3.2 to 6.6
Accept: 3.1 or lower

The warning system is only a reference for simplicity, but a convenient sign indicating when the management team should pay attention to vibration on a train. The bigger picture needs to be explored before any action should be taken or conclusions drawn about this train because there could be local variations within the historical VI values. In addition, from the just before wheel re-profiling curve in Figure 51, 90 out of the 163 samples have VI values below 3.2. That is 55.2% of wheels before maintenance were below the Alert line. In other words, re-profiling of those wheels is not necessary, time and resources can be saved.

Figure 52 is displayed as a case study of the application of the 3A-Warning system. The curve values vary from 1.5 to 8 at an increasing rate. It then drops to a 1.8, lower level. The first time VI reaches a lower limit of 3.2 is at the data point 700 and the growing trend then continues. The upper limit is reached at data point 2,100. The trend further grows until 8.0, before going for maintenance. After maintenance, the VI values dropped immediately to the 1.8 level. In this case, it took time to grow from the Alert to Alarm level. Even after reaching the Alarm stage, before taking any action on the train, the management team still had to consider more information, such as whether any other train had higher VI values than this one.

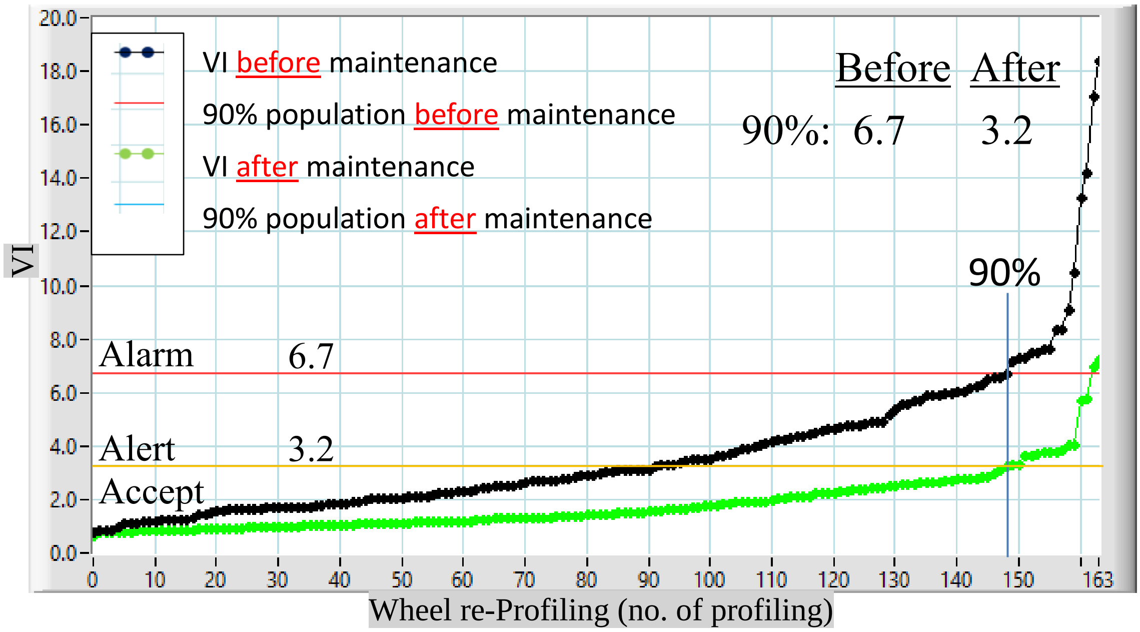

Figure 51. The 3A-Warning system (Accept, Alert and Alarm).

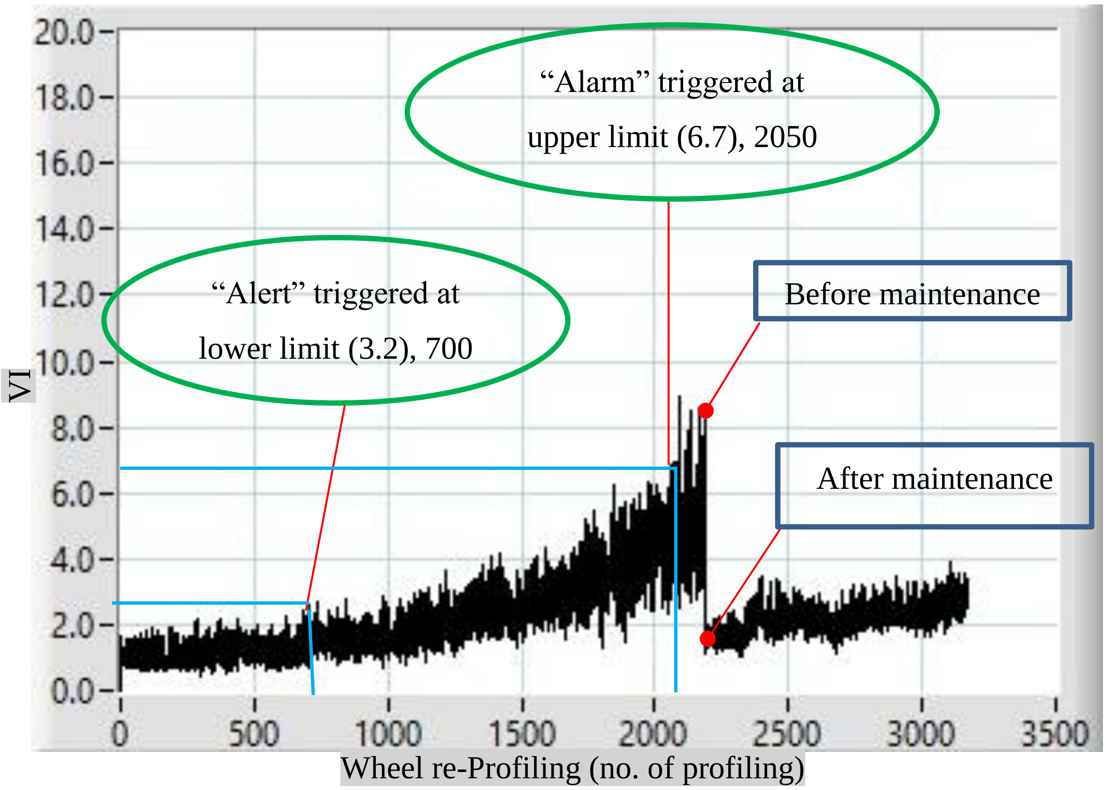

Figure 52. A 3A-Warning example. The wheel is re-profiled when VI reached 8 at 2,100 travels.

7.4.5 Other Applications of Studying Vibration

The railway monitoring system is a case study for the application of the Vibration Index (VI) sensing system. This system can also be utilized for other motor vehicles and machinery involving rotary parts because their degradations due to vibration may follow the P-F curve [23]–[25] which could be identified by this system. Literature on application using strain/stress to monitor escalators has been published [181]. In addition, applications to elevators, cable cars and trams are likely to be investigated soon. The reasons are the same as for the railway system in which vehicles consuming high levels of electrical power and generating electrical noise that interferes traditional electric type sensors, but optical sensors are immune against electrical noise.

7.5 Chapter Summary

This chapter reports the physical establishment of SRHM system, signal processing techniques, definition of vibration, Data Mining processing and the use of VI. Graphs exhibit the structure and connections of the sensor network. Vibration is introduced and defined, in relation to wheel/rail interaction, and VI calculation as well as its interpretation are presented. In addition, the critical components for monitoring the health condition of a railway are described and compared. The technologies for applying sensor-based measurement to the Track/Rail, Wheels, Bearings and Gearboxes are listed in a Table. Data Mining is also presented with appropriate data for this study. Finally, the interpretation of historical VI values is related to a 3A-Warning system given as a simple description related to VI amplitude.

Chapter 8 **Railway Condition Monitoring Decision-Making Support**

8.1 Introduction

In this chapter, a statistical point of view is brought to the analysis of historical VI values. It also explores VI values before and after wheel re-profiling and the application of these values facilitating the decision on whether to undertake maintenance or not. The bathtub curve used in reliability analysis and the Weibull distribution are used in modelling the data. An algorithm for predicting when train maintenance is next needed, is proposed. A method balancing between "scraping" and condition-based maintenance is also introduced in relation to wheel re-profiling. Consequently, the lifetime of a wheel is maximized and the cost is minimized.

8.2 Weibull Reliability Analysis and Bathtub Curve Modelling

Failure analysis is the modelling method employed in this project for analyzing the historical VI values of the whole fleet of trains. Actually, making use of fleet maintenance data relates to "lifetime" analysis of the fleet. To do this, the Weibull distribution [182] is made use of. The Weibull distribution states that failure occurrences versus time takes a bathtub shape as shown in Figure 53. In other words, machine failure rates usually follow the bathtub curve. The Infant Phase (1) has a high but decreasing rate of failure when machines are new and some components faulty. After a period of running, in the Phase (2) of Normal Lifetime, the surviving or repaired machines, run at a lower and constant failure rate for a relatively long period. Lastly, in the Wear-out Phase (3) stage, machines exhibit higher and increasing rates of failure as they age and reach the end of their lives. Eventually, the cost of retaining normal operation of the machines is too high.

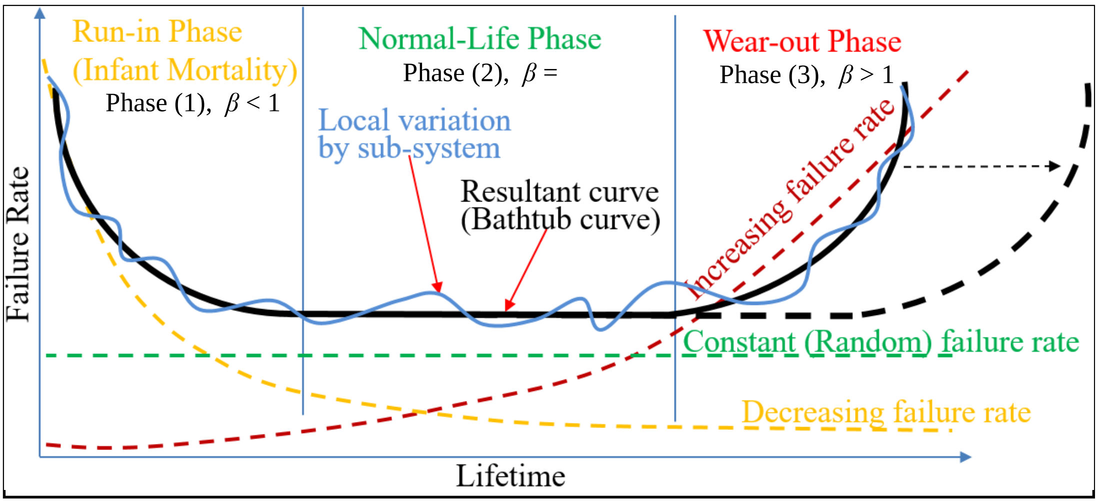

Figure 53. Bathtub curve of the lifetime of a complex machine.

The failure rate of a train fleet also follows the bathtub curve. Since a train is a giant machine composed of different components, each component is an individual sub-system which itself behaves in a "bathtub" shape manner. Thus, a fleet may include a large number of small bathtub curves, each as shown in Figure 53. The distribution of small bathtubs are supposed to be random among the fleet, and when attached together, the overall bathtub assumption still holds for the whole system. Thus, when sampling the giant bathtub at an instant of time, all small bathtubs are automatically embedded. The resultant bathtub curve is notionally presented as the blue line with local variations. Condition monitoring attempts to extend the lifetime are shown in the dotted line in black.

In this study, failure data is presented in the time domain (or mileage). Analyses investigate the health condition of the fleet based on current failure data. The data is sampled in snapshots of time over the whole lifetime of the entire fleet. The intervals between snapshots should suit the degradations of the units under test. In fact, the degradation of a railway system is very slow, and is measured in decades. The sampling period therefore is six months for condition monitoring. The historical health condition trend is reflected as the failure rate of the fleet and the bathtub curve phases are estimated accordingly.

The concept of failure analysis is not limited to total function failure but a common and fair measurement [154], [183]. That means the establishment of a vibration itself is also a "failure" in this study. Among the formulae in the Weibull distribution, the most relevant is the Probability Density Function (PDF) [65] as is selected here. To explain clearly, the graphical presentation is shown in Figure 54 while the PDF mathematical expression is given by equation (8.1):

$$f(T) = \frac{\beta}{\eta}\left(\frac{T-\gamma}{\eta}\right)^{\beta-1} e^{-\left(\frac{T-\gamma}{\eta}\right)^{\beta}} \tag{8.1}$$

$$f(T) \geq 0, \qquad T \geq 0 \; or \; \gamma, \qquad \beta > 0, \qquad \eta > 0, \qquad -\infty < \gamma < \infty$$

β is the shape parameter, also known as the Weibull slope,
η is the scale parameter,
γ is the location parameter.

As γ, the location parameter remains constant and located at zero, it can therefore be ignored. Thus, the formula becomes a two-parameter Weibull PDF function and can be re-written as equation (8.2):

$$f(T) = \frac{\beta}{\eta}\left(\frac{T}{\eta}\right)^{\beta-1} e^{-\left(\frac{T}{\eta}\right)^{\beta}} \tag{8.2}$$

The shape parameter β describes the different phases of failure in the bathtub curve as shown in Figure 53. When $\beta < 1$, the lifetime is in the Infant phase with decreasing failure rate; for $\beta = 1$, the lifetime is in the Normal Lifetime phase with constant failure rate; For $\beta > 1$, the lifetime is in the Wear-Out phase with an increasing failure rate.

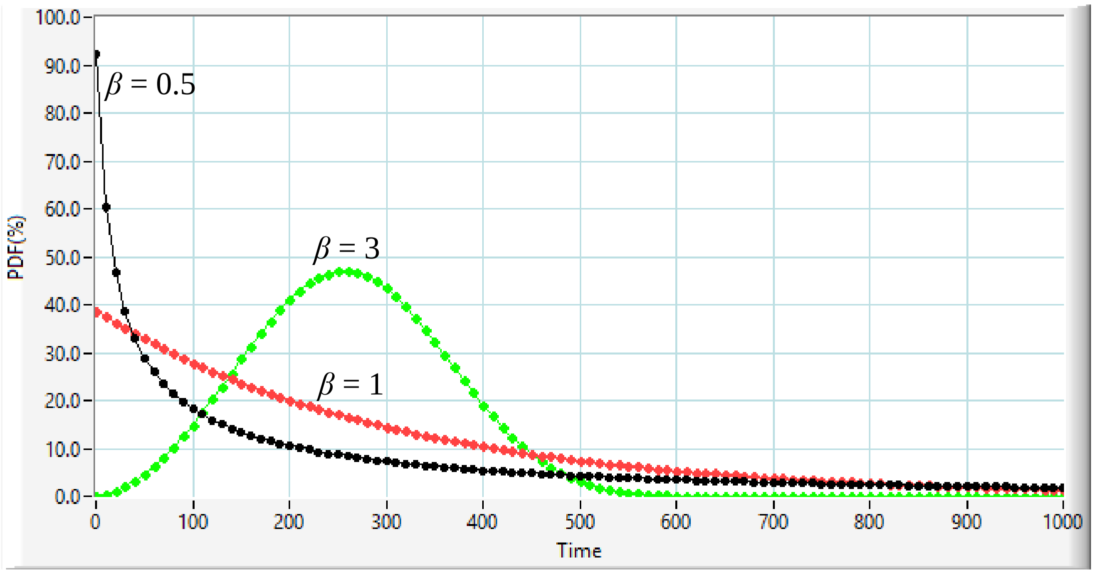

Figure 54. Graphical presentation of Weibull distribution.

8.3 Results and Discussion

In the SRHM system, the objective is not only to monitor the health condition of trains, but also to provide information for management decision-making support [97] in prioritizing maintenance schedules. In order to increase efficiency and usage, the direct involvement of the management is recommended. That involves giving them fast responses and up-to-date maintenance details so that they enjoy using the system and benefit from saving time and making correct final decisions.

The management also try to (a) maximize production capacity by shortening breakdown induced delays, (b) be environmentally friendly, (c) enhance employee safety. This is the concept of Multi-Criteria Decision-Making Methods (MCDM) in maintenance [184] and is assumed in this research.

8.3.1 Weibull Distribution Modelling

The two-parameter PDF Weibull distribution function can now be used to analyze the historical VI values of the SRHM system. The historical VI data covering nearly one year (360 days) for 30 trains were collected from 1st September 2014 to 26th August 2015. During the testing period, each train made 10 rounds a day for ~310 days (~65 days for maintenance checking-up). With 8 cars in a train, a total of 750,000 VI values have been calculated as plotted in Figure 55. The VI values are divided into three periods. Period 1 is the first six months for reference as a control with no VI values fed back for maintenance. Period 2 is the next three months when high VI values were taken as the first priority of maintenance. Period 3 is the last three months when high VI values were referred more frequently for maintenance action.

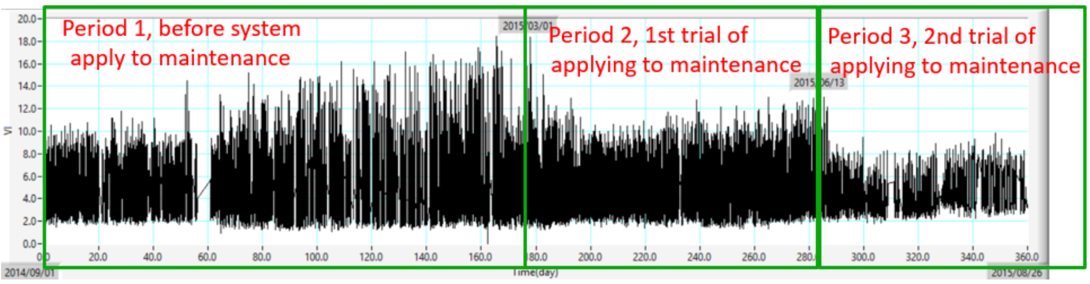

Figure 55. VI values of 30 trains and long last for 360 days.

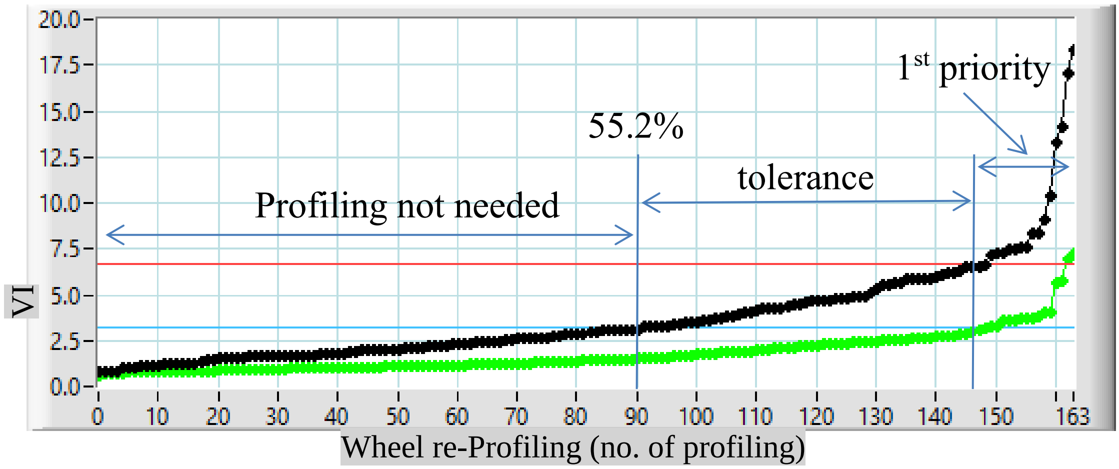

Figure 56. The Weibull distribution of VI values in the reference period. The maximum VI values are 18.4 & 7.3 before and after applying to maintenance.

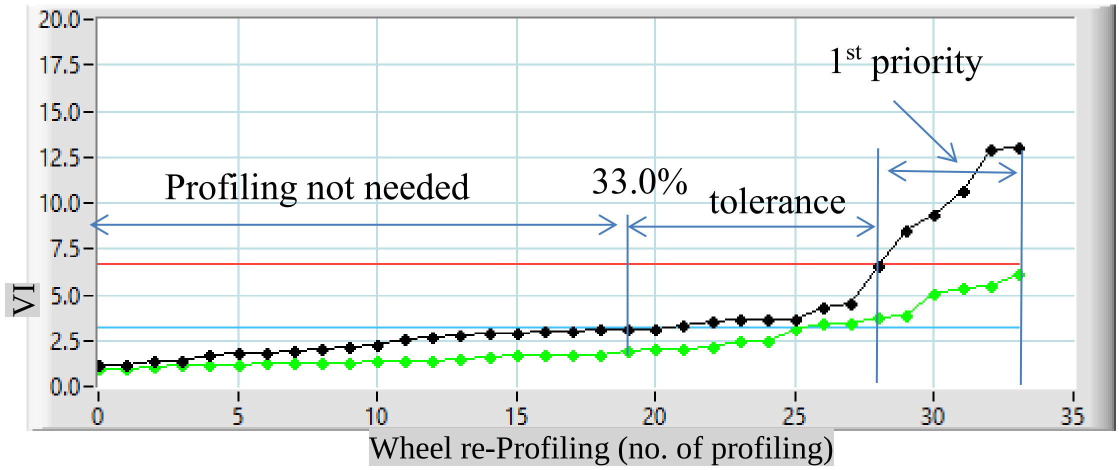

Figure 57. The Weibull distribution of VI values in Period 2. The maximum VI is reduced from 12.9 to 6.0 after the 1st trial of applying VI values to maintenance.

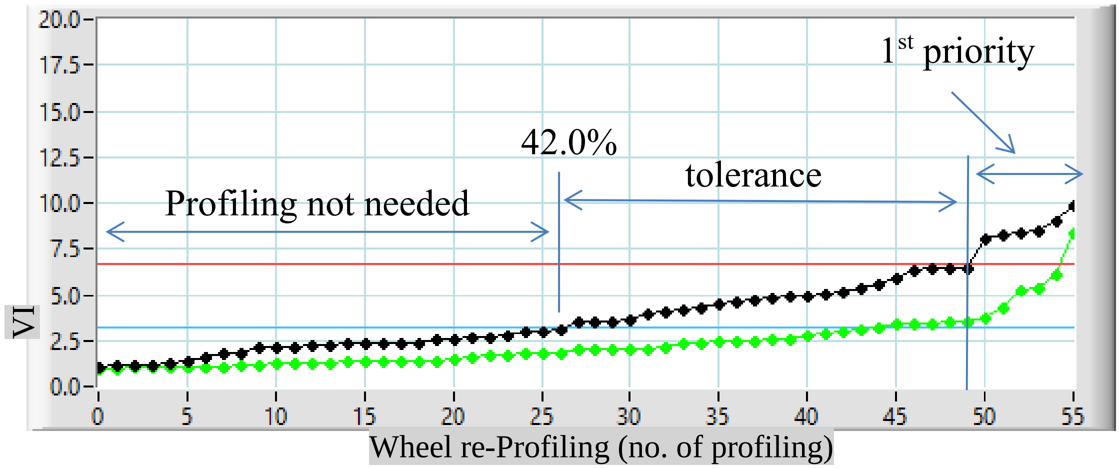

Figure 58. The Weibull distribution of VI values of Period 3. The maximum VI is reduced from 9.9 to 8.4 after the 2nd trail of applying VI values to maintenance.

After each period of maintenance, the pair of VI values before (black) and after (green) wheel re-profilings were recorded by the SRHM system as shown in Figure 56, Figure 57 and Figure 58 for Period 1, Period 2 and Period 3, respectively, of Figure 55. The data were then sorted in ascending order for ease of analysis. The characteristics of the envelope changes in the three Periods showing the effect of feeding back the VI values to maintenance. The highest VI values are given higher maintenance priorities although maintenance may not be taken as planned since other factors such as corrective maintenance have to be considered at the same time.

Figure 56 is the Weibull plot of the VI values for the reference data Period 1. The maximum value of 18.4 before maintenance is extremely high. The curves (green) after maintenance in all these three figures, show that VI values have been significantly reduced with less variation. The maximum VI values after maintenance are 7.3, 6.0 and 8.4 in periods 1, 2 and 3 respectively.

Figure 57 relates to Period 2, the next three months. The VI values are used to prioritize maintenance scheduling simultaneously with the existing preventive maintenance (by time) strategy. The outcome is significant with envelope drops from 16 in the reference period to the level of 10 shown in Figure 55. The maximum VI values before maintenance drop from 18.4 in Period 1 to 12.9.

Figure 58 relates to Period 3, another three months after the reference period. The envelope drops further from 10 in Period 2 to the 6.0 shown in Figure 55. The maximum VI values before maintenance further dropped from 12.9 to 9.9. That means the OOR had been significantly improved after the year of testing.

According to the 3A-Warning system, wheels with VI values below the Alert should not be re-profiled. However, they were re-profiled, in fact, during the testing period. In other words, the re-profiling effort was not necessary and could have been saved. Referring to Figure 56, Figure 57 and Figure 58, 55.2%, 33.0% and 42.0% of wheel re-profiling from Period 1 to Period 3 respectively was not necessary. To sum up, the use of VI values in maintenance will not only improve OOR but also reduce the usage of the resources. This demonstration proves that FBG sensors could be used as a very effective decision-making support tool in railway maintenance management. With the fusion of more FBG sensors in the SRHM system, predictions of failure [19], [185] may also be possible.

Utilizing the two-parameter Weibull PDF function, the VI values were then fitted into equation (7.5) for curve fitting purpose as shown in Figure 59. The Weibull slope parameter β and the values of VI were used to estimate the maintenance quality level of the fleet. Lower values of β represent better maintenance quality. The black curve (β = 0.80) for the vibration before maintenance is obviously higher than the green curve (β = 0.77) relating to after maintenance. It reflects that the maintenance quality of the fleet is equivalent to a point near the Infant phase approaching the Normal-Life quality in the bathtub curve. The black curve with lower value (~0.5) and lower slope at the beginning than the middle part of the curve, then grows to a higher value (~15) at an increasing rate near the end. The average values are very low, at 2.73 and 2.00 respectively, before and after maintenance and much lower than the Alert value of 3.2 in the 3A-Warning system.

In addition, the Weibull distribution can be applied to a single car. The plotting of historical VI values for a car with Weibull fitted curve is shown in Figure 60. This car with β equal to 0.98 is higher than the 0.80 for the whole fleet before wheel re-profiling. Therefore, more attention should be paid to this particular train when considering maintenance priority.

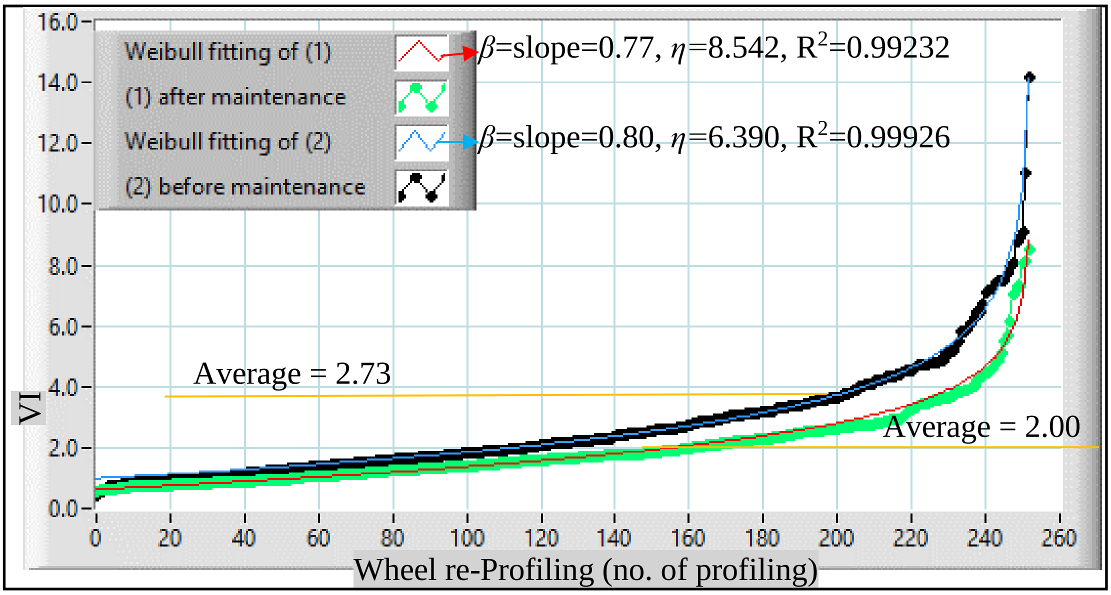

Figure 59. The Weibull curve fittings of VI curves before and after maintenance

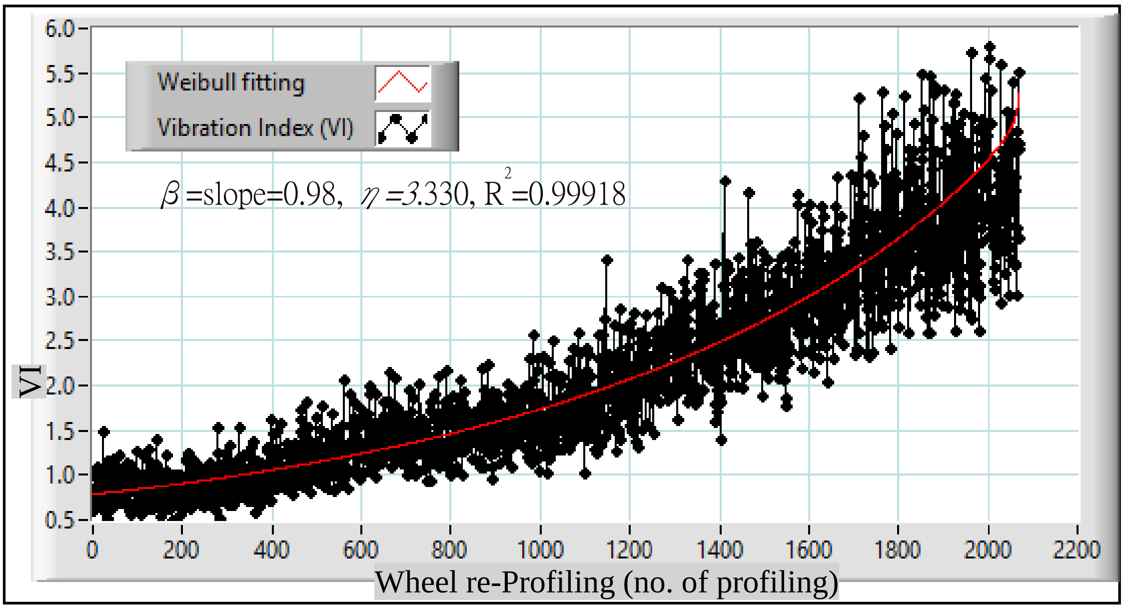

Figure 60. Weibull curve fitted for a car with historical VI values.

8.3.2 The Fleet Health Condition Level Chart

The Fleet Health Condition Level (FHCL) chart shown in Figure 61 is a reference standard for estimating the overall maintenance performance over the long-term. Line A gives the VI values just before maintenance, representing the current quality level of the whole fleet before applying the decision-making support tool. The quality level could be poorer than Line A if the maintenance work is poor when the rate of wearing-out is too high and aging is too fast. Line B is a threshold to separate those VI values beyond the Alarm region. Line C represents the VI values after going through maintenance works. This line represents the best quality and the values stay low. Line D is a threshold to separate those VI values beyond the Alert region. Line E is a virtual line balancing the effort and quality level and is the targeted standard to be reached by management.

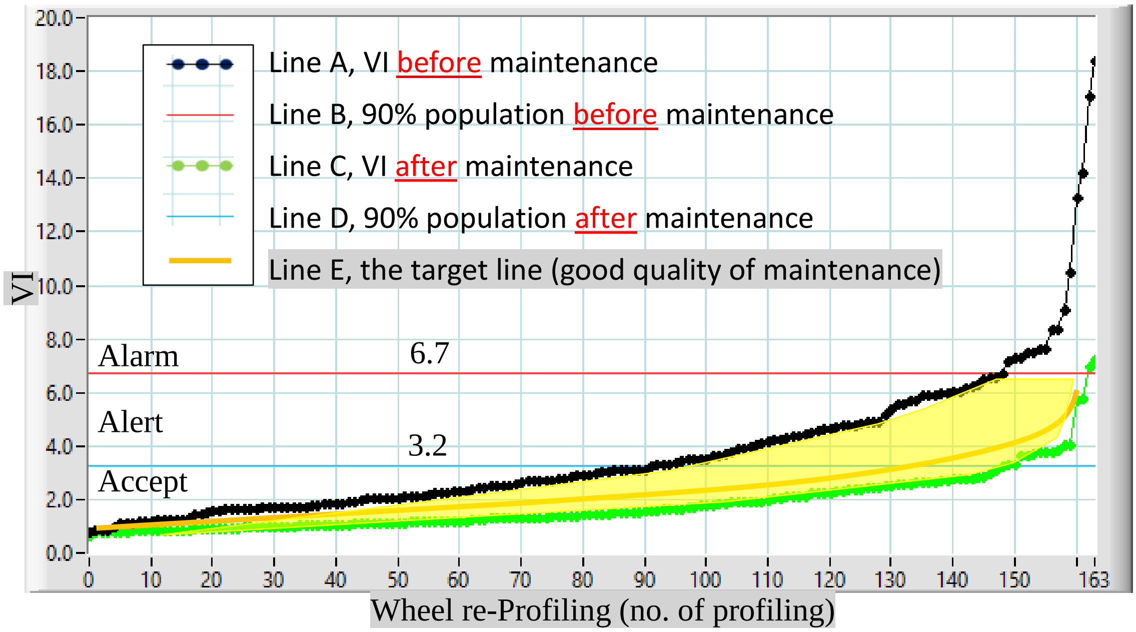

Figure 61. The Fleet Health Condition Level Chart.

The yellow area:

The FHCL chart in Figure 61 quantifies the overall health quality level of the whole fleet. Management can monitor the health condition of the fleet in real-time using the past data, best data and targeted health quality. The tunnel (yellow area) between Line A and Line C is the quality standard tolerance. The area of the tunnel should be kept as narrow as possible while the baseline of VI should be kept low. The highest points in Line A should be considered for decision-making support action, prioritizing the maintenance schedule towards narrowing the yellow area.

The Baseline of the Fleet Health Condition Level Chart:

Line C of Figure 61, the bottom line of the fleet health quality contains values just after maintenance. However, this only represents the current best quality health level. It will change gradually over time. According to the theory of failure analysis in the Weibull curve, with aging, health quality level will worsen no matter how well maintenance works are performed [186]. Of course, the better the maintenance work performed, the lower will be the rate of worsening. In other words, with the trend of the historical data baseline, the baseline of the FHCL chart can be used to monitor the aging condition of the trains.

To sum up, the FHCL chart provides background support to the management as a reference for managing the health quality of the fleet as well as that of an individual train. The principle of the FHCL chart is based on statistics with theoretical support, thus is easily understood by management and acceptable as a decision-making support tool.

8.3.3 Facilitating Decision-Making Support for Management

Maintenance priority decision-making is a logical process. This study provides more information and identifies more factors, making the system more intelligent and efficient. These factors include (1) VI values, (2) historical VI values, (3) rate VI changes, and (4) the number of cars having high VI values. Cases in Figure 62 and Figure 63 illustrate the use of the system in the decision-making. Three choice scenarios are listed below for management to use. In the case of the following example, if the management selects Factor (4) as the first priority, Train A will go to maintenance earlier than train B.

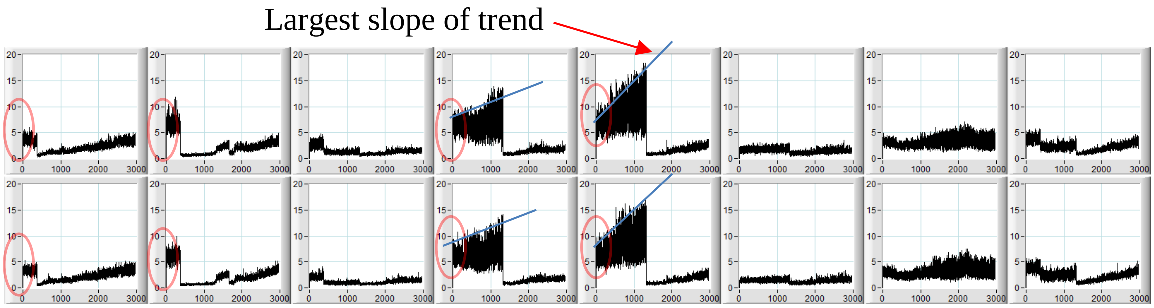

Figure 62. Train A has 6 cars with high VI values.

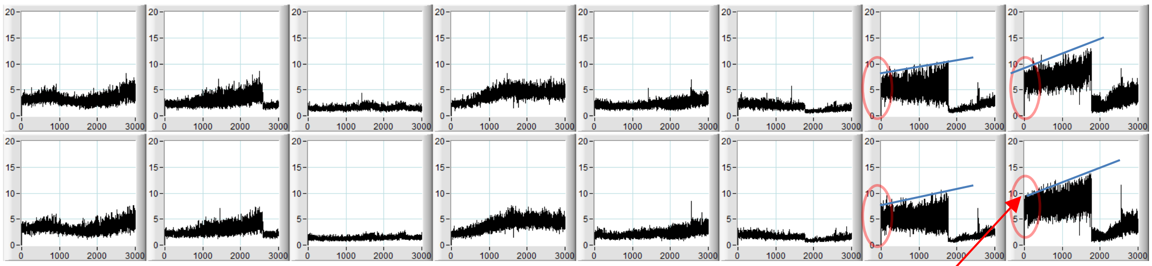

Figure 63. Train B has 4 cars with high VI values.

Scenario 1: If only the highest train VI value is considered, Train B will be taken for maintenance, since the initial VI value in Car 5 of Train A is a bit lower than that in Car 8 of Train B.

Scenario 2: If the number of cars with high values is considered, Train A will be taken for maintenance, since it has 4 cars with high values compared with only 2 cars in Train B.

Scenario 3: If the slope of the trend is considered, Train A will be taken for maintenance, since the slope in Car 5 is the steepest and steeper than any in Train B.

With these preference Scenarios, a system decision tree can provide decision-making support information. However, management has to also consider other factors, in making a final decision. If only these three Scenarios are considered, Train A should be sent for maintenance first as six high-value cars can be tackled at the one time. This increases the efficiency of the maintenance work and reduces the overall VI values of the fleet in a shorter time. In addition, the time needed to complete maintenance is also a factor. The amount of time for a train to complete maintenance is around 10 days.

<u>Maximize the Lifetime with Minimum Resources</u>

Once understanding the relationship between vibration and OOR, the next question to ask is how to minimize OOR and thereby maximize wheel lifetime with minimum resources. Research by the Lioyd's Register in [54], found that when wheel re-profiling is carried out only when a serious OOR condition exists, the lifetime of a wheel will be reduced. In the meantime, a test was conducted which proved that to maximize lifetime, re-profiling of the wheel should occur at fixed short mileage intervals (70,000 km) so that the thickness of the material removed is minimized.

There is no doubt that the lifetime of a wheel can be maximized by reducing the thickness of cuts at short mileage intervals. However, this process consumes a large amount of resources. Also relevant is that, not all wheels suffer the same amount of degradation rate, but they still consume the same amount of resources in the cutting processes. In other words, applying the same regime to all wheels is not reasonable and wastes resources. Thus, a more meticulous regime should be introduced to balance both lifetime and resources consumption.

Lines applying to these different regimes are illustrated in Figure 64. Regime (a) was proposed by Lioyd's Register in [54] with short and fixed mileages. This regime can maximize lifetime but needs more resources. Regime (b) as used in the old days, only re-profiles a wheel when its OOR is very serious. This regime requires less resources but reduces lifetime. A balanced solution, Regime (c), compromises between Regime (a) and (b), by re-profiling the wheel just before the OOR condition at which the high rate of degradation increase region begins (non-linear increase region) as shown in Figure 83. With Regime (c), the wheels with lower degradation rates could even achieve longer lifetimes than those in Regime (a) and save more resources at the same time.

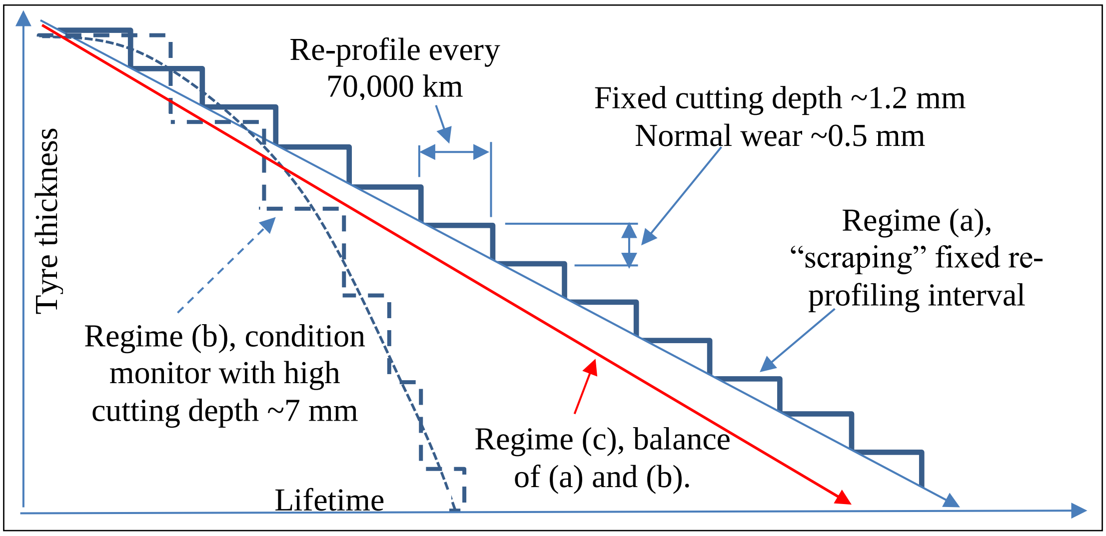

Figure 64. Wheel re-profiling using Regime (a) allows a longer lifetime but uses huge resources. Regime (b) uses limited resources but reduce lifetime. Regime (c) is a balance of Regime (a) and Regime (b) and need intelligent control.

The VI values of a wheel, assuming a Weibull distribution, are shown in Figure 65. The curve can be divided into a “Low increase region” and a “High increase region”. In the “Low increase region”, the VI value increases slowly then at an increasing rate in the “High increase region”. To maintain a long lifetime, VI values should always be kept in the “Low increase region” to maintain low OOR values as recommended by the 3A-Warning system.

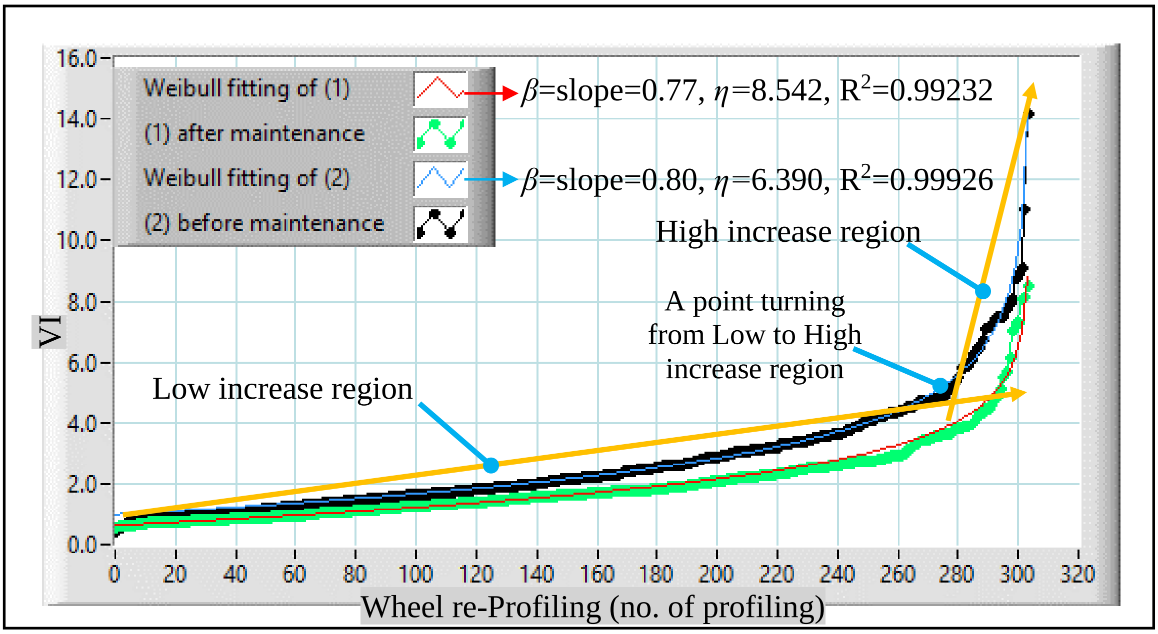

Figure 65. The trend of VI values is simplified into Low and High increase regions. The VI value is supposed safe before the point turning into the High increase region.

8.3.4 Contributions to Modelling the Vibration Data

The contributions of modelling and analysis of vibration data for condition monitoring purposes proposed in this study are listed below. Firstly, the correlation between the vibrations due to wheel/rail interaction and the Out-Of-Roundness (OOR) of wheels were proved experimentally. Vibration was significantly reduced after wheel re-profiling [20]. Secondly, the Weibull distribution has been applied to degradation analysis and shown fitted well with the vibration historical trend, as shown in Figure 65. Indeed, it is found that wheel re-profiling should be performed when the VI value has reached a turning point before it goes into the increasing degradation region as shown by the Weibull distribution in Figure 65. Otherwise, the wheel lifetime would be reduced, according to the internationally renowned railway company -Lloyd's Register Rail Europe [54].

8.3.5 Comparing the SRHM System with Existing Methodology

Gotcha Monitoring Systems [9] is an existing and commercially available system similar to the Smart Railway Health-Condition Monitoring (SRHM) system being investigated in this study, it is developed by Lloyd's Register Rail Europe. The similarities include, (1) both use optical fiber sensors [187]. (2) both measure the vibration influenced by wheel/rail interaction, (3) both use historical data to present vibration trends. However, the theoretical background is never revealed in Gotcha because it is a commercial secret, whereas the underlying theoretical background of the SRHM is fully elaborated and discussed in this study. Furthermore, it is noted that (1) Gotcha serves to provide propriety information only for track users and track owners as the basis for a fee-charging system whereas the SRHM system is specially designed for safety enhancement and maintenance efficiency improvement via condition monitoring. (2) The SRHM system includes track settlements level measurements. Gotcha provides no such information at present. (3) The modular design approach of SRHM allows additional functions to be plugged into the system to cater for future expansions in the development of a comprehensive smart railway system based on the underlying theory discussed.

8.3.6 Change of Maintenance Practices

The Smart Railway Health-Condition Monitoring (SRHM) System is designed for long-term decision-making support in railway maintenance. The system has just finished its Testing and Commissioning (T&C) stage for a short period. Therefore, there are no statistical figures related to maintenance cost saving available. On the other hand, many complimentary feedbacks from engineers and technical staff have been received. The SRHM system provides comprehensive information regarding the health conditions of different trains and cars that change their maintenance practices especially in prioritizing the maintenance schedules between different trains and cars. For example, the corporation which uses the proposed SHRM system is now very confident in selecting the trains for wheel re-profiling, because they all have high Vibration Index (VI) values which are proven to be highly correlated to the existence of imperfections such as dents on the wheels. The VI values for all trains are routinely reported and comparisons are easily made. In other words, the engineers are confident that the trains selected for maintenance are the correct ones and thus the overall reliabilities of the trains are improved.

8.4 Chapter Summary

In this chapter, the Weibull distribution is introduced for failure analysis purposes. The bathtub curve is proposed for modelling of the failure rate. Evaluation of the readiness for maintenance action, based on VI values, is described. Trains with high VI values will receive maintenance first. The results show that after one year of trial, the maximum fleet VI values dropped from 18.4 to 9.9. In addition, 55.2% of wheel re-profiling activity was not needed since it occurred when OOR values were still within acceptable limits. Three scenarios are presented of the decision-making logic which minimizes the overall OOR and takes a shorter time. The FHCL chart is derived as a background guide, supporting management in monitoring the health quality of the fleet and individual trains also. Finally, a regime which balances the maximum lifetime with minimum resources is proposed by applying wheel re-profiling just after the point where the Weibull distribution turns into the region of high degradation increase.

Chapter 9 **Future Developments**

9.1 Introduction

Future work will mainly be based on the intelligent employment of more data and information. For more data, sensors can be added to enrich the designs of the algorithms. For more information, data of greater diversity will be input to the system, and more meaningful information extracted. In addition, other than the data from sensors, data will be deriving from the maintenance work itself, such as OOR measurements made in the depot, data such as the parts repaired/replaced, and data from other condition monitoring systems, are also useful.

9.2 Data Fusion of Events and Other Systems

A train is an extremely complex moving machine. Vibration sources are multiple. Any changes to vibration could be due to wear at wheel and track. Events [87] such as the replacement of parts and other types of preventive maintenance may affect parts of the structure. Therefore, data relating to all events, maintenance tasks and condition monitoring systems [147] may be useful for separating and eliminating any error information, i.e. other than OOR, in order to increase accuracy and functionality.

9.3 Miniature of FBG-Based Accelerometer

The existing FBG strain sensors installed on the track rail measure both dynamic and static strain. However, the frequency response may be biased towards the lower frequencies as the track rail is tightly mounted and its mass is heavy. A FBG-based accelerometer [188] is recommended for installation on the track to measure higher frequencies. In the meantime, the size and material of the sensor chassis should be compliant with related safety requirement. Alternatively, smaller lighter FBG-based accelerometers are preferred [189].

9.4 FBG-Based Microphone

Because of its high level of intelligence, sensor fusion in railway systems [190] is an effective monitoring approach. Use of a FBG-based microphone [191] is proposed for detecting acoustic signals generated by wheel/rail interaction. The interaction noise generated is another form of vibration signal that may be useful in identifying different types of failure and defect.

9.5 Alternative Method for VI Calculation (Gaussian Fitting)

The VI proposed in this study is based on cars, rather than wheels. The calculation takes account of the vibration of all eight wheels in the two bogies. However, the peak vibration when the wheel acts on the tip of the sensor, is supposed of high value. The proposed new method aims to detect this peak. The fundamental waveform is assumed to be of Gaussian distribution shown in Figure 66. The red curve is the Gaussian fitted waveform and the blue curve is the raw signal emitted when a wheel passes the sensor. Therefore, the vibration is extracted by subtracting the Gaussian fitted waveform from the raw data. This approach may be more representative of degradation to a single wheel than the existing method. However, the strain amplitudes caused by the train weight is also very high and the signal-to-noise ratio may not be very good. Thus, more signal processing steps may be needed.

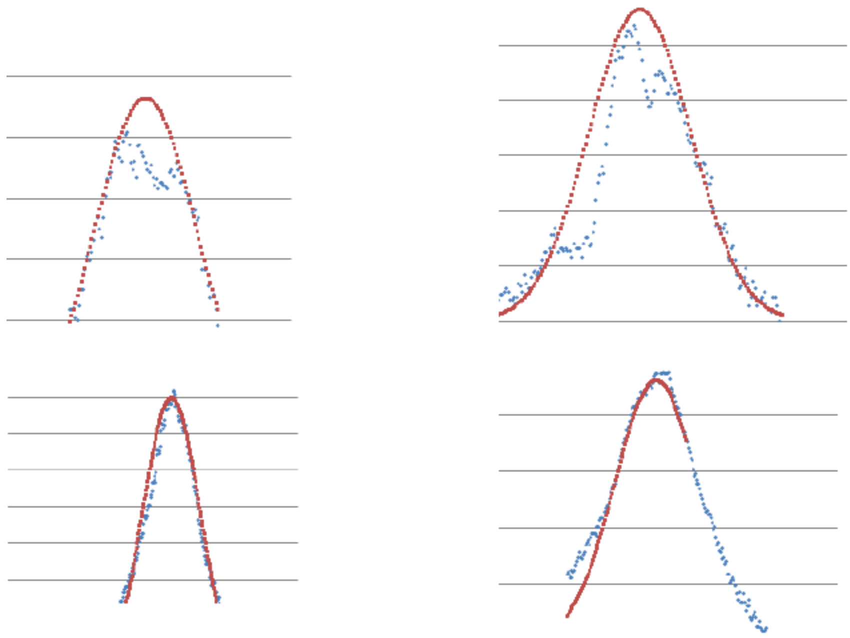

Figure 66. Proposed Gaussian fitted envelopes for four example waveforms with peaks when wheels at the tip of FBG sensors.

9.6 Residual Usable Lifetime Prediction of a Wheel

The Residual Usable Lifetime (RUL) prediction [192], [82], [193] for a wheel is proposed as part of the necessary future study. The approach is to keep a continuing record of wheel re-profiling thickness. With a database of information about the wheels, the usage and residual lifetime forecasting is possible. The information needed to support the forecasting includes (1) the current thickness of the tyre, (2) the minimum thickness allowed, (3) thickness profiled each time, (4) the rate of degradation, and (5) historical data over the lifetime of the wheels. Knowing the RUL of the whole fleet, just-in-time ordering of wheels is possible, saving on currency flow, space and manpower.

9.7 Chapter Summary

To fully utilize and develop the SRHM system in the future, more data and information in both volume and diversity are proposed to increase the benefit of the maintenance scheduling. Sensors to provide more data include FBG types of accelerometer and microphone. Data relating to different events and different condition monitoring systems are also highlighted. An alternative approach for calculating VI is also discussed. With more information, RUL predictions for the whole fleet can be achieved.

Chapter 10 **Conclusions**

In this research, the use of FBG-based i) Track Settlement Level Sensors, ii) Axle Counting Sensors, iii) Weight Balance (WB) Sensors, and iv) Vibration Index (VI) sensors have been developed in the context of railway condition monitoring. Furthermore, a SRHM System has also been established for real-life usage and the continuous verification of sensors. A VI sensor was selected as a demonstration example for one year of data collection and evaluation. Based on historical data, a regime for balancing the use of maintenance resources with wheel lifetimes in relation to wheel re-profiling policy is advised as decision-making support in prioritizing the maintenance schedule.

The key technologies such as information technologies, maintenance strategies, vibration effects due to the OOR of wheels on railway cars are reviewed in Chapter 2. A detailed review of optical fiber sensing including distributed sensing and the FBG are introduced separately in Chapter 3. The four sensors development and their applications are reported in the remaining chapters as follows.

10.1 Settlement Level Sensor

A track settlement level sensor is a FBG connecting a float and the base of the sensor body, which detects the liquid level inside. An external tank supplies liquid to the sensor and acts as a reference. The experimental result showed the sensitivity to be 0.103 nm/mm. The diameter of the sensor is 80 mm and it is around 200 mm high. This sensor is based on 80 μm of cladding and a 9 μm core single-mode fiber. It is more sensitive than the traditional 125 μm fiber. Experimental data also suggests that the sensor's operating temperature range was -30°C to +80°C and that the temperature error is minor at 0.008 nm/°C.

10.2 Axle Counting Sensor

An axle counting sensor is a FBG mounted on the track with an interrogation device and processing software in a computer. The research focused upon the processing algorithm used to analyze the wavelength data as trains pass through. The results show that the proposed X-crossing and D-crossing method complement each other. When used together in axle counting, accuracy is very high. The results show a 100% accuracy after 1,680,000 axles had passed through the sensors in three locations over five months. The limitation is that the computer and interrogation systems may crash every 2 months, requiring close human supervision.

10.3 Weight Balance Sensor

A weight balance (WB) sensor is also a FBG mounted on a rail with an interrogation device and processing software in a computer. The research focused upon the calculation of dynamic weight and the balance of the two wheels on each axle. During the study, a finite element simulation and an experiment were performed to explore the distribution of sensitives on the rail to help determine the locations of FBG installation. An approach was verified which gave the best candidate with an approximately 10% error. Weight balance of the wheels was also investigated but proved not useful for estimation of derailment at the Nadal Limit, as the lateral force on the wheel was not measured in the experiment. Instead, an alternative solution, namely Off-loading ratio was derived based on the weight difference bearing down on the left and right hand rails.

Another experiment on car wheels profiling was carried out. The high inter-axle vibration signals results allowed the FBG sensor to determine the OOR of wheels. This proved that by measuring rail vibration, good estimates of the OOR of wheels can be obtained and used for condition monitoring in real-time.

10.4 Smart Railway Health-Condition System

A VI sensor, like the other sensor, is a FBG mounted on a rail with an interrogation device and processing software in a computer. A VI is derived from wheel/rail interaction vibrations, mainly reflections the OOR of a wheel. A RFID reader on the trackside is connected to the SRHM to match the trains with the recorded raw data obtained from the eight VI sensors on the rails. An algorithm for calculating the VI of a car has been developed. It should be noted that a single system is enough on a railway line, serving the whole fleet in fully automatic mode, on in-service non-stop trains.

A long-term test of nearly one year (360 days), of VI data deriving from 30 trains was carried out. In order to relate the data to maintenance strategies, a Weibull reliability analysis model was employed in this study. The slopes of the Weibull fitted curves before and after wheel re-profiling are proposed as representing the quality of the fleet, and hence the degree of need for maintenance. From the experiences of maintenance personnel, and statistical analysis, it was agreed that measured VI values can be used as thresholds for assigning different VI values to the categories of Accept, Alert or Alarm, a so-called 3A-Warning system. The system automatically sends messages to the relevant people with a detailed report once thresholds are triggered.

10.5 Railway Condition Monitoring Decision-Making Support

In order to fulfil the decision-making support function, the VI values, by car, are plotted graphically for visualization of OOR trends. Each individual train is compared with the whole fleet. The train with the highest VI values is then prioritized for maintenance based on a rule-based artificial intelligence algorithm developed during the research.

The results show that after a year of application of the SRHM system, the highest VI values in the fleet improved from 18.4 to 9.9, and 55.2% of the wheel re-profiling workload could have been saved by adopting the 3A-Warning system. For decision-making support purposes, the relationship between VI and OOR was further investigated in relation to the prioritizing of maintenance. Performing wheel re-profiling at high VI values could shorten the lifetime of the wheels according to Gotcha's research. Instead, a regime for balancing resources usage with wheel lifetimes has been proposed based on the use of the point on the Weibull distribution curve just before the high rated increase region of the curve within the FHCL chart derived from historical wheel re-profiling VI values.

10.6 Academic Values of the Study

This research has verified that the benefits of FBG sensors to humanity are increased by the application of information technologies in railway condition monitoring. With the fusion of individual sensors with the system, alongside the appropriate information technologies, more intelligent decision-making support for railway maintenance decision was achieved. The SRHM system makes a huge contribution to the railway system because firstly, the overall maintenance quality is constantly monitored and the current quality is available for reviewing at any time by management. Secondly, wheel OOR is inspected in-service in non-stop mode and is fully automatic. Thirdly, maintenance work is now more effective because the decision-making support system provides information on the exact train next requiring maintenance. Finally, labor, costs and time for maintenance are reduced, the lifetime of train wheels is lengthened, and safety and service quality are increased.

Appendix A Vibration Index Cases

Different cases of VI values and their waveforms are shown below. The black color curve represents the signal from FBG on the left rail and red color represents the signal from the right rail. Pay attention to the vibration of the wavelet signal between peaks. If the wavelet signal is more serious, the VI value on the right column is higher.

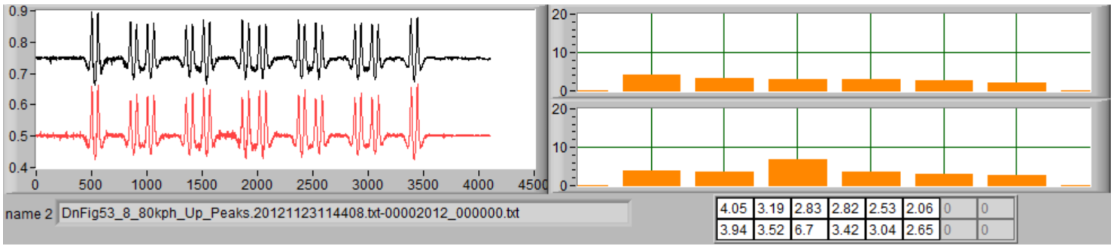

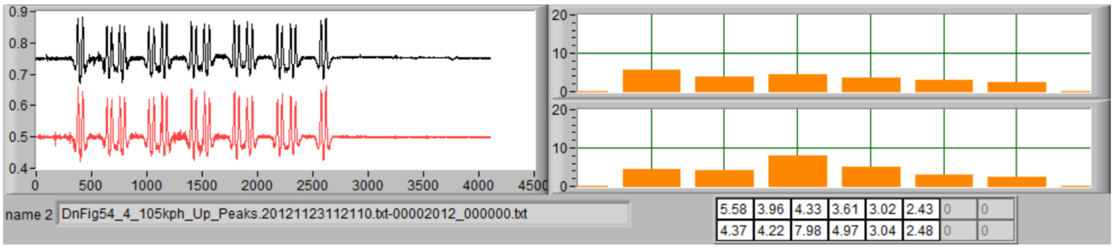

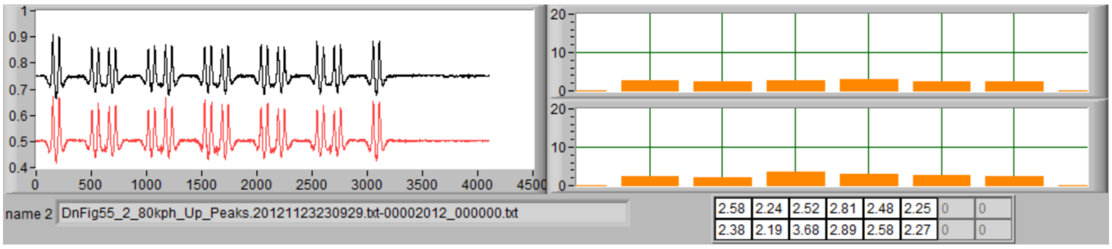

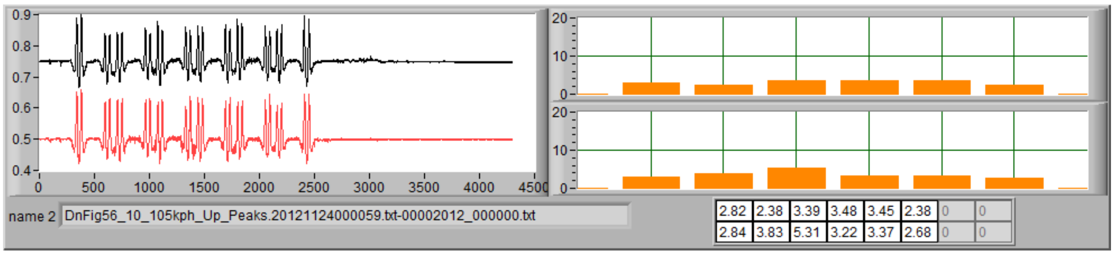

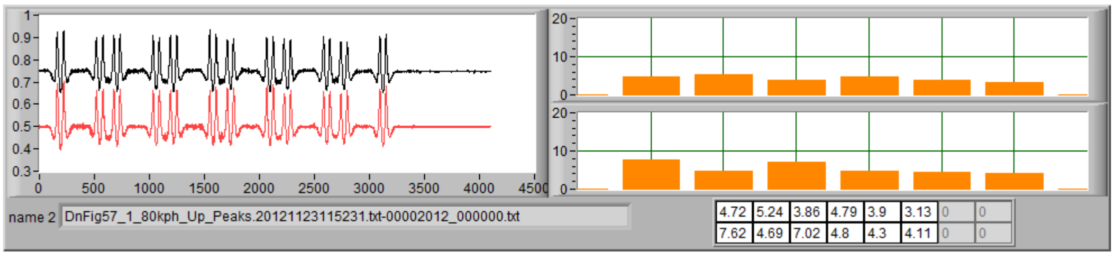

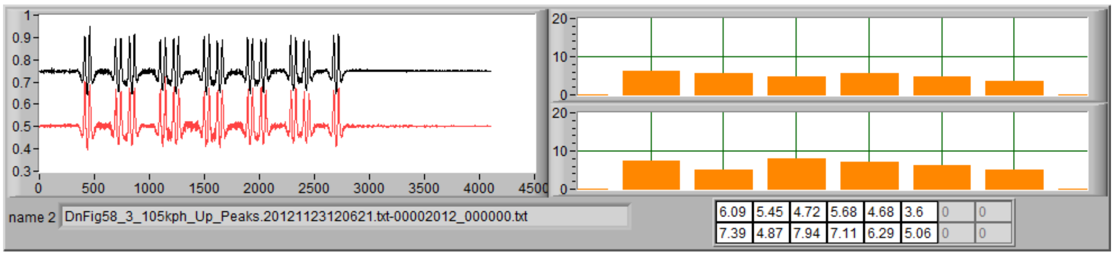

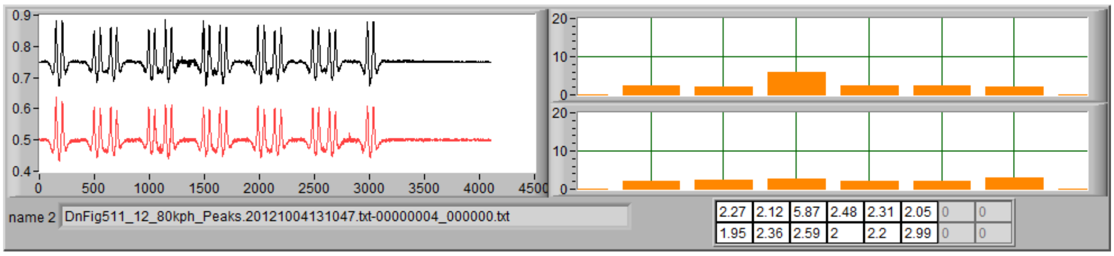
name 2 DnFig511_12_80kph_Peaks.20121004131047.txt-00000004_000000.txt
2.27 2.12 5.87 2.48 2.31 2.05 0 0
1.95 2.36 2.59 2 2.2 2.99 0 0

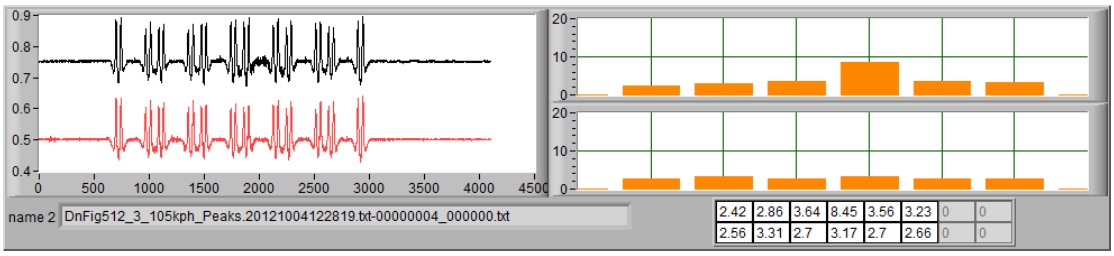
name 2 DnFig512_3_105kph_Peaks.20121004122819.txt-00000004_000000.txt
2.42 2.86 3.64 8.45 3.56 3.23 0 0
2.56 3.31 2.7 3.17 2.7 2.66 0 0

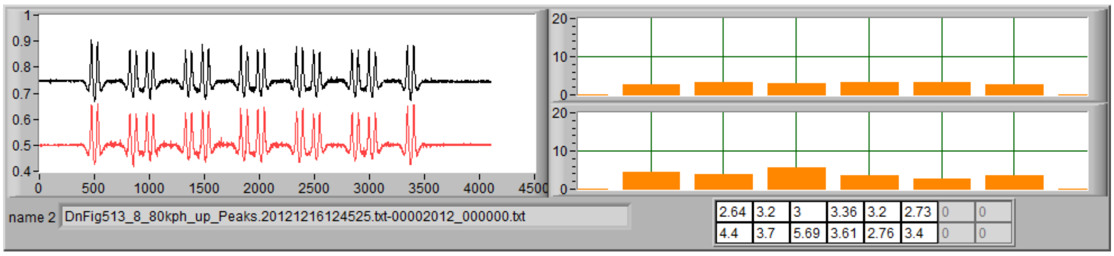
name 2 DnFig513_8_80kph_up_Peaks.20121216124525.txt-00002012_000000.txt
2.64 3.2 3 3.36 3.2 2.73 0 0
4.4 3.7 5.69 3.61 2.76 3.4 0 0

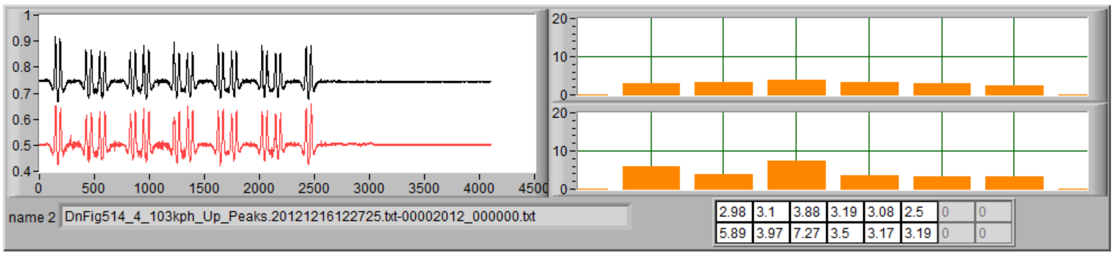
name 2 DnFig514_4_103kph_Up_Peaks.20121216122725.txt-00002012_000000.txt
2.98 3.1 3.88 3.19 3.08 2.5 0 0
5.89 3.97 7.27 3.5 3.17 3.19 0 0

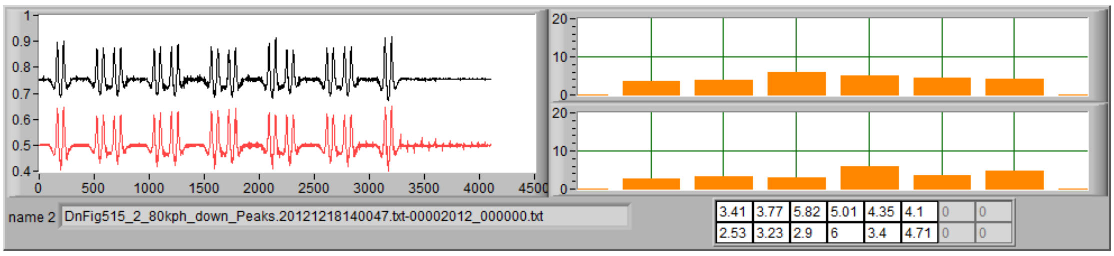
name 2 DnFig515_2_80kph_down_Peaks.20121218140047.txt-00002012_000000.txt
3.41 3.77 5.82 5.01 4.35 4.1 0 0
2.53 3.23 2.9 6 3.4 4.71 0 0

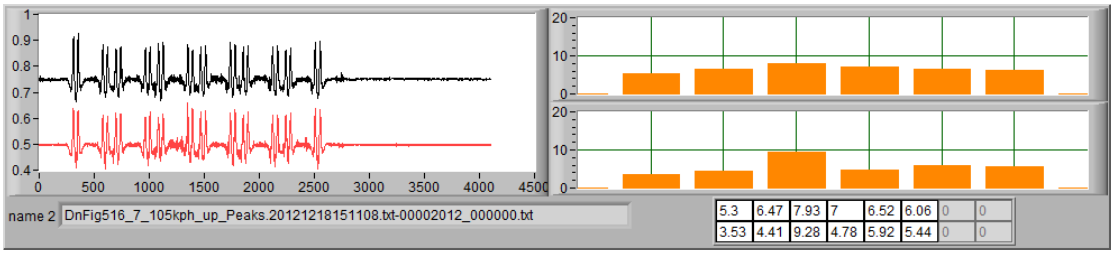
name 2 DnFig516_7_105kph_up_Peaks.20121218151108.txt-00002012_000000.txt
5.3 6.47 7.93 7 6.52 6.06 0 0
3.53 4.41 9.28 4.78 5.92 5.44 0 0

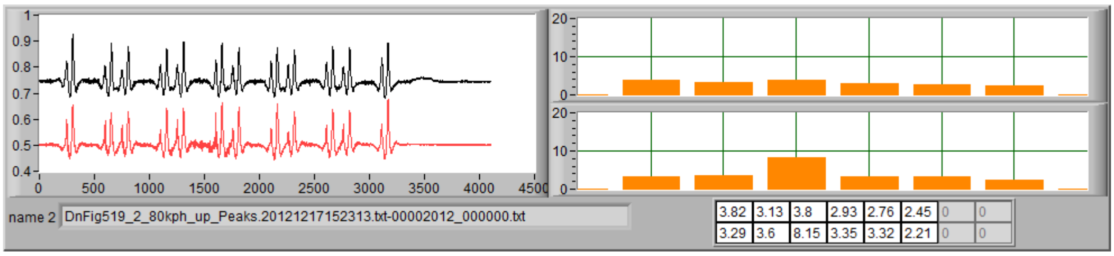
name 2 DnFig519_2_80kph_up_Peaks.20121217152313.txt-00002012_000000.txt
3.82 3.13 3.8 2.93 2.76 2.45 0 0
3.29 3.6 8.15 3.35 3.32 2.21 0 0

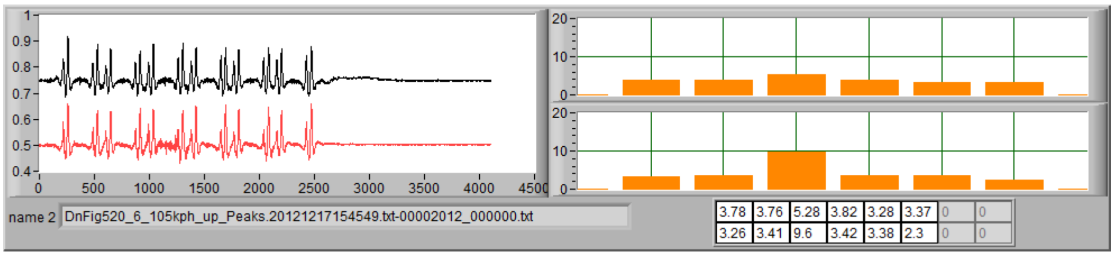
name 2 DnFig520_6_105kph_up_Peaks.20121217154549.txt-00002012_000000.txt
3.78 3.76 5.28 3.82 3.28 3.37 0 0
3.26 3.41 9.6 3.42 3.38 2.3 0 0

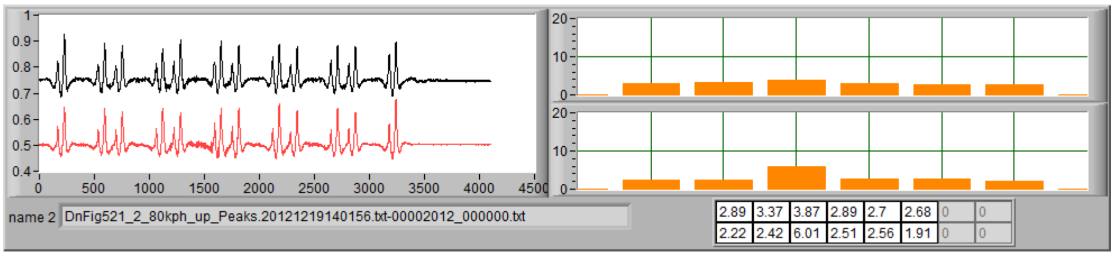
name 2 DnFig521_2_80kph_up_Peaks.20121219140156.txt-00002012_000000.txt
2.89 3.37 3.87 2.89 2.7 2.68 0 0
2.22 2.42 6.01 2.51 2.56 1.91 0 0

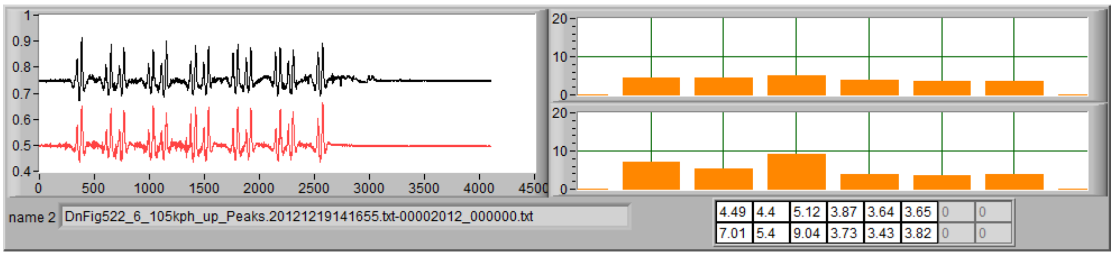
name 2 DnFig522_6_105kph_up_Peaks.20121219141655.txt-00002012_000000.txt
4.49 4.4 5.12 3.87 3.64 3.65 0 0
7.01 5.4 9.04 3.73 3.43 3.82 0 0

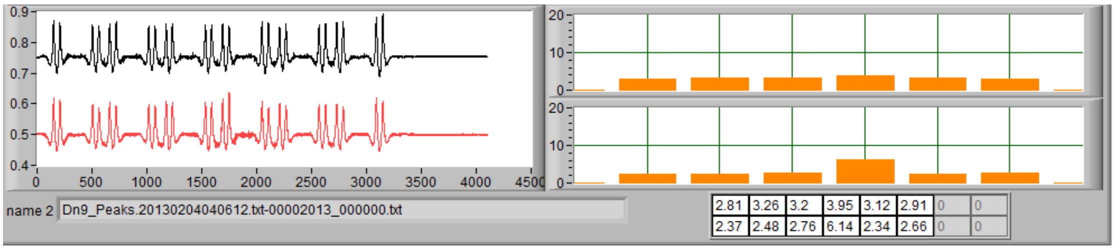
name 2 Dn9_Peaks.20130204040612.txt-00002013_000000.txt
2.81 3.26 3.2 3.95 3.12 2.91 0 0
2.37 2.48 2.76 6.14 2.34 2.66 0 0

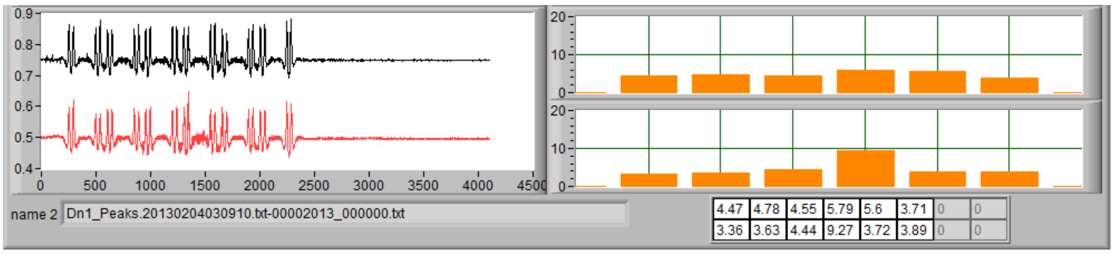
name 2 Dn1_Peaks.20130204030910.txt-00002013_000000.txt
4.47 4.78 4.55 5.79 5.6 3.71 0 0
3.36 3.63 4.44 9.27 3.72 3.89 0 0

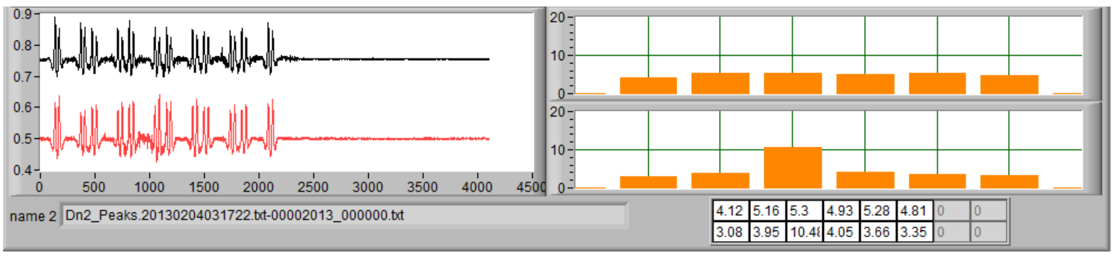
name 2 Dn2_Peaks.20130204031722.txt-00002013_000000.txt
4.12 5.16 5.3 4.93 5.28 4.81 0 0
3.08 3.95 10.4 4.05 3.66 3.35 0 0

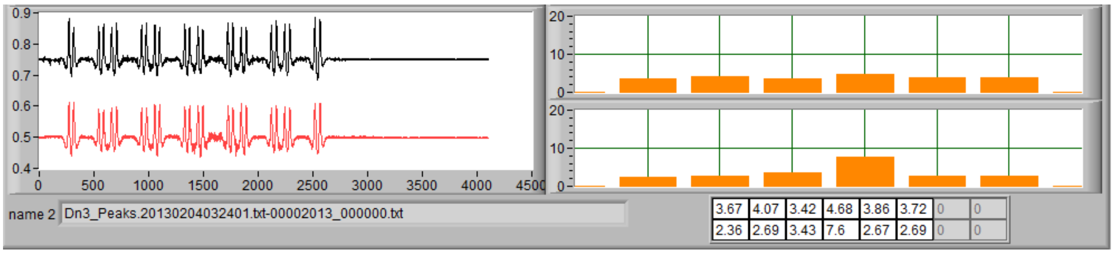
name 2 Dn3_Peaks.20130204032401.txt-00002013_000000.txt
3.67 4.07 3.42 4.68 3.86 3.72 0 0
2.36 2.69 3.43 7.6 2.67 2.69 0 0

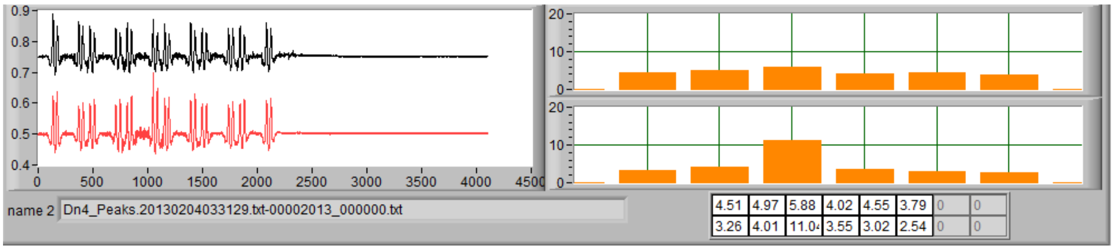
name 2 Dn4_Peaks.20130204033129.txt-00002013_000000.txt
4.51 4.97 5.88 4.02 4.55 3.79 0 0
3.26 4.01 11.0 3.55 3.02 2.54 0 0

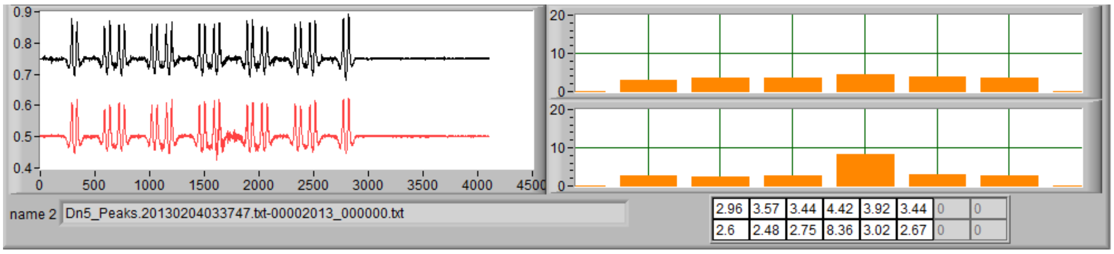
name 2 Dn5_Peaks.20130204033747.txt-00002013_000000.txt
2.96 3.57 3.44 4.42 3.92 3.44 0 0
2.6 2.48 2.75 8.36 3.02 2.67 0 0

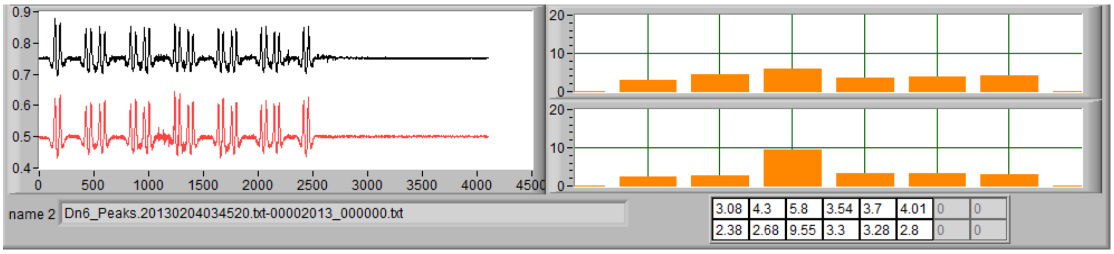
name 2 Dn6_Peaks.20130204034520.txt-00002013_000000.txt
3.08 4.3 5.8 3.54 3.7 4.01 0 0
2.38 2.68 9.55 3.3 3.28 2.8 0 0

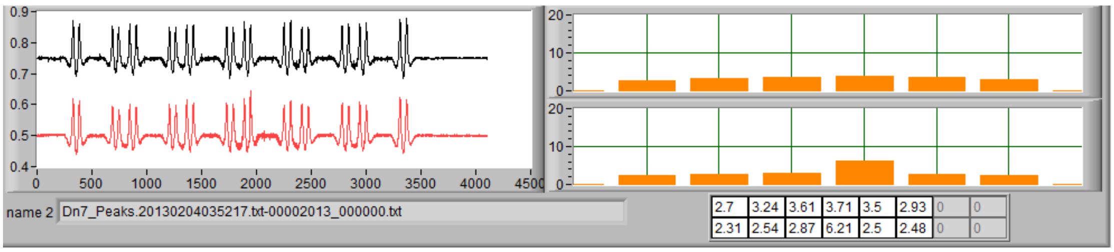
name 2 Dn7_Peaks.20130204035217.txt-00002013_000000.txt
2.7 3.24 3.61 3.71 3.5 2.93 0 0
2.31 2.54 2.87 6.21 2.5 2.48 0 0

Appendix B VI Trend of 8 Sensors in the 8 Cars of a Train

The FGB waveforms of all 8 sensors for measuring the 8 cars of a train. These waveforms show the consistency of the signals from the 8 FBG sensors. The X-axis is the number of rounds to run in-service. The maximum scale of 3,000 represent 300 days of VI as a train runs 10 rounds a day. A pair of sensors was down for 20 days as shown in the missing data pints from 2,100 to 2,300 at the right column.

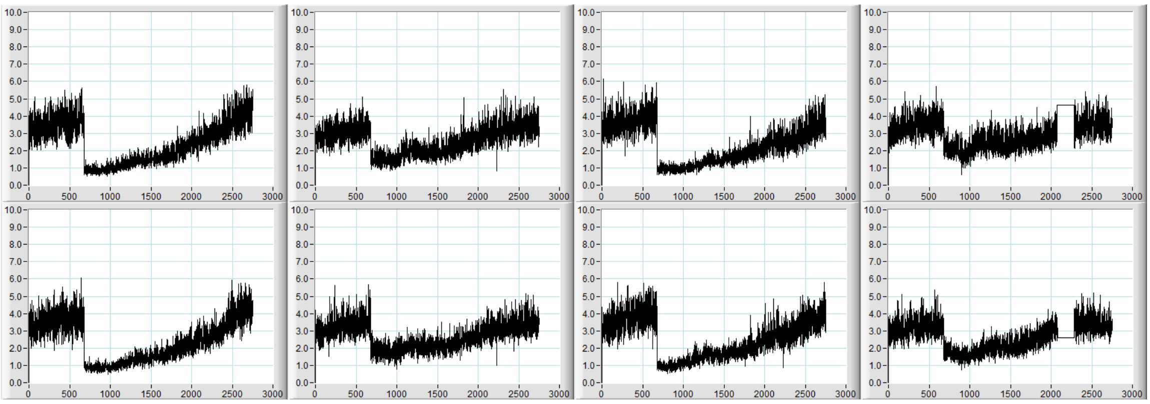

All 8 sensors output of car 1

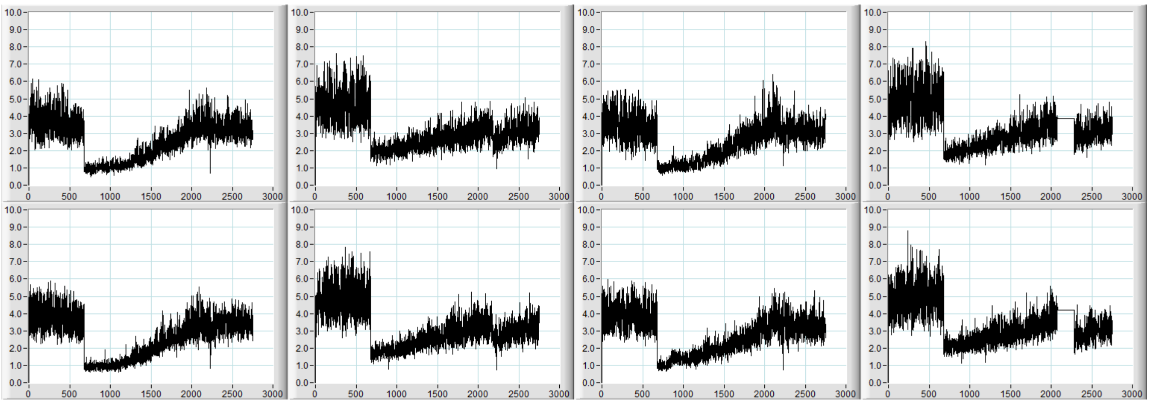

All 8 sensors output of car 2

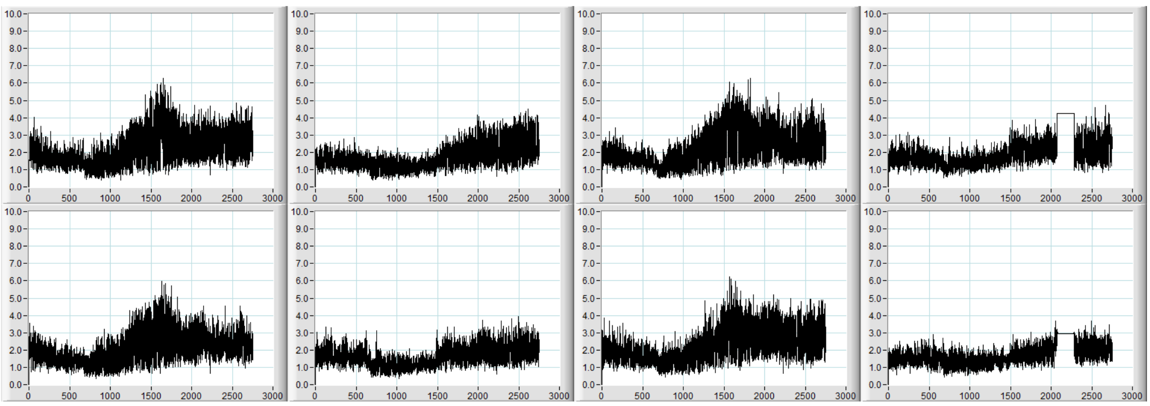

All 8 sensors output of car 3

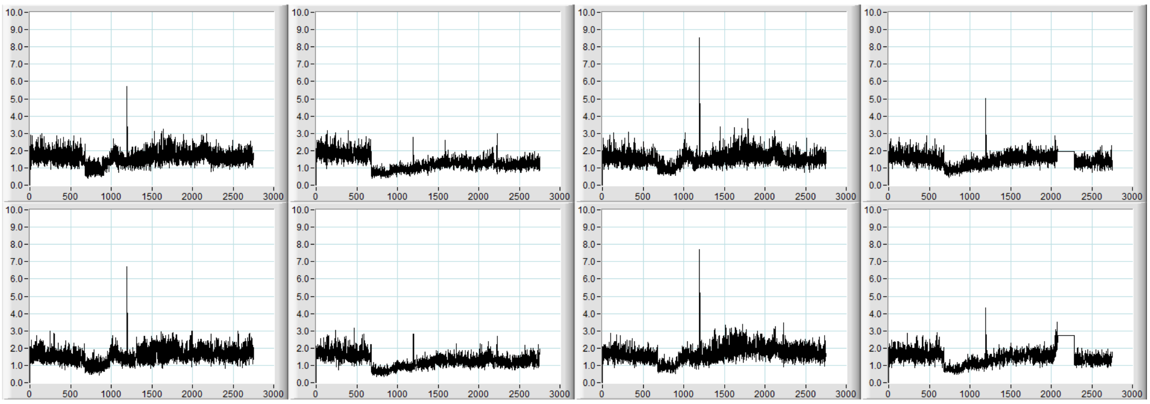

All 8 sensors output of car 4

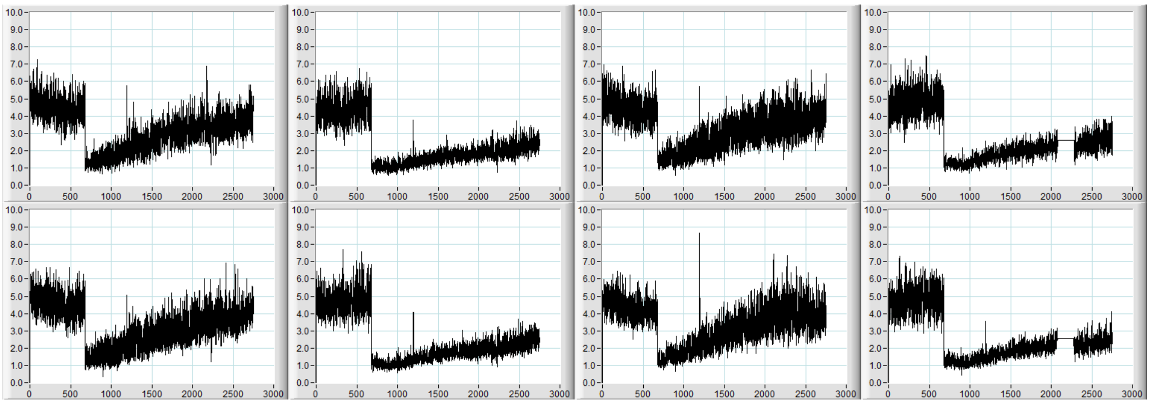

All 8 sensors output of car 5

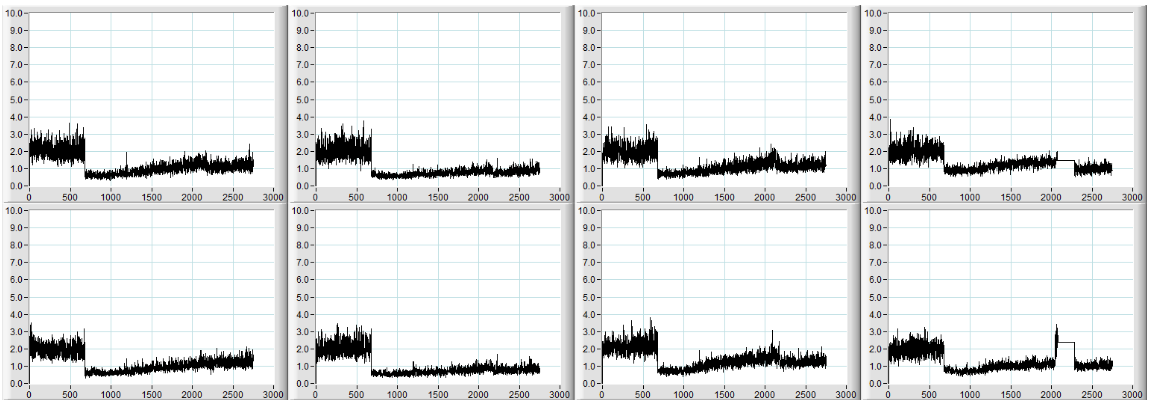

All 8 sensors output of car 6

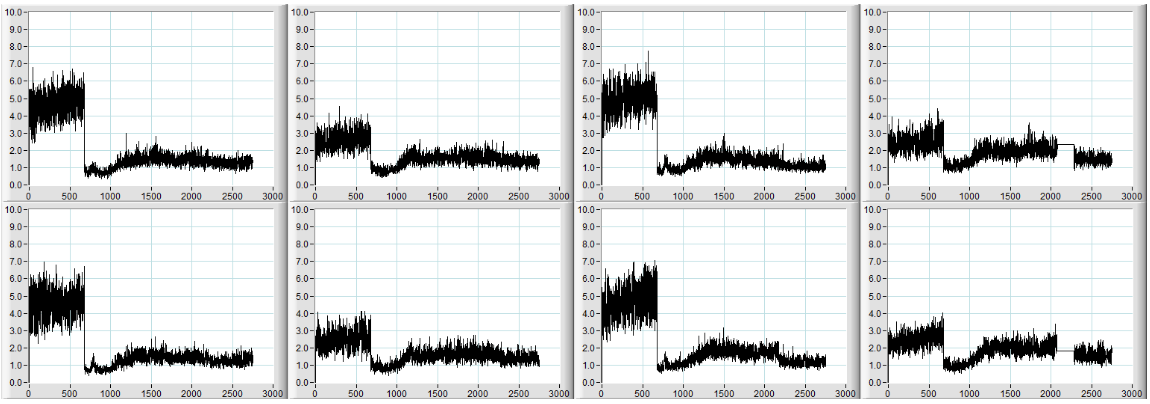

All 8 sensors output of car 7

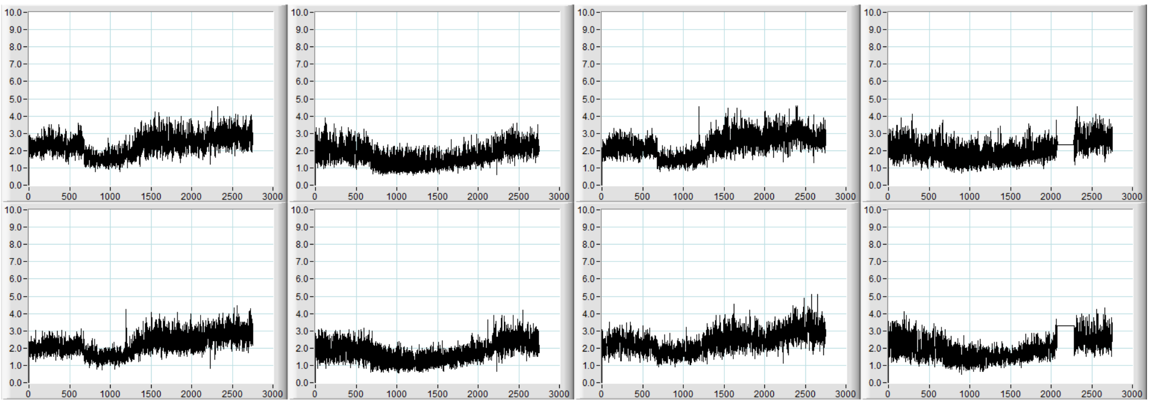

All 8 sensors output of car 8

Appendix C Historical VI of the Fleet from High to Low

This appendix lists out the most serious VI of the train from high to low. They are train number 27, 6, 17, 21, 5, 2, 28, 11, 10, 3 and 1 respectively.

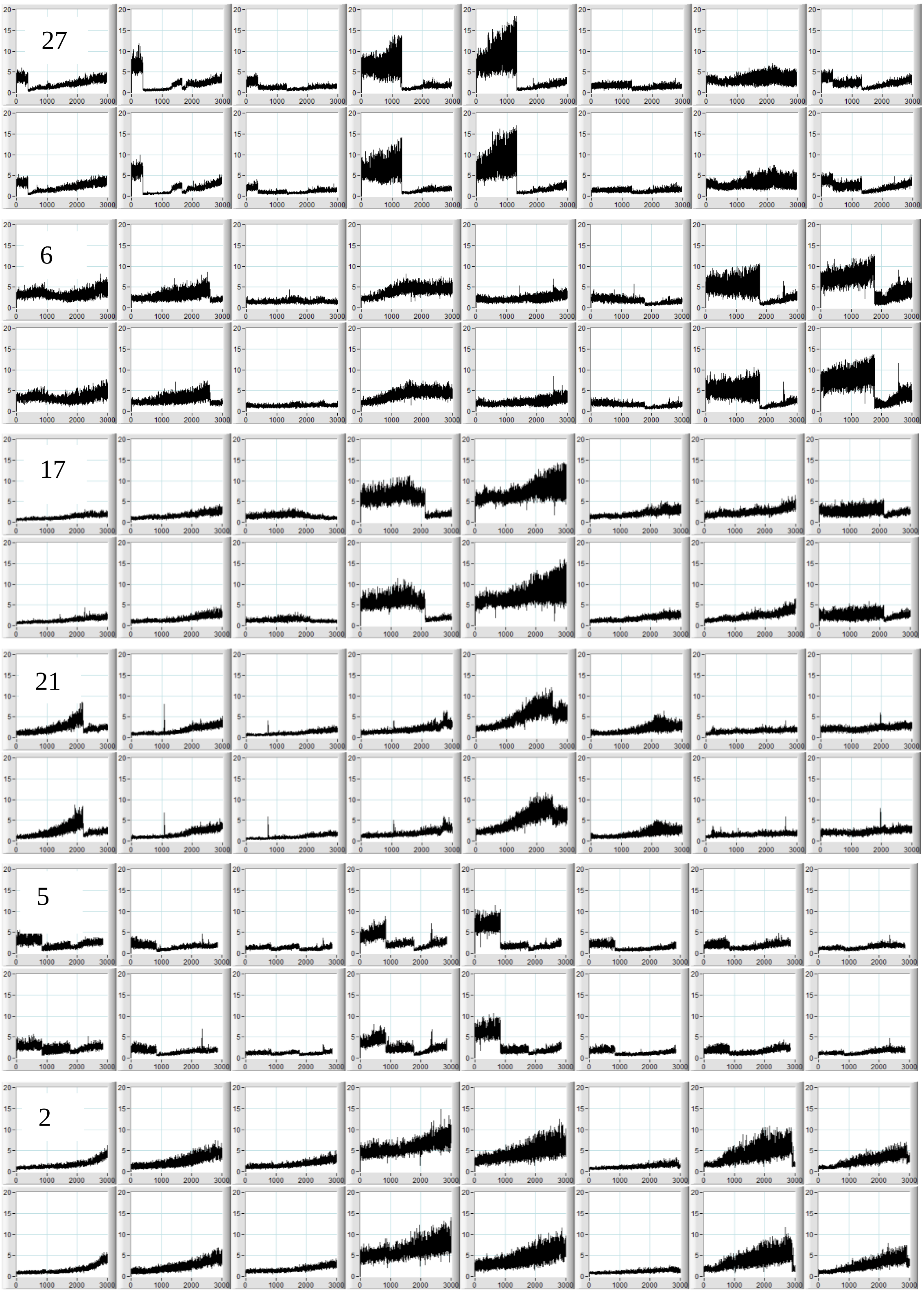

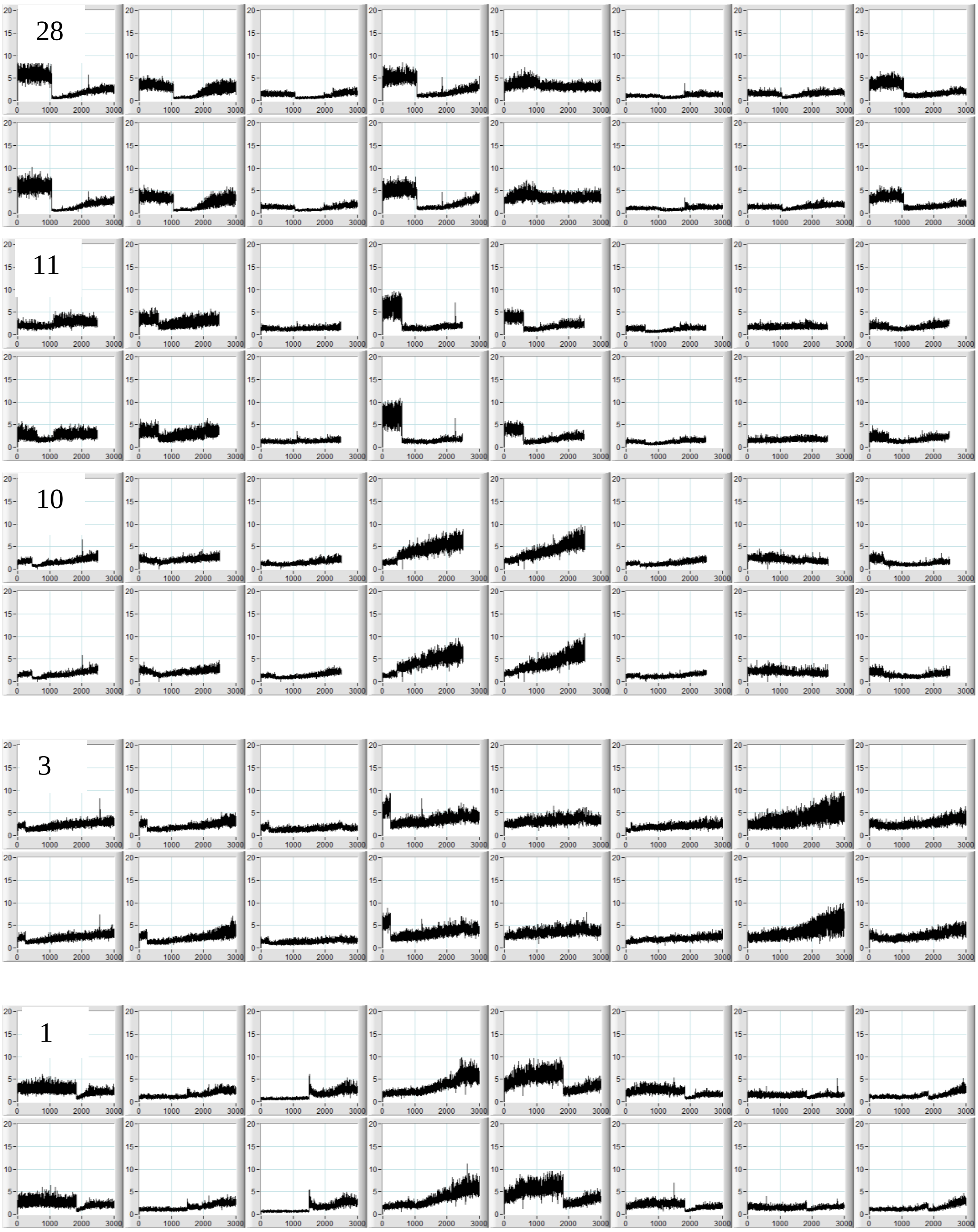
28
11
10
3
1

Appendix D Historical VI with Lowest Values in the Fleet

Graphs listed below are the six trains with lowest VI values.

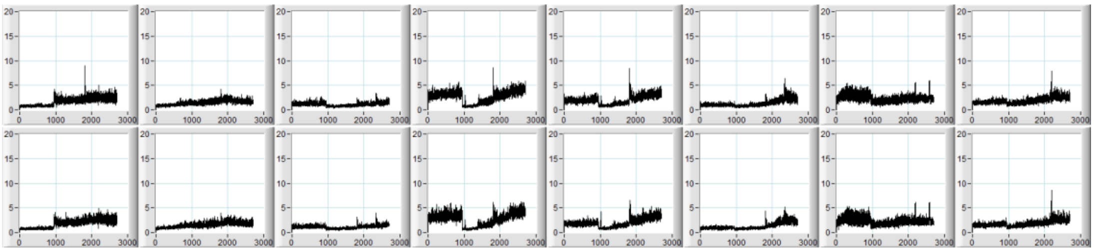

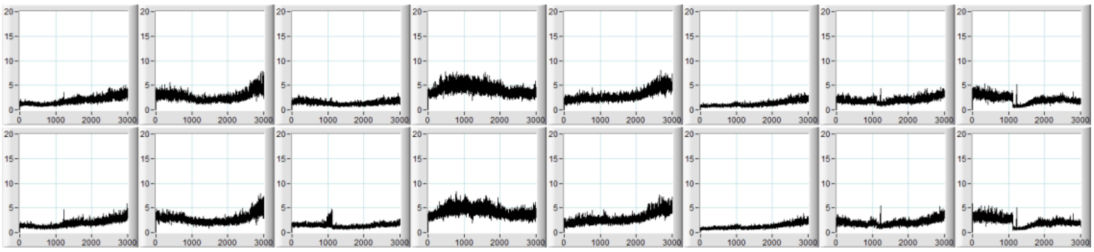

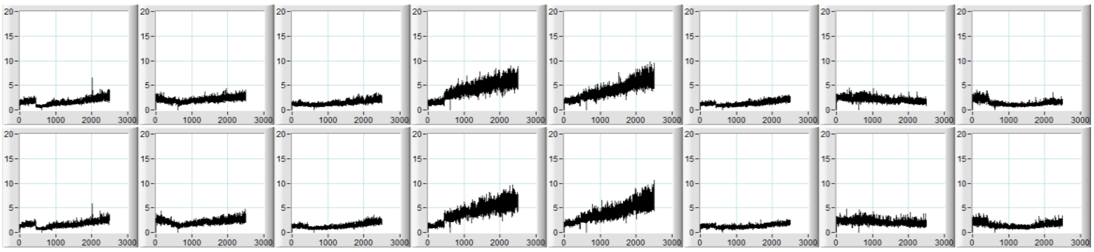

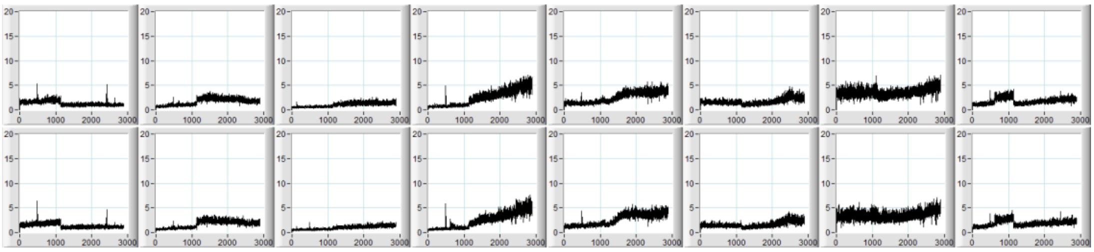

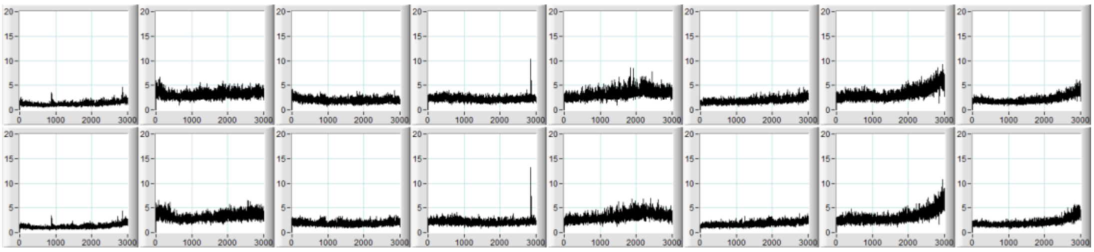

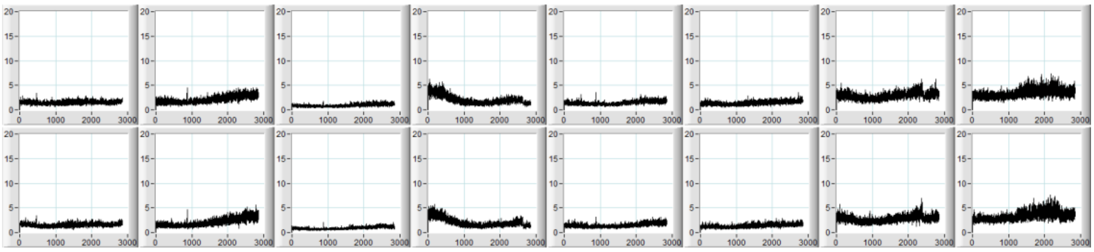

Appendix E Waveforms of 8 Sensors

The following eight waveforms are from the eight FBG strain sensors on the rail. The left column of waveforms # 8, #7, #4 and #3 are from the left hand rail. The right column of waveforms #6, #5, #2 and #1 are from the right. Since the train is approaching the sensors from #8 first, then #7, #4 and lastly #3. The time delay is less in #8 then more in #7 and most serious in #3.

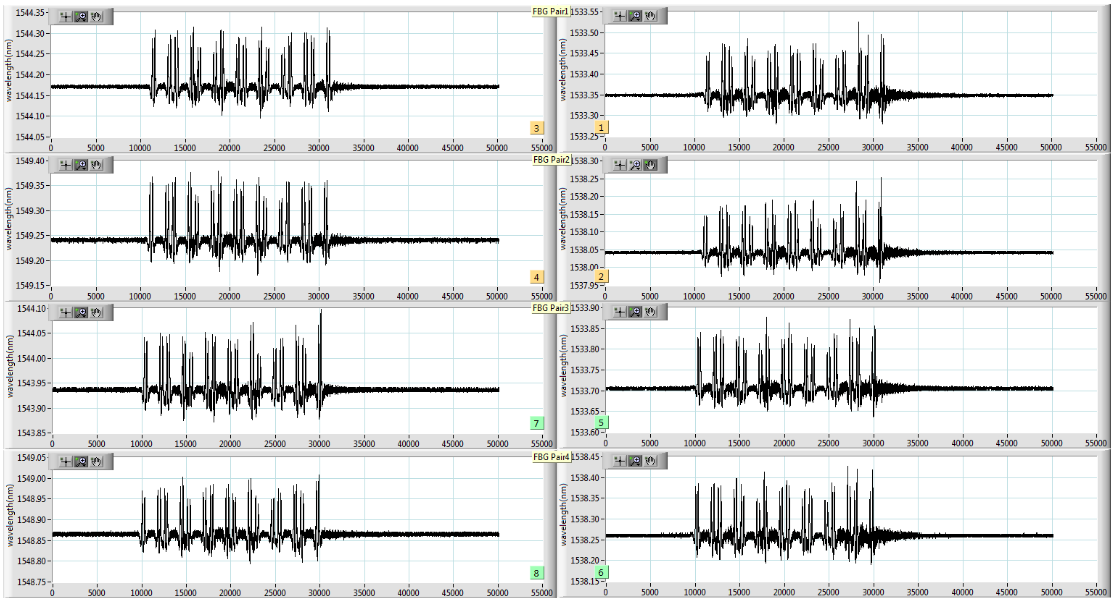

Appendix F Flowcharts of the Sub-Systems

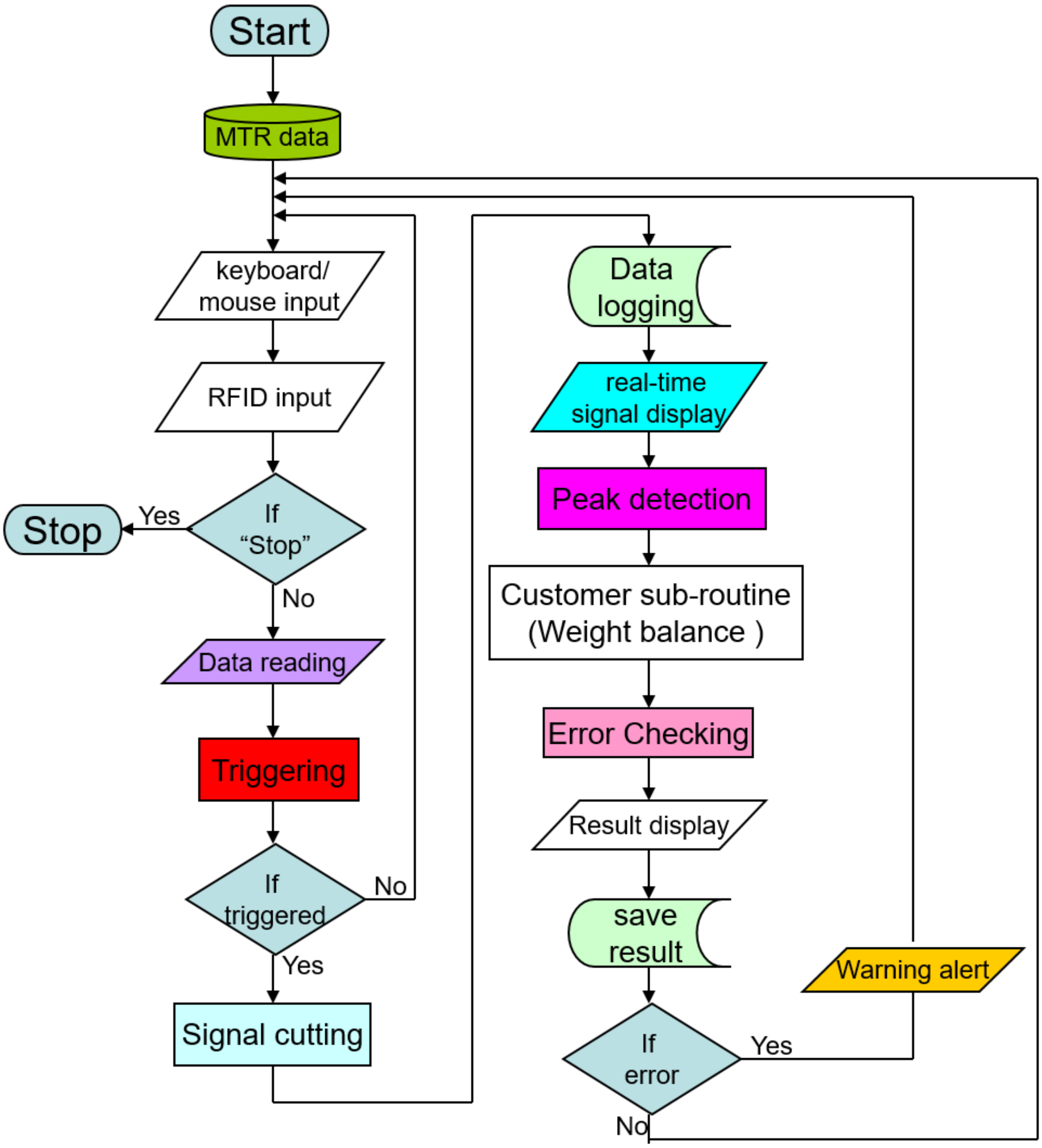

Flow Chart of "Weight balance" calculation sub-system.

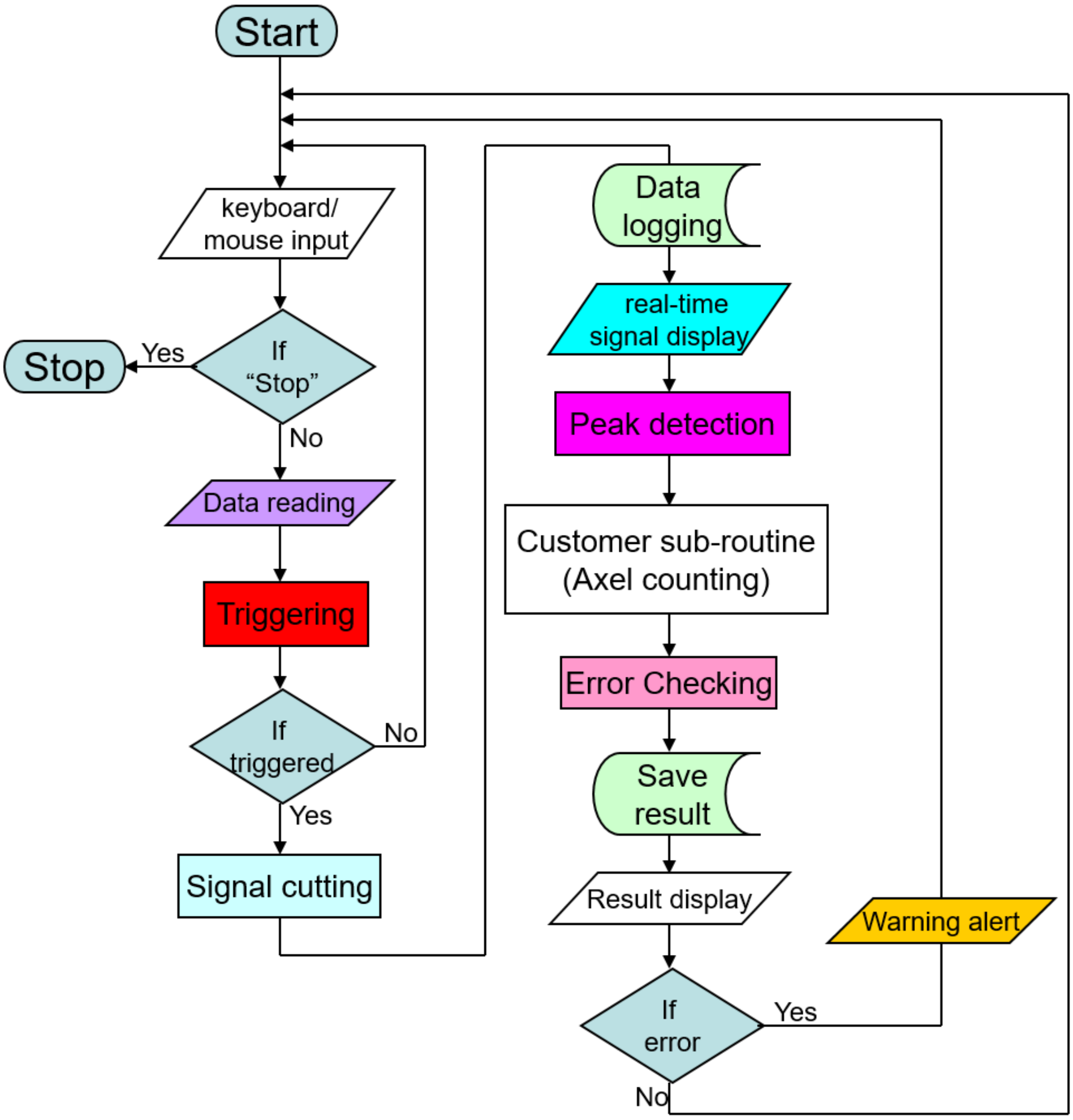

Flow Chart of "Axle Counting" calculation sub-system.

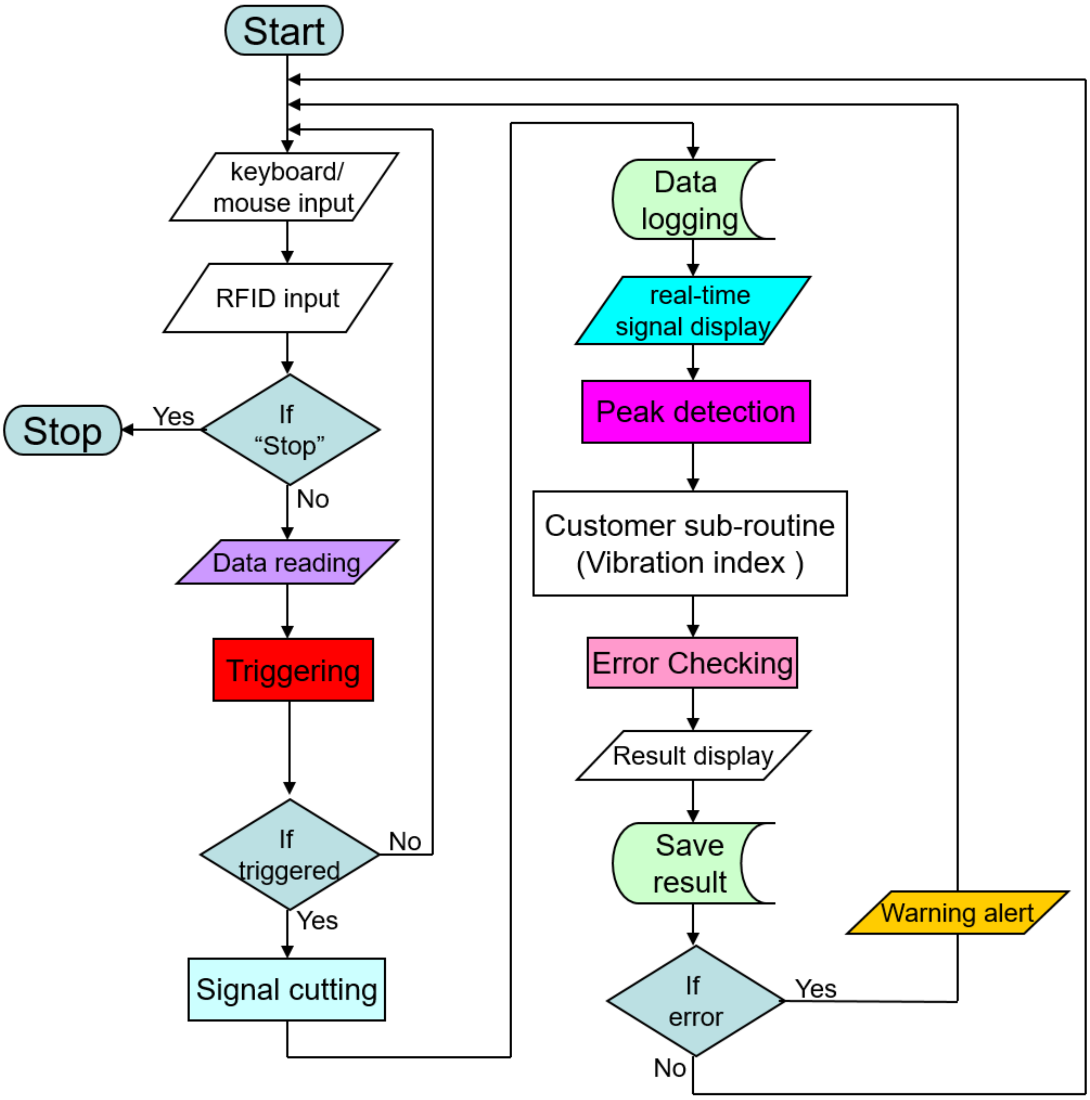

Flow Chart of "Vibration Index" calculation sub-system.

References

[1] K. O. Hill and G. Meltz, “Fiber Bragg grating technology fundamentals and overview,” *J. Light. Technol.*, vol. 15, no. 8, pp. 1263–1276, 1997.

[2] S. J. Mihailov, “Fiber bragg grating sensors for harsh environments,” *Sensors*, vol. 12, no. 2, pp. 1898–1918, 2012.

[3] A. Cusano, A. Cutolo, and J. Albert, “Fiber Bragg Grating Sensors: Recent Advancements, Industrial Applications and Market Exploitation,” Sharjah : Bentham Science Publishers, 2011, p. 332.

[4] A. D. Kersey *et al.*, “Fiber grating sensors,” *J. Light. Technol.*, vol. 15, no. 8, pp. 1442–1463, 1997.

[5] C. C. L. H. Y. A. K. M. C. W. H. C. S. Y. L. H. T. and Y. Q. Ni, “Optical sensor networks for structural health monitoring of canton tower,” *14th Asia pacific Vib. Conf.*, 2011.

[6] W. H. Chung *et al.*, “Structural monitoring of Tsing Ma Bridge using fiber Bragg grating sensors,” *6th Chinese Optoelectron. Symp.*, no. c, pp. 144–146, 2003.

[7] L. K. Cheng *et al.*, “Dynamic load monitoring of the Tsing Ma Bridge using a high-speed FBG sensor system,” *2nd Eur. Work. Struct. Heal. Monit.*, vol. 2004, 2004.

[8] A. AHMADI, S. GUPTA, R. KARIM, and U. KUMAR, “Selection of Maintenance Strategy for Aircraft Systems Using Multi-Criteria Decision Making Methodologies,” *Int. J. Reliab. Qual. Saf. Eng.*, vol. 17, no. 03, pp. 223–243, 2010.

[9] Lloyd’s Register Rail Europe BV, “Gotcha Monitoring Systems,” 2011.

[Online]. Available: http://www.gotchamonitoringsystems.com/references.php#UK.

[10] T. Farrington-Darby, L. Pickup, and J. R. Wilson, "Safety culture in railway maintenance," *Saf. Sci.*, vol. 43, no. 1, pp. 39–60, 2005.

[11] P. Weston, P. Li, and C. Ling, "Track and vehicle condition monitoring during normal operation using reduced sensor sets," *HKIE Trans.*, vol. 13, no. January 2015, pp. 47–54, 2006.

[12] J. Vatn, "Maintenance optimisation," 2007.

[13] E. Brynjolfsson and S. Yang, "Information Technology and Productivity: A Review of the Literature," *Adv. Comput.*, vol. 43, no. C, pp. 179–214, 1996.

[14] K. Lee, K. Lee, and S. Ho, "Exploration of using FBG sensor for derailment detector," *WSEAS Trans. Top. Syst.*, vol. 3, no. 6, pp. 2433–2439, 2004.

[15] N. K. Poon, B. M. H. Pong, C. P. Liu, and C. K. Tse, "Essential-coupling-path models for non-contact EMI in switching power converters using lumped circuit elements," *IEEE Trans. Power Electron.*, vol. 18, no. 2, pp. 686–695, 2003.

[16] M. Sondalini, "Change to Component Health Monitoring for Massive Equipment Reliability Improvement," vol. 61, no. 0. Lifetime Reliability, pp. 1–9, 2009.

[17] M. Baqqar, M. Ahmed, and F. Gu, "Data mining for gearbox condition monitoring," *17th Int. Conf. Autom. Comput.*, no. September, pp. 138–142, 2011.

[18] M. Palo, D. Galar, T. Nordmark, M. Asplund, and D. Larsson, "Condition monitoring at the wheel/rail interface for decision-making support," *Proc. Inst. Mech. Eng. Part F J. Rail Rapid Transit*, vol. 228, no. 6, pp. 705–715,

2014.

[19] R. A. Smith, “The wheel-rail interface - Some recent accidents,” *Fatigue Fract. Eng. Mater. Struct.*, vol. 26, no. 10, pp. 901–907, 2003.

[20] C. C. Lai *et al.*, “Development of a fiber-optic sensing system for train vibration and train weight measurements in Hong Kong,” *J. Sensors*, vol. 2012, 2012.

[21] D. R. Anderson, “Detecting flat wheels with a fiber-optic sensor,” *ASME/IEEE 2006 Jt. Rail Conf. JRC2006*, pp. 25–30, 2006.

[22] C. Wei, Q. Xin, W. H. Chung, S. Y. Liu, H. Y. Tam, and S. L. Ho, “Real-time train wheel condition monitoring by fiber Bragg grating sensors,” *Int. J. Distrib. Sens. Networks*, vol. 2012, 2012.

[23] M. Gehloff, “A Common Misunderstanding about Reliability Centred Maintenance,” *McGraw-Hill*, vol. 61, no. 0. DTM Consulting Services Inc., pp. 1–6, 2013.

[24] S. Sethiya, “Condition Based Maintenance (CBM),” *Secy. to C.*, 2006.

[25] M. Gehloff, “PF curve 101-Keep it simple,” vol. 2012, no. Sept. 2. DTM Consulting Services Inc., pp. 1–6, 2013.

[26] T. G. CHONDROS, A. D. DIMAROGONAS, and J. YAO, “Vibration of a Beam With a Breathing Crack,” *J. Sound Vib.*, vol. 239, no. 1, pp. 57–67, 2001.

[27] F. Besnard, K. Fischer, and L. Bertling, “Reliability-Centred Asset Maintenance - A step towards enhanced reliability, availability, and profitability of wind power plants,” *IEEE PES Innovative Smart Grid Technologies Conference Europe, ISGT Europe*, 2010. [Online]. Available: http://www.plantservices.com/articles/2010/09bestpractices/.

[28] Deployed_Instruments, "Optical Sensing Interrogator sm130." Micron Optics, Inc., USA, pp. 1–4, 2009.

[29] A. Ekberg and E. Kabo, "Fatigue of railway wheels and rails under rolling contact and thermal loading-an overview," *Wear*, vol. 258, no. 7–8, pp. 1288–1300, 2005.

[30] G. Schram, "A Bayesian-network Decision Support System for Bearing Failure Mode Analysis," *BNAIC'01 Spons.*, 2001.

[31] R. Want, "An Introduction to RFID Technology," *PERVASIVEcomputing*, pp. 1–49, 2006.

[32] W. Zhang, "Study on Internet of Things application for High- speed Train Maintenance , Repair and Operation (MRO)," no. Citcs, pp. 8–12, 2012.

[33] M. Bebbington, C. D. Lai, and R. Zitikis, "Useful periods for lifetime distributions with bathtub shaped hazardrate functions," *IEEE Trans. Reliab.*, vol. 55, no. 2, pp. 245–251, 2006.

[34] H. F. Hamada, Michael; S., Wilson; A. G., Reese; C. S.; Martz, "Repairable System Reliability," *Bayesian Reliab.*, 2008.

[35] H. E. Ascher, "Evaluation of Repairable System Reliability Using the ``Bad-As-Old'' Concept," *IEEE Trans. Reliab.*, vol. R-17, no. 2, 1968.

[36] R. Davis and P. Willmott, "Total productive maintenance," *Asset Maint. Manag.*, vol. 14, no. 1, p. 1999, 1999.

[37] J. Abbott, "When old trains are better than new," BBC NEWS, Dover, 2002.

[38] "Executive Management's Report. Hong Kong Transport Operations," *Annu. Rep. 2014*, pp. 1–47, 2014.

[39] P. R, "Strain gauge transducer signal conditioning circuitry," Patent US3841150, 1973.

[40] Q. Chen and P. Lu, “Fiber Bragg Gratings and Their Applications as Temperature and Humidity Sensors,” *At. Mol. Opt. Phys. New Res.*, pp. 235–260, 2008.

[41] M. Kreuzer, “Strain measurement with fiber bragg grating sensors,” *HBM, Darmstadt, S2338-1.0 e*, 2006.

[42] L. Wang and C. Shu, “Distributed fiber strain sensor using stimulated Brillouin scattering based slow light,” *IEEE Photonic Soc. 24th Annu. Meet.*, vol. 4, pp. 929–930, 2011.

[43] C. C. Lai, H. Y. Au, M. S. Y. Liu, S. L. Ho, and H. Y. Tam, “Development of level sensors based on fiber bragg grating for railway track differential settlement measurement,” *IEEE Sens. J.*, vol. 16, no. 16, pp. 6346–6350, 2016.

[44] C. L. Wei *et al.*, “A fiber Bragg grating sensor system for train axle counting,” *IEEE Sens. J.*, vol. 10, no. 12, pp. 1905–1912, 2010.

[45] K. Tam, HY and Liu, SY and Chung, WH and Ho, TK and Ho, SL and Lee, “Smart railway sensor network using fiber bragg gratings as sensing elements,” *Techno-Press*, 2005.

[46] A. Rastegari and M. Mobin, “Maintenance decision making, supported by computerized maintenance management system,” *Proc. - Annu. Reliab. Maintainab. Symp.*, vol. 2016–April, 2016.

[47] M. R. K. Mookiah, U. Rajendra Acharya, C. M. Lim, A. Petznick, and J. S. Suri, “Data mining technique for automated diagnosis of glaucoma using higher order spectra and wavelet energy features,” *Knowledge-Based Syst.*, vol. 33, pp. 73–82, 2012.

[48] J. Han, “Data mining : concepts and techniques,” *J. Chem. Inf. Model.*, p. 703,

2012.

[49] N. Y. Mahamoud, P. Dehombreux, M. Pirlot, and H. E. Roble, “Decision-support approach for selecting the suitable maintenance policy,” *IEEE Int. Conf. Ind. Eng. Eng. Manag.*, vol. 2016–Decem, pp. 1355–1359, 2016.

[50] I. Bâra, A., & Lungu, “Improving Decision Support Systems with Data Mining Techniques,” *Improv. Decis. Support Syst. with Data Min. Tech.*, no. 3, pp. 1–5, 2012.

[51] N. Elgendy and A. Elragal, “Big Data Analytics in Support of the Decision Making Process,” *Procedia Comput. Sci.*, vol. 100, pp. 1071–1084, 2016.

[52] A. Johansson, “Out-of-round railway wheels-assessment of wheel tread irregularities in train traffic,” *J. Sound Vib.*, vol. 293, no. 3–5, pp. 795–806, 2006.

[53] Yangkai *et al.*, “Research on the principle of railway wheel out-of-roundness on-line dynamic detecting system based on Laser measurement,” *FENDT 2014 - Proceedings, 2014 IEEE Far East Forum Nondestruct. Eval. New Technol. Appl. Increasingly Perfect NDT/E*, pp. 217–220, 2014.

[54] I. Vermeij, T. Bontekoe, G. Liefting, and J. Peen, “Optimisation of Rolling Stock Wheelset Life through Better Understanding of Wheel Tyre Degradation,” *Int. J. Railw.*, vol. 1, no. 3, pp. 83–88, 2008.

[55] M. Hartung, “Ch1. Introduction and background.,” in *Vibration-based Condition Monitoring: Industrial, Aerospace and Automotive Applications*, vol. 63, no. 2, R. B. Randall, Ed. 2011 John Wiley & Sons, Ltd, 2011, pp. 1–23.

[56] Y. Kano, S. Hasebe, C. Huang, and T. Yamada, “New type linear variable differential transformer position transducer,” *IEEE Trans. Instrum. Meas.*,

vol. 38, no. 2, pp. 407–409, Apr. 1989.

[57] B. S. Dunn and P. Maintenance, “Plant Maintenance Resource Center Maintenance Terminology - Some Key Terms Maintenance Terminology - Some Key Terms,” pp. 1–19, 1993.

[58] A. H. C. Tsang, “Condition-based maintenance: tools and decision making,” *J. Qual. Maint. Eng.*, vol. 1, no. 3, pp. 3–17, 1995.

[59] R. Stanislaw and J. Marcin, “Use of Condition Monitoring in the Proactive Maintenance Strategy,” *Springer Int. Publ.*, vol. 1, pp. 601–610, 2015.

[60] G. L. Ag, “Guidelines for Machinery Condition Monitoring,” *Lloydia (Cincinnati)*, vol. 1, no. 1, pp. 1–12, 2004.

[61] M. J. Roemer, G. J. Kacprzynski, and R. F. Orsagh, “Assessment of data and knowledge fusion strategies for prognostics and health management,” *Aerosp. Conf. 2001, IEEE Proc.*, vol. 6, pp. 2979–2988, 2001.

[62] ISO 13373-1, “Condition monitoring and diagnostics of machines — Vibration condition monitoring — Part 1: General procedures,” *Int. Organ. Stand.*, vol. 1, 2002.

[63] ISO 13381-1, “Preview Condition monitoring and diagnostics of machines -- Prognostics -- Part 1: General guidelines,” *Int. Organ. Stand.*, vol. 1, 2004.

[64] D. A. Tobon-Mejia, K. Medjaher, and N. Zerhouni, “The ISO 13381-1 standard’s failure prognostics process through an example,” *2010 Progn. Syst. Heal. Manag. Conf. PHM ’10*, 2010.

[65] R. B. Abernethy, *The New Weibull Handbook, Fifth Edition. Chapter 1. An overview of weibull analysis.* 536 Oyster Road, North Palm Beach, 1979.

[66] A. P. Patra, *Maintenance Decision Support Models for Railway Infrastructure using RAMS & LCC Analyses*. 2009.

[67] Marketsandmarkets.com, "Machine Condition Monitoring Market by Monitoring Type," *marketsandmarkets.com*, 2016. [Online]. Available: http://www.marketsandmarkets.com/Market-Reports/machine-health-monitoring-market-29627363.html. [Accessed: 01-Jan-2017].

[68] C. Monitoring, "A new standard for Condition Monitoring," no. June, pp. 13–14, 2011.

[69] P. B. Case and T. Systems, "POSS ® Point machine monitoring."

[70] H. Trains and P. Trains, "COMORAN : Condition Monitoring for Railway Applications."

[71] D2S_International, "I-RAIL, An Intelligent On-line High-Speed Rail Condition Monitoring System Deployed Via Passenger and Freight Trains." European Commission, Belgium, pp. 1–4, 2012.

[72] Alemi, F. Corman, and G. Lodewijks, "Review on condition monitoring approaches for the detection of railway wheel defects," *Proc. Inst. Mech. Eng. Part F J. Rail Rapid Transit*, vol. 0, no. 0, pp. 1–21, 2016.

[73] Cognizant, "Intelligent Infrastructure for Next-Generation Rail Systems," *Cogniz. 20-20 insights*, no. August, 2013.

[74] M. Monteiro, "Vibrations induced by trains Case Study : Extension of track platform of Gare do Oriente," pp. 1–10, 2009.

[75] "Noise and Vibration from High-speed Trains," p. 435, 2001.

[76] P. J. Remington, "Estimation of Wheel/Rail Interaction Forces in the Contact Area Due To Roughness," *J. Sound Vib.*, vol. 193, no. 1, pp. 83–102, 1996.

[77] C. E. Hanson, P. E. Jason, C. Ross, and D. A. Towers, "High-Speed Ground Transportation Noise and Vibration Impact Assessment," *U.S. Dep. Transp. Fed. Transit Adm.*, no. September 2012, pp. 1–248, 2012.

[78] Tata Consultancy Services, "Remote Condition Monitoring of Rail Assets Driving intelligent and efficient rail operations," no. 2013, pp. 1–5, 2014.

[79] B. F. Spencer, M. E. Ruiz-Sandoval, and N. Kurata, "Smart sensing technology: Opportunities and challenges," *Struct. Control Heal. Monit.*, vol. 11, no. 4, pp. 349–368, 2004.

[80] E. Aboelela, W. Edberg, C. Papakonstantinou, and V. Vokkarane, "Wireless sensor network based model for secure railway operations," *2006 IEEE Int. Perform. Comput. Commun. Conf.*, no. January 2005, pp. 623–628, 2006.

[81] V. J. Hodge, S. O. Keefe, M. Weeks, and A. Moulds, "Wireless Sensor Networks for Condition Monitoring in the Railway Industry: A Survey," *IEEE Trans. Intell. Transp. Syst.*, vol. 16, no. 3, pp. 1088–1106, 2015.

[82] J. Ben Ali, B. Chebel-Morello, L. Saidi, S. Malinowski, and F. Fnaiech, "Accurate bearing remaining useful life prediction based on Weibull distribution and artificial neural network," *Mech. Syst. Signal Process.*, vol. 56, pp. 150–172, 2015.

[83] A. Sandryhaila and J. M. F. Moura, "Big data analysis with signal processing on graphs: Representation and processing of massive data sets with irregular structure," *IEEE Signal Process. Mag.*, vol. 31, no. 5, pp. 80–90, 2014.

[84] M. Kamber and I. Database, "Data Mining : Concepts and Techniques Chapter 9 . Mining Complex Types Mining Complex Data Objects : An Example : Plan Mining by Divide and Generalization-Based Sequence," *Syst. Res.*, pp. 1–18, 2001.

[85] J. Tutcher, "Ontology-driven data integration for railway asset monitoring applications," *Proc. - 2014 IEEE Int. Conf. Big Data, IEEE Big Data 2014*, pp. 85–95, 2015.

[86] J. M. Easton, J. R. Davies, and C. Roberts, “Ontology Engineering The “What’s”, “Why’s”, and “How’s” of Data Exchange,” *Int. J. Decis. Support Syst. Technol.*, vol. 3, no. 1, pp. 40–53, 2011.

[87] A. Holst, J. Ekman, and S. Larsen, “Abnormality Detection in Event Data and Condition Counters on Regina Trains,” *Railway Condition Monitoring, 2006. The Institution of Engineering and Technology International Conference on*. pp. 53–56, 2006.

[88] X. Wu, X. Zhu, G. Q. Wu, and W. Ding, “Data mining with big data,” *IEEE Trans. Knowl. Data Eng.*, vol. 26, no. 1, pp. 97–107, 2014.

[89] A. Nunez, J. Hendriks, Z. Li, B. De Schutter, and R. Dollevoet, “Facilitating maintenance decisions on the Dutch railways using big data: The ABA case study,” *Proc. - 2014 IEEE Int. Conf. Big Data, IEEE Big Data 2014*, pp. 48–53, 2015.

[90] A. Thaduri, D. Galar, and U. Kumar, “Railway assets: A potential domain for big data analytics,” *Procedia Comput. Sci.*, vol. 53, no. 1, pp. 457–467, 2015.

[91] E. Fumeo, L. Oneto, and D. Anguita, “Condition based maintenance in railway transportation systems based on big data streaming analysis,” *Procedia Comput. Sci.*, vol. 53, no. 1, pp. 437–446, 2015.

[92] B. L., “A brief history of decision making,” *Harvard Business Review*, vol. 84, no. 1. p. 32, 2006.

[93] S. Alter, “A Taxonomy of Decision Support Systems,” *Sloan Management Review*, vol. 19, no. 1. pp. 39–56, 1977.

[94] D. Trees, “Introduction to Decision Trees 14,” *Event (London)*.

[95] H. Guler, “Decision Support System for Railway Track Maintenance and Renewal Management,” *J. Comput. Civ. Eng.*, vol. 27, no. 3, pp. 292–306,

May 2013.

[96] E. V. Ocalir-Akunal, “Decision Support Systems in Transport Planning,” *Procedia Eng.*, vol. 161, pp. 1119–1126, 2016.

[97] S. K. Linden and K. R. Petty, “He Use of Metro (Model of the Environment and Temperature of the Roads) in Roadway Operation Decision Support Systems,” vol. 53, no. 9, pp. 1689–1699, 2013.

[98] L.-P. Crevier and Y. Delage, “METRo: A New Model for Road-Condition Forecasting in Canada,” *J. Appl. Meteorol.*, vol. 40, no. 11, pp. 2026–2037, 2001.

[99] N. Rodríguez-Padial, M. Marín, and R. Domingo, “Strategic Framework to Maintenance Decision Support Systems,” *Procedia Eng.*, vol. 132, pp. 903–910, 2015.

[100] K. O. Hill, Y. Fujii, D. C. Johnson, and B. S. Kawasaki, “Photosensitivity in optical fiber waveguides: Application to reflection filter fabrication,” *Appl. Phys. Lett.*, vol. 32, no. 10, pp. 647–649, 1978.

[101] H. Tam *et al.*, “Distribution Optical Sensor System on the 610-m Guangzhou New TV Tower,” pp. 2–4, 2011.

[102] K. Yu, C. Lai, C. Wu, Y. Zhao, C. Lu, and H. Tam, “A High-Frequency Accelerometer Based on Distributed Bragg Reflector Fiber Laser,” *IEEE Photonics Technol. Lett.*, vol. 26, no. 14, pp. 1418–1421, 2014.

[103] K. O. Hill, B. Malo, F. Bilodeau, D. C. Johnson, and J. Albert, “Bragg gratings fabricated in monomode photosensitive optical fiber by UV exposure through a phase mask,” *Appl. Phys. Lett.*, vol. 62, no. 10, pp. 1035–1037, 1993.

[104] P. Ferdinand, S. Magne, V. Dewynter-Marty, C. Martinez, S. Rougeault, and

M. Bugaud, “Applications of Bragg grating sensors in Europe,” *Opt. Fiber Sensors*, vol. 16, pp. 14–19, 1997.

[105] T. H. T. Chan *et al.*, “Fiber Bragg grating sensors for structural health monitoring of Tsing Ma bridge: Background and experimental observation,” *Eng. Struct.*, vol. 28, no. 5, pp. 648–659, 2006.

[106] “Grating Based Temperature Sensors - Temperature Calibration and Thermal Response Temperature,” Micron Optics, Inc. Grating, 2008.

[107] C. Elliott, V. Vijayakumar, W. Zink, and R. Hansen, “National Instruments LabVIEW: A Programming Environment for Laboratory Automation and Measurement,” *J. Lab. Autom.*, vol. 12, no. 1, pp. 17–24, 2007.

[108] T. Liu, D. Wang, R. Raenaei, X. Chen, L. Zhang, and I. Bennion, “A low-cost multimode fiber Bragg grating sensor system,” 2005, vol. 5634, p. 54.

[109] X. Sang, C. Yu, and B. Yan, “Bragg gratings in multimode optical fibres and their applications,” *J. Optoelectron. Adv. Mater.*, vol. 8, no. 4, pp. 1616–1621, 2006.

[110] Changgui Lu and Yiping Cui, “Fiber Bragg grating spectra in multimode optical fibers,” *J. Light. Technol.*, vol. 24, no. 1, pp. 598–604, 2006.

[111] G. Meltz, W. W. Morey, and W. H. Glenn, “Formation of Bragg gratings in optical fibers by a transverse holographic method,” *Opt. Lett.*, vol. 14, no. 15, p. 823, Aug. 1989.

[112] T. (Micron O. Graver, “How do FBG sensor interrogators work,” *Micron Optics Inc*, 2008. [Online]. Available: http://www.micronoptics.com/how-do-fbg-sensor-interrogators-work/.

[113] A. Güemes, A. Fernandez-Lopez, and A. Lozano, “Fiber Optic Distributed Sensing,” *NATO-STO Lect. Ser.*, pp. 1–16, 2014.

[114] L. Schenato, *A Review of Distributed Fibre Optic Sensors for Geo-Hydrological Applications,* vol. 7, no. 9. 2017.

[115] E. D. Moore, “Advances in Swept-Wavelength Interferometry for Precision Measurements,” University of Colorado, Boulder, 2011.

[116] K. Kishida, Y. Yamauchi, and A. Guzik, “Study of optical fibers strain-temperature sensitivities using hybrid Brillouin-Rayleigh system,” *Photonic Sensors*, vol. 4, no. 1, pp. 1–11, Mar. 2014.

[117] S. B. Mahar, “Spontaneous Brillouin Scattering Quench Diagnostics for Large Superconducting Magnets,” 2008.

[118] Z. Xue, J. Shi, Y. Yamauchi, and S. Durucan, “applied sciences Fiber Optic Sensing for Geomechanical Monitoring : (1) -Distributed Strain Measurements of Two Sandstones under Hydrostatic Confining and Pore Pressure Conditions,” *Appl. Sci.*, vol. 2103, no. 1, 2018.

[119] M. L.-A. R.A. Perez-Herrera, “Fiber optic sensor networks,” *Opt. Fiber Technol.*, vol. 19, no. 6, pp. 689–699, 2013.

[120] H. Guo, G. Xiao, N. Mrad, and J. Yao, “Fiber Optic Sensors for Structural Health Monitoring of Air Platforms,” *Sensors*, vol. 11, no. 4, pp. 3687–3705, Mar. 2011.

[121] T. Dahlberg, “Railway track settlements - a literature review,” pp. 1–41, 2004.

[122] B. E. Zuada Coelho, *Dynamics of railway transition zones in soft soils*. 2011.

[123] A. Paixão, E. Fortunato, and R. Calçada, “The effect of differential settlements on the dynamic response of the train-track system: A numerical study,” *Eng. Struct.*, vol. 88, pp. 216–224, 2015.

[124] Y. Mizuno, Y. Fujino, K. Kataoka, and Y. Matsumoto, “Development of a

Mobile Sensing Unit and Its Prototype Implementation," *Tsinghua Sci. Technol.*, vol. 13, no. October, pp. 223–227, 2008.

[125] "S8 VIBRATING WIRE SETTLEMENT CELL Description." Soil Instruments Ltd., pp. 0–3.

[126] A. Simonetti, "A Measurement Technique for the Vibrating Wire Sensors Andrea Wire Sensors," *IEEE*, pp. 1–6, 2012.

[127] Y. Dai, Q. Sun, S. Tan, J. Wo, J. Zhang, and D. Liu, "Highly sensitive liquid-level sensor based on dual-wavelength double-ring fiber laser assisted by beat frequency interrogation.," *Opt. Express*, vol. 20, no. 25, pp. 27367–76, 2012.

[128] M. Zaynetdinov, E. M. See, B. Geist, G. Ciovati, H. D. Robinson, and V. Kochergin, "A fiber Bragg grating temperature sensor for 2-400 K," *IEEE Sens. J.*, vol. 15, no. 3, pp. 1908–1912, 2015.

[129] Y. Q. Ni, Y. Xia, W. Y. Liao, and J. M. Ko, "Technology innovation in developing the structural health monitoring system for Guangzhou New TV Tower," *Struct. Control Heal. Monit.*, vol. 16, no. 1, pp. 73–98, Feb. 2009.

[130] S. W. Hughes, "Measuring liquid density using Archimedes' principle," *Phys. Educ.*, vol. 41, no. 5, pp. 445–447, 2006.

[131] R. J. Black, D. Zare, L. Oblea, Y.-L. Park, B. Moslehi, and C. Neslen, "On the Gage Factor for Optical Fiber Grating Strain Gages," *Proc. Soc. Adv. Mater. Process Eng.*, 2008.

[132] "Optical Sensing Interrogators – what distance." Micron Optics, 2008.

[133] C. S. Fibers, "1310 / 1550 nm Reduced Clad and Bend Insensitive Select," *East*, p. 9001, 2011.

[134] A. to Z. of A to Z Materials, "Stainless Steels - Introduction To The Grades And Families," pp. 1–8, 2011.

[135] "ES CompleatTM Lifetime Heavy Duty Fully Formulated Antifreeze/Coolant." Cummins Filtration, 2014.

[136] "Miniature One-touch Fittings One-touch Mini," no. 650. SMC, South San Francisco, pp. 18–26.

[137] Y. J. Rao, "Recent progress in applications of in-fibre Bragg grating sensors," *Opt. Lasers Eng.*, vol. 31, no. 4, pp. 297–324, 1999.

[138] K. Y. Lee, K. K. Lee, and S. L. Ho, "Exploration of using FBG sensor for axle counter in railway engineering," *WSEAS Trans Syst.*, vol. 3, no. 6, pp. 2440–2447, 1978.

[139] A. Jhunjhunwala, "Axle counter based block signaling for safe and efficient train operations," *IEEE*, pp. 824–828, 1999.

[140] A. Taguchi, "Development of a Train Detection System and a Spread Spectrum Transmission System for Track Circuit," *IEEE*, pp. 1922–1926, 1997.

[141] N. Nedelchev, "Influence of earth connection on the operation of railway track circuits," *IEE Pro.-Electr. Power Appl*, vol. 144, no. 3, pp. 215–219, 1997.

[142] I. Lucic, "Holistic safety performance forecasting for train detection system," *Conf. Proc. - IEEE Int. Conf. Syst. Man Cybern.*, vol. 3, pp. 2973–2978, 2005.

[143] A. Othonos and K. Kyriacos, "Fiber Bragg Gratings—Fundamentals and Applications in Telecommunications and Sensing," *Artech House*, 1999.

[144] Z. Wen, X. Jin, and W. Zhang, "Contact-impact stress analysis of rail joint region using the dynamic finite element method," *Wear*, vol. 258, no. 7–8. pp. 1301–1309, 2004.

[145] “routemap of railway network in Hong Kong.” MTRC, 2016.

[146] Z. Zhou, T. Graver, L. Hsu, and J. Ou, “Techniques of Advanced FBG Sensors: Fabrication, Demodulation, Encapsulation, and Their Application in the Structural Health Monitoring of Bridges,” *Pacific Sci. Rev.*, vol. 5, pp. 71–76, 2003.

[147] F. Terms, “Unconventional Method of Train Detection Using Unconventional Method of Train Detection Using Fibre Optic Sensors,” vol. 3733, no. July, 2017.

[148] C. Miee, M. Ap, S. L. H. Miee, M. Ceng, and H. K. Chan, “Light Rail Cars Structural Integrity Studies of the Body shells of Light Rail Cars,” vol. 3733, no. August, 2017.

[149] H. Iijima; H. Yoshida; K. Suzuki;Y. Yasuda, “A Study on the Prevention of Wheel-Climb Derailment at Low Speed Ranges,” *JR EAST Tech. Rev.*, no. 30, pp. 21–24, 2008.

[150] R. G. Marquis, Brian, “Application of the Nadal Limit to the prediction of wheel climb derailment,” in *ASME/ASCE/IEEE 2011 Joint Rail Conference*, 2011, pp. 1–8.

[151] J. S. Koo and S. Y. Choi, “Theoretical development of a simplified wheelset model to evaluate collision-induced derailments of rolling stock,” *J. Sound Vib.*, vol. 331, no. 13, pp. 3172–3198, Jun. 2012.

[152] “Resistance of Railway Vehicles to Derailment and Roll-Over (GM/RT2141),” *Railw. Gr. Stand.*, vol. 3, no. April, pp. 1–29, 2009.

[153] T. Erdogan, “Fiber grating spectra,” *J. Light. Technol.*, vol. 15, no. 8, pp. 1277–1294, 1997.

[154] R. M. Goodall and C. Roberts, “Concepts and Techniques for Railway

Condition Monitoring," *Railw. Cond. Monit. 2006. Inst. Eng. Technol. Int. Conf.*, pp. 90–95, 2006.

[155] X. Liu, M. R. Saat, P. Christopher, and L. Barkan, "Analysis of Causes of Major Train Derailment and Their Effect on Accident Rates," *Transp. Res. Rec. 2289.1*, no. December 2012, pp. 154–163, 2015.

[156] M. Kiley, "Basics of Oil Condition Monitoring Through Oil Analysis," 2016.

[157] S. Sheng, "Investigation of oil conditioning, real-time monitoring and oil sample analysis for wind turbine gearboxes," *Am. Wind Energy Assoc. Proj. Perform. Reliab. Work.*, 2011.

[158] A. Bracciali and F. Piccioli, "Elimination of Failures in Railway Gearboxes by Regenerative Coasting," in *Civil-Comp Proceedings*, 2014, vol. 104, no. April.

[159] K. Lang, Z. Xing, W. Dong, and X. Gao, *Proceedings of the 3rd International Conference on Electrical and Information Technologies for Rail Transportation (EITRT) 2017*, vol. 483. Singapore: Springer Singapore, 2018.

[160] A. S. Sait and Y. I. Sharaf-Eldeen, "A Review of Gearbox Condition Monitoring Based on vibration Analysis Techniques Diagnostics and Prognostics," no. April, 2011, pp. 307–324.

[161] P. Wilcox, "Long Range Inspection of Rail Using Guided Waves," in *AIP Conference Proceedings*, 2003, vol. 657, pp. 236–243.

[162] P. Navaraja, "Crack Detection System for Railway Track By Using Ultrasonic and Pir Sensor," *IJAICT*, vol. 05, no. 1, pp. 126–130, 2014.

[163] A. Amini, M. Entezami, and M. Papaelias, "Onboard detection of railway axle bearing defects using envelope analysis of high frequency acoustic emission signals," *Case Stud. Nondestruct. Test. Eval.*, vol. 6, pp. 8–16, Nov.

2016.

[164] D. Wang, P. W. Tse, and K. L. Tsui, "An enhanced Kurtogram method for fault diagnosis of rolling element bearings," *Mech. Syst. Signal Process.*, vol. 35, no. 1–2, pp. 176–199, Feb. 2013.

[165] T. S. Azoh, B. Djeumako, and B. S. Fotsing, "Modeling of train track vibrations for maintenance perspectives: application," *Eur. Sci. J.*, vol. 10, no. 21, pp. 260–275, 2014.

[166] C. Esveld and A. De Man, "Use of Railway Track Vibration Behaviour for Design and Maintenance," *IABSE Symp.*, vol. 87, pp. 39–45, 2003.

[167] C. Wei, Z. Cai, H. Y. Tam, S. L. Ho, and Q. Xin, "Reliability verification of a FBG sensors based train wheel condition monitoring system," *Proc. - 2012 Int. Conf. Intell. Syst. Des. Eng. Appl. ISDEA 2012*, pp. 1091–1094, 2012.

[168] P. B. Morice and G. D. Base, "The design and use of a demountable mechanical strain gauge for concrete structures," *Mag. Concr. Res.*, vol. 5, pp. 37–42, 1953.

[169] J. B. Khurgin, "Slow light in various media: a tutorial," *Adv. Opt. Photonics*, vol. 2, no. 3, p. 287, 2010.

[170] G. Mariscal, Ó. Marbán, and C. Fernández, "A survey of data mining and knowledge discovery process models and methodologies," *Knowl. Eng. Rev.*, vol. 25, no. 02, pp. 137–166, Jun. 2010.

[171] T. Poibeau, H. Saggion, J. Piskorski, and R. Yangarber, "Information Extraction: Past, Present and Future. Chapter 2. Multi-source, Multilingual Information Extraction and Summarization," in *Theory and Applications of Natural Language Processing*, 2013, pp. 23–50.

[172] G. Bellinger, D. Castro, and A. Mills, "Data , Information , Knowledge , and

Wisdom,” *Syst. Think.*, p. 5, 2004.

[173] R. L. Ackoff, “From data to wisdom,” *J. Appl. Syst. Anal.*, vol. 16, no. 1, pp. 3–9, 1989.

[174] J. F. Courtney, “Decision making and knowledge management in inquiring organizations: toward a new decision-making paradigm for DSS,” *Decis. Support Syst.*, vol. 31, no. 1, pp. 17–38, May 2001.

[175] G. Vivó-Truyols, J. R. Torres-Lapasió, A. M. Van Nederkassel, Y. Vander Heyden, and D. L. Massart, “Automatic program for peak detection and deconvolution of multi-overlapped chromatographic signals: Part I: Peak detection,” *J. Chromatogr. A*, vol. 1096, no. 1–2, pp. 133–145, 2005.

[176] E. Berlin and K. Van Laerhoven, “Sensor networks for railway monitoring: Detecting trains from their distributed vibration footprints,” *Proc. - IEEE Int. Conf. Distrib. Comput. Sens. Syst. DCoSS 2013*, pp. 80–87, 2013.

[177] E. Rahm and H. H. Do, “Data Cleaning: Problems and Current Approaches,” *Bull. Tech. Comm. Data Eng.*, vol. 23, no. 4, pp. 3–13, 2000.

[178] W. P. B Chandrasekaran, “Data Validation During Diagnosis, A Step Beyond Traditional Sensor Validation,” *AAAI*, pp. 778–782, 1987.

[179] J. D. Chung, J. G. Kim, and D. S. Bae, “Safety Diagnosis of Collided Subway Electric Multiple Units (EMUs),” *Key Eng. Mater.*, vol. 297–300, pp. 1876–1881, 2005.

[180] N. C. Karmakar, S. M. Roy, S. Preradovic, T. D. Vo, and S. Jenvey, “Development of Low-Cost Active RFID Tag at 2 . 4 GHz,” *Network*, vol. 0, no. September, pp. 1602–1605, 2006.

[181] N. C. C. Kiang and S. L. Ho, “Application of WPT and FBG techniques for prognostic of escalator abnormality: A case study of degraded step wheel,”

HKIE Trans. Hong Kong Inst. Eng., vol. 21, no. 1, pp. 21–34, 2014.

[182] W. L. Lim, G. R. McDowell, and A. C. Collop, "The application of Weibull statistics to the strength of railway ballast," *Granul. Matter*, vol. 6, no. 4, pp. 229–237, 2004.

[183] A. Bendell, "Proportional hazards modelling in reliability assessment," *Reliab. Eng.*, vol. 11, no. 3, pp. 175–183, 1985.

[184] D. Sabaei, J. Erkoyuncu, and R. Roy, "A review of multi-criteria decision making methods for enhanced maintenance delivery," *Procedia CIRP*, vol. 37, pp. 30–35, 2015.

[185] A. W. D. Parameters, "Weibull Distribution Parameters for Fault Feature Extraction of Rolling Bearing," pp. 69–74, 2011.

[186] A. K. Jardine, P. M. Anderson, and D. S. Mann, "Application of the Weibull proportional hazards model to aircraft and marine engine failure data," *Qual. Reliab. Eng. Int.*, vol. 3, no. October, pp. 77–82, 1987.

[187] N. and B. TagMaster, "Wheel Flat Detection and Axle Load Measurement," 2016.

[188] H. Y. Au, S. K. Khijwania, and H.-Y. Tam, "Fiber Bragg grating based accelerometer," *Proc. SPIE*, vol. 7004, no. L, p. 70042S–70042S–4, 2008.

[189] J. A. Bucaro and N. Lagakos, "Lightweight fiber optic microphones and accelerometers," *Rev. Sci. Instrum.*, vol. 72, no. 6, pp. 2816–2821, 2001.

[190] A. Mirabadi, N. Mort, and F. Schmid, "Application of sensor fusion to railway systems," *Multisens. Fusion Integr. Intell. Syst. 1996. IEEE/SICE/RSJ Int. Conf.*, pp. 185–192, 1996.

[191] L. Mohanty, L. M. Koh, and S. C. Tjin, "Fiber Bragg grating microphone system," *Appl. Phys. Lett.*, vol. 89, no. 16, pp. 1–4, 2006.

[192] N. Chen and K. L. Tsui, “Condition monitoring and remaining useful life prediction using degradation signals: revisited,” *IIE Trans.*, vol. 45, no. July, pp. 939–952, 2013.

[193] P. Umiliacchi, L. David, and F. Romano, “Predictive maintenance of railway subsystems using an Ontology based modelling approach,” pp. 1–10, 2011.

END.